Title

Cell-cell junctions: the role of actin and viruses in modulating epithelial barrier function

Author

Hamkins-Indik, Tiama

Publication Date

2021

Peer reviewed|Thesis/dissertation

Cell-cell junctions: the role of actin and viruses in modulating epithelial barrier function

By

Tiama Hamkins-Indik

A dissertation submitted in partial satisfaction of the

requirements for the degree of

Joint Doctor of Philosophy
with University of California, San Francisco

in

Bioengineering

in the

Graduate Division

of the

University of California, Berkeley

Committee in charge:

Professor Daniel A. Fletcher, Chair
Professor Tamara Alliston
Professor David Bilder

Spring 2021

Cell-cell junctions: the role of actin and viruses in modulating epithelial barrier function

Abstract

Cell-cell junctions: the role of actin and viruses in modulating epithelial barrier function

by

Tiama Hamkins-Indik

Doctor of Philosophy in Bioengineering

University of California, Berkeley

Professor Daniel A. Fletcher, Chair

Barriers are critical in the body, and dysregulation of barriers is a hallmark of many diseases, including irritable bowel disease, leaky cancer vasculature, and many viral infections. Epithelial paracellular permeability, what passes between cells, is regulated by the tight junction which is formed by specialized adhesive membrane proteins, adaptor proteins, and the actin cytoskeleton. Despite the tight junction's critical physiological role, a molecular-level understanding of how tight junction assembly sets the permeability of epithelial tissue is lacking. In chapter 2, we identify a 28-amino acid sequence in the tight junction adaptor protein ZO-1 that is responsible for actin binding and show that this interaction is essential for tight junction barrier function. In contrast to the strong interactions with actin at the adherens junction, we find that the affinity between ZO-1 and actin is surprisingly weak, and we propose a model based on kinetic trapping to explain how affinity could affect tight junction assembly. Finally, by tuning the affinity of ZO-1 to actin, we demonstrate that epithelial monolayers can be engineered with a spectrum of permeabilities, which points to a new target for treating transport disorders, addressing viral breakdown of cell-cell barriers, and improving drug delivery.

Viruses are known to dysregulate epithelial barriers by targeting tight junctions. The current SARS-CoV-2, the virus responsible for COVID-19, outbreak has created a devastating global health crisis that has been exacerbated by limited treatment options. Similarly, last year there were 39-56 million flu cases and 24,000-62,000 flu deaths in the USA. In chapter 3, we investigate the potential role of SARS-CoV-2 E protein and the influenza NS1 protein in one major symptom of both COVID-19 and influenza – breakdown of epithelial barrier function. Tight junctions are organized by proteins containing PDZ domains, which bind to PDZ binding motifs (PBM) at the C-terminus of other proteins. To test the importance of the E protein PBM and NS1 protein PBM on epithelial barrier function, we built ectopic expression cell culture models and measured tight junction protein localization and barrier function. We found that the PBM of NS1 from different strains of influenza had a variable effect on barrier function, with most PBMs significantly

decreasing barrier function despite variable amino acid sequence. In contrast, we found that the PBM of the E protein of SARS-CoV-2 did not affect barrier function in our cell culture experiments, though expression of the full-length E protein did reduce barrier function in lung epithelial cells.

Our work has revealed how actin binding at the tight junction influences barrier function, but there is a lack of molecular tools to modulate actin binding in live cells. In chapter 4, we present the development of a switchable actin binder that binds to actin only when a cell-permeable small molecule is administered. The switch comprises three fused protein domains – an actin-binding motif and two flanking domains that heterodimerize to block actin binding. For the actin-binding motif, we chose the actin binding site (ABS) of ZO-1 and sandwiched it between truncated Bcl-xL and the modified peptide, BH3, whose binding can be disrupted by the small molecule A-1155463. We show that the switchable actin binder colocalizes with actin in the presence of the small molecule and is tunable; with increasing concentration of the small molecule, there is increasing colocalization of the switchable actin binder with actin. To demonstrate functionality of the probe, we engineered ZO-1 with the switchable actin binder and found that inducing actin binding modulated barrier function. As a second demonstration of the switchable actin binder, we found that tethering the actin cortex to the plasma membrane altered macrophage phagocytosis and receptor enrichment. As indicated by these results, a switchable actin binder that controls when, where, and how much actin binding occurs in live cells has the potential to be a useful and versatile tool for investigating the role of actin networks in cells.

Dedicated to my family

Table of Contents

Acknowledgements

Words cannot express my gratitude for the support I received during my graduate studies; I could not have done this without the community of people around me. I am so lucky to be surrounding by such incredible people, thank you.

I thank Dr. Dan Fletcher for his guidance and support during grad school. Thank you for giving me the freedom to follow the science, and explore any question I found interesting. For the scientific discussions muddling through experiment troubleshooting, guiding which questions to follow, envisioning possible mechanisms, and crafting stories. As an advisor, Dan always listens and helps me navigate the challenges of grad school. He connected me with his community of scientists, and help me build my own. He always values my opinions and voice, providing me with many avenues to share my research and my ideas. He assembled an incredible collection of scientists and engineers in his lab, and the support and scientific insight made the daily and sometimes grueling work of science so enjoyable.

The Fletcher Lab is full to the brim with world-class scientists, and it has been an honor to rub shoulders with the best of the best. Thanks to Amanda Meriwether for her unerring support, kindness, and brilliance. She always pushed me to think bigger and smarter. Her energetic competence was so motivating to me. I appreciate her big-picture thinking combined with the organizational aptitude to make big plans into reality. In addition to her scientific prowess, she also cares deeply about building an inclusive and supportive community in the Fletcher Lab, at UC Berkeley, and within the greater bioengineering community. We have such stimulating discussion on education, science and the intersection with diversity, equity, and inclusion. I want to express my gratitude to Dr. Marija Podolski for her guidance throughout my studies, and especially for our work studying actin binding during macrophage phagocytosis. Her positive outlook and words of encouragement provided such sustenance and made me eager to come into lab and carry out challenging and failure-laden experiments. Thanks to Dr. Brian Belardi for collaborating on our work examining actin binding at the tight junction. He always pushed me to delve deeper into the literature and to design experiments with rigor and purpose. The sums of our experience, his background in chemistry and mine in bioengineering, was greater than the parts and allowed us to explore how biochemical interactions can influence cell function. I learned a lot from him, especially about molecular biology tools, protein engineering, and the tight junction. Thanks to Lienna Chan, Vikki Qian, and Roni Weissman, three undergraduate researchers who worked with me, for focusing their scientific minds on projects with me. I am grateful for my time working with Lienna who brought enthusiasm and diligence to every project, and began our work examining out viruses break down cell-cell barriers. I have deep appreciation for Vikki, who brought a quiet thoughtfulness to her work, and executed her experiments with attention to detail and skill. Many thanks to Roni, who brings curiosity and cheer to our experiments and who executed complex experiments in the wake of the uncertainty of the pandemic. Thanks to Dr.

Caitlin Cornell for her astute and probing questions and her energizing spirit to keep us going through the trials and tribulations of science. Thanks to Dr. Kathy Wei for sharing her knowledge of proteins and protein engineering with me and discussing the ins and outs of building the switchable actin binder. Thanks to Andrew Harris for teaching me techniques, sharing literature with me, and having discussion with me about all things actin. My appreciation goes to Dr. Max Armstrong, for his candid advice and help with building anything in lab. Max was always there to talk, and was a huge support to me in lab. Thanks to Dr. Carmen Chan for her leadership in lab, pushing science to the limits, and motivating me with a can-do attitude to learn new techniques and adapt old ones. Thanks to Dr. Sungmin Son for his thoughtful feedback and biophysics discussions. For her tenacity and support, thanks to Maria de Leon Derby, who always made me feel valued and who taught me about her projects. To Liya Oster, for her leadership on all projects biophysics: fusion, lipids, and interfaces, and for her compassion and experiment design discussions. Thanks to Eva Schmidt for her mentorship and experiment guidance. Thanks to Emily Suter, for her energy, science know-how, stellar experiment design and interpretation, and input on my projects. Thanks to Paulina Kettel for teaching me assays and working on macrophage experiments with me. Thanks to Kaden Southard for his scientific contributions in lab and during our shared commute, as well as his kindness and compassion as I navigated grad school. Thanks to Abdul Bhuiya for his diagnostic development expertise, cheerful support, and device design consultations. Thanks to Victor Gomez for keeping everything in lab running smoothly, taking over nearly all of my lab jobs, and for his support and advice. For their scientific insight, experimental troubleshooting, and comradery, thanks to Dr. Neil Switz, Jordi Silvestri, Ari Joffe, Dr. Sho Takatori, Dr, Dan Friedman, Dr. Mike D'Ambrosio, Dr. Henry Pickard, Dr. Ben Ricca, Dr. Matthew Bakalar, and Dr. Alba Diz-Munoz. Thank you, Fletcher Lab!

My gratitude goes to Dr. Irina Conboy for her mentorship and guidance on updating the curriculum for Cell Biology for Engineers and contributing critical feedback as a member of my qualifying exam committee. I loved working on writing labs, devising projects, and learning how to teach with Dr. Conboy. As a member of my qualifying exam, Dr. Conboy helped me hone in on scientific questions with specific experiments and helped me understand the context of my work. I learned so much, thank you.

Thanks to my qualifying exam committee, Dr. Dan Fletcher, Dr. Irina Conboy, Dr. Tamara Alliston, and Dr. David Bilder for their input, guidance, and critiques of my research proposal. The experiments I outlined during my qualifying exam provided the sturdy foundation for our work exploring actin binding at the tight junction, and the input I received was invaluable. In a similar vein, thank you to Dr. Dan Fletcher, Dr. Tamara Alliston, and Dr. David Bilder for being on my dissertation committee. Thanks for asking persistent questions and for helping to bring my ambitious experimental plans to a more pragmatic state. I appreciate the discussion on how to build a career as a bioengineer and the support to make my career dreams come true.

I am so grateful for my friends for their laughter, joy, steadfastness, and for always being a phone call away. Thanks to Zoë Steier for her unyielding heart and walking with me step for step, literally and figuratively, through grad school. For our explorations of nature, and long conversations to help me figure out so many things, including: experiments, Berkeley bureaucracy, classes, and navigating life. Thank you! Thanks to Meg Cook for, oh dear, I can't seem to find the right words. For being funny and ridiculous, for the support through the good and the bad, for always cheering me up. For the comfort I always find in hearing your voice on the phone. Thanks to Alya Madrid for her never-ending support. For always reaching out, even when I get busy and distracted. For helping me grow and change, being goofy, dancing from one day to the next, and so much more. Thanks to Max Armstrong, David Piech, Thomas Carey, and Justin Lopez, for their unwavering support and helping me to relax and have fun. Thanks for the evening talks, giant martinis, thanksgiving traditions, bay area hikes, Cleveland sport team fandom, inquisitive questions, and all-around good times. Thanks to Jacob Izlraelevitz, Leah Mendelson, Raphael Cherney, Rebecca Cherney, Ian Cutler, Emma Sokoloff-Rubin, Elias Sanchez-Eppler, Elena Cohen, David Sheppard-Brick, Molly Lieberman, Rachita Navara, Sandra Lam, Stacey Entel, and Erin Glaser for their friendship and support.

Thank you to my family for their faith in my ability, loving me exactly as I am, and always being there. Thanks to my incredible partner, Tim Ando, for his belief in me, for building me up, and for taking care of me when the going got tough. For his whimsy and goofiness and always knowing how to make me laugh. For telling me I can do anything I set my mind to and supporting my career and my well-being in equal measure. For planning the most incredible travels and taking me around the world. Tim has such kindness and empathy, and I deeply value his support during grad school. Thanks to Chihoko Ando for supporting me with food, conversations, and travel during graduate school. Thanks go to my grandparents, Monica Hamkins, Clark Hamkins, Harriet Hershenov, Bernie Hershenov, and Barry Indik for their warmth, love, and care. I send my deepest gratitude to my mom, SuEllen Hamkins, for being a role model, supporting me, helping me see my strengths, and for prioritizing seeing each other in person even though we were on opposite sides of the continent. She is the embodiment of warmth and love, and her passionate spirit rejuvenates me and keeps me going. My love of science was kindled from a very young age, and she always supported my pursuit of career as an engineer. I have always felt surrounded by love, thank you. Many thanks to my dad, Jay Indik, for his love, support, and jokes. He encouraged and supported my interest in math and science as a kid, and as my research got more complex always sought to understand what I was working on. Always a phone call away, he has been there whenever I've needed him. Thanks to the one and only, Frances Hamkins-Indik. Thank goodness they were here when I moved across the country for grad school. They have been there for me at every turn of the road: to complain with me, to commiserate, and to schlump around, and relax with. They make my commute all the better by keeping me company on the phone with our morning grumblings. It's been so important to balance the rigor of grad school with the fun of exploring the bay area, eating food, and goofing around with Fran; thanks for being there for me.

Chapter 1 – Introduction

The goal of this introduction is to summarize and communicate my complex research topic, epithelial barrier function, in an accessible manner to a broad audience. Please see individual chapters for introductions targeted at a scientific audience.

Cell-cell barriers

Barriers in the body

Barriers in our bodies are critical[1,2]. Our skin is a protective barrier keeping the world outside and us inside; our skin has evolved to be robust and difficult to break through[3–5]. Our blood vessels have evolved to hold blood and withstand pressure while also delivering nutrients to every cell in the body by allowing nutrients to pass through the blood vessel walls[6,7] (Figure 1A). The blood brain barrier, or the blood vessels in the brain, are some of the most selective barriers in the body. These blood vessels prevent almost everything in the blood stream from getting into our brain, except for nutrients and oxygen[8]. Our intestines allow energy rich food to pass into the blood stream while preventing pathogens and parts of food that we can't digest to pass through. Barriers in our body vary. Some, like the skin and the blood brain barrier are incredibly tight[9]. Others, like many blood vessels are allow for a lot of transport across the barrier. In this dissertation I will share our research answering questions about these barriers. How are barriers in the body built and maintained? How are they broken down by viruses? Can we engineer cell barriers?

Introducing the tight junction

Our organs, like our skin, blood vessels, and intestines, are formed from cells that are connected to each other. One way that our organs control what passes through them is by controlling what passes between cells, be it proteins, ions, or even other cells. Broadly speaking, the closer together the cells are, or the tighter they are, and the less passes between them. Cell have different ways of sticking to each other with different proteins that are called cell-cell junctions. The aptly named tight junction is the cell-cell junction that is responsible for what passes between cells[2] (Figure 1B).

Before I explain who the players are in the tight junction, I want to start with a brief overview of the building blocks of cells themselves. The cells in our body are like water balloons filled with proteins and genetic material organized with structured proteins and lipid compartments. The water balloon of the cell is called the plasma membrane and is made out of lipids which separate the inside of the cell from the outside of the cell, like a stable bubble. Proteins are encoded in the genetic material in the cell and comprise the physical structures in the cell as well as the molecular machines that build them, just like metal can be the frame of the house and the material that the tools to build the house are made of. Now back to the tight junction. There are proteins embedded in the plasma membrane of the cell, and some of these stick to proteins on other cells like Velcro[10]. The tight junction is the collection of proteins in the membrane that stick to each other to bring cells close to each other as well as the proteins inside the cell that organize and orchestrate the proteins in the membrane[11] (Figure 1B).

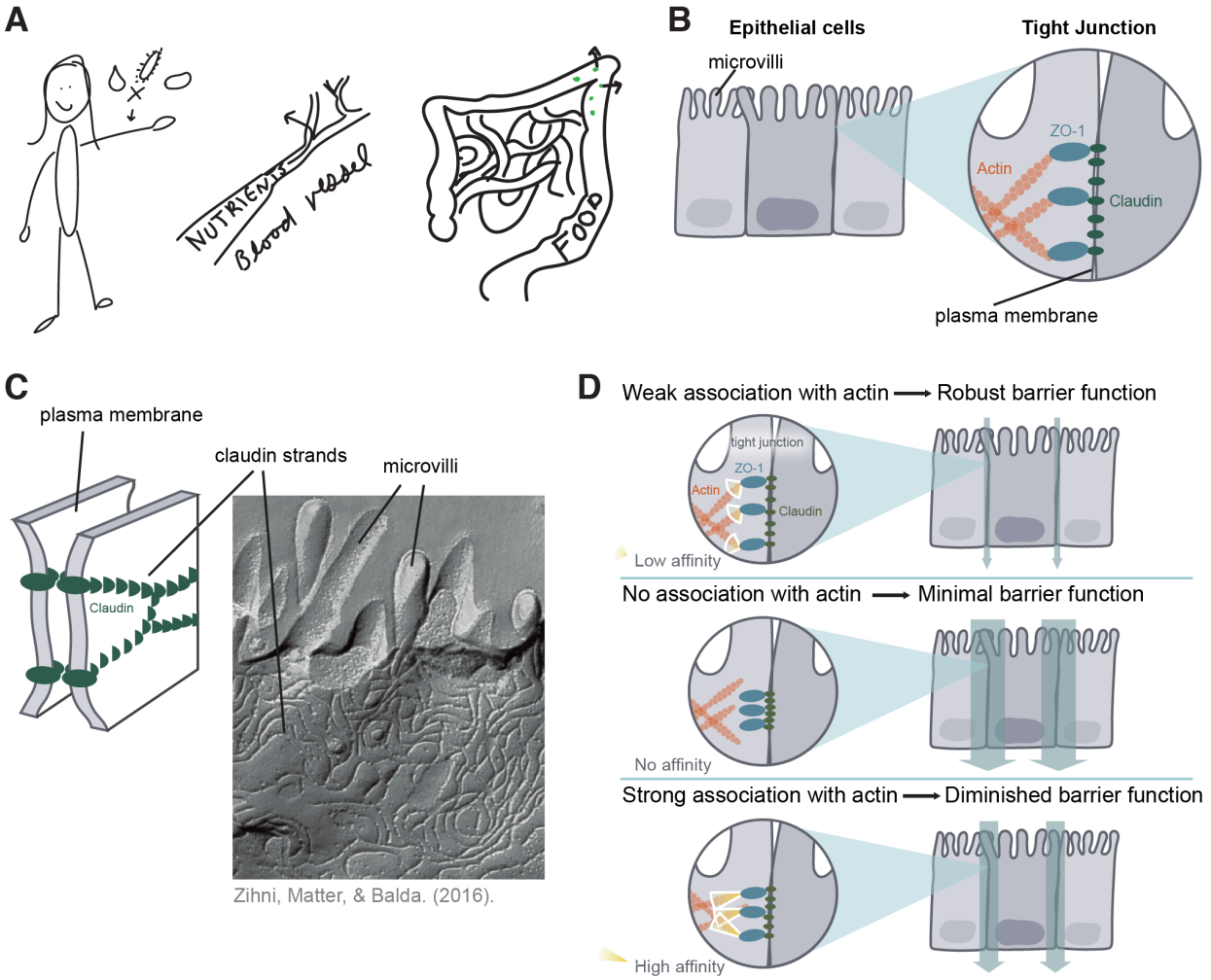

Figure 1 Introducing the tight junction and how a link with actin at the tight junction regulates barrier function

A) Barriers in our body are critical, including our skin, blood vessels, and our intestines.

B) At the top of epithelial cells are tight junctions, cell-cell junctions that zipper cells together closely and regulate what passes between cells. Claudins bind to each other in opposing membranes and ZO-1 provides a link to the actin cytoskeleton.

C) Claudin is a protein in the membrane that form strands in the membrane, shown here is an EM micrograph of claudin strands that form a meshwork in the cell membrane.

D) We found that a weak association with actin results in robust barrier function, no association with actin results in minimal barrier function, and, surprisingly, a strong association with actin results in diminished barrier function.

What are the proteins of the tight junction? There are hundreds of proteins associated with the tight junction, and one family of proteins that Velcros cells together are claudins. Unlike Velcro, claudins bind to itself in long strands in the plane of the cell membrane and the strands in one cell bind to strands in another cell. When you look at these strands in cells you see a beautiful meshwork, and generally speaking the more strands we see the stronger the barrier is in the cells[12,13] (Figure 1C). Inside the cell, one family of proteins that bind to claudins are ZO family proteins (ZO-1, ZO-2, ZO-3)[14–16]. ZO family proteins bind to a whole host of proteins at the tight junction,

including structural proteins inside the cell[14–17]. I am interested in whether the link to structural proteins is important for organizing tight junction and the overall barrier of cell layers.

The actin cytoskeleton and tight junctions

The cell cytoskeleton is comprised of structural proteins inside the cell. Just like our own skeletons, the cytoskeleton (cyto- is Greek for cell, skeleton means, well, skeleton) gives physical form to the flexible membrane, like tent poles give shape to a fabric tent. The cytoskeleton is made up of individual proteins bind together into filaments, like Legos snapped together, forming different shapes and structures. As the human skeleton grows and changes, the cell cytoskeleton can continually elongate and disassociate—it is dynamic, intricate, and constantly moving. The cytoskeleton and the proteins that interact with the cytoskeleton give rise to many key functions of cells, like cell migration, muscle cell contraction, cell division, cell signaling, and cell-cell junctions[18–23].

For the actin cytoskeleton, the protein called actin binds to itself to make actin filaments (Figure 3A). Actin binding proteins regulate rates of polymerization and dissociation and whether actin filaments are bundled together like woven rope or form a branched network more like mesh. Actin binding proteins also help determine where actin filaments are in the cell[18]. The actin cytoskeleton is found in every cell of our body. Actin filaments are bound to tight junction proteins, and we know that actin is important for building barriers[15,24] (Figure 1B).

As scientists, we have tools to control how much of the actin in a cell is polymerized into filaments and how much is floating around in the cell as individual proteins. One drug, called cytochalasin D, prevents actin from polymerizing into filaments. When this drug is given to cells, we see that the claudin strands dissociate; there are far fewer strands and they are less connected[25]. In the presence of cytochalasin D, barrier function, or how much of something can travel from the top of a cell layer to the bottom of a cell layer, is increased[26]. In other words, a whole lot more stuff gets through cell layers when the actin can't form filaments. This suggests that actin in the form of filaments is critical for the organization of the tight junction. Another study examined whether claudin strands in the membrane of a cell are aligned with actin filaments. They found that, that yes, indeed, they are aligned with actin filaments and that ZO-1 acts as a linker and binds to both claudin strands and actin filaments[27] (Figure 1B). These studies led me to our main research question, what is the role of actin binding to ZO-1 for barrier function? Is ZO-1 bound to actin strongly or weakly?

A weak link with actin organizes tight junctions to control barrier function

To answer our questions about ZO-1 and actin, we used cell culture models. Practically, this means we grow mammalian cells in the lab to look at tight junction proteins under the microscope and evaluate barrier function. We used a DNA editing technology called CRISPR/Cas9 to create ZO protein "knockout" cells, which are normal cells except that the ZO proteins have been removed.

CRISPR/Cas9 was revolutionary because it allows scientists to make specific DNA edits almost anywhere in the genome—a huge technological leap from previous methods[28]. To make our cell lines, we used CRISPR/Cas9 to cut the DNA of the cell, specifically in the ZO protein genes. Because each gene codes for one specific protein, cutting the ZO genes prevents that protein from ever being made. In the knockout cells we saw that claudins and other tight junction proteins were no longer localized to cell-cell junctions. Without ZO proteins it appeared that there was no tight junction. Our next question was whether this translated to a decrease in barrier function.

To know how good the barrier is we use an assay to measure barrier function, or how tight the tight junction is. To accomplish this, we grow the cells on a porous plastic membrane and then measure how tiny molecules called ions cross the cell layer. We put electrodes on either side of the cell layer and measure the electrical resistance across the cell layer—the greater the electrical resistance the tighter the layer. In our knockout cells, it was almost as though the cells were not there. Lots of ions got through the cell layer, while normal cells formed a barrier to ions traveling across the cells. In short, knocking out ZO proteins essentially obliterated the barrier function of the cells.

We next wanted to answer the question, is ZO-1 binding to the actin cytoskeleton important for barrier function? We took our knockout cells and had the cells make the ZO-1 protein again, but this time we could make changes to ZO-1. We engineered the cells to make full length ZO-1 and ZO-1 missing the small part of ZO-1 that binds to actin. The cells were leakier when ZO-1 could not bind actin, confirming our hypothesis that actin binding at the tight junction was important for the cell barrier.

But why is ZO-1 binding to actin important for barrier function? Tight junction proteins, like claudin, were in the same place in cells, at the cell-cell junction no matter if ZO-1 could bind to actin. Claudin was still at the tight junction. This was surprising, if the proteins aren't different at the tight junction, then how come the barrier function is different?

Just like actin grows, shrinks and moves, we hypothesized that how the tight junction is connected to actin affects how the tight junction fluctuates, moves and stabilizes. To understand how actin binding could alter barrier function we replaced the actin binding site of ZO-1 with actin binding domains from other proteins. There are hundreds of proteins that bind to actin, and some bind strongly to actin while others bind weakly. When we measured barrier function in cells with the actin binding site of ZO-1 replaced with strong binders we found something we didn't expect. We found that when ZO-1 was strongly bound to actin, there was reduced barrier function; more ions could pass through the cell layer. This was unexpected, because we had assumed, wrongly it turns out, that if ZO-1 was strongly bound to actin it would stabilize and strengthen the claudin strands in the membrane. What we saw was the opposite, when ZO-1 was weakly bound to actin we saw an increase in barrier function.

We built a computer model to understand how it could be that a weak link with actin results in better barrier function. This model predicted that when claudin strands were tightly bound to actin filaments the claudin strands could get trapped in bunched up configurations and were not well-aligned with the actin filaments. When the claudin strands were weakly bound to actin filaments the claudin strands could be more aligned with the actin filaments. Our model predicted that for both weak and strong binding to actin the same proteins will be found in the membrane, just as we saw in our cells. Our model also predicts that for weak binding to actin we would expect the tight junction to extend further in the membrane than the strong binders. To validate our computer model we imaged the spread of ZO-1 at the tight junction, but we had to use a new super-resolution imaging technique because the tight junction is too small to see with conventional fluorescent imaging. We found that the distribution of ZO-1 in the membrane was different depending on how tightly ZO-1 is bound to actin. When ZO-1 was weakly linked to actin, ZO-1 was more spread out. When ZO-1 was strongly linked to actin, ZO-1 was less spread out.

Overall, we found that how ZO-1 binds to actin changes barrier function. Surprisingly, we found that a weak link with actin results in more robust barrier function while a strong link with actin results in reduced barrier function. We suggest that the weak link with actin allows the claudin strands to better align with the actin filaments, resulting in an overall longer tight junction (Figure 1D). While our research is many years away from generating a cure, if we understand how barriers in cells are built in the first place we can start to tackle some of the barrier related diseases from a mechanistic standpoint.

Viruses and cell barriers

Viral infection is one such disease that can result in a loss of barrier function. We initially focused on how influenza targets tight junction proteins to decrease barrier function, but as COVID-19 left death and destruction in its wake, we turned our attention to using tools and techniques we developed for studying barrier function and tight junctions towards COVID-19 (Figure 2).

Barrier function is critically connected to some of the most severe symptoms of both influenza and SARS-CoV-2 (the virus responsible for COVID-19) such as fluid accumulation in the lung leading to decreased oxygen transport and difficulty breathing[30–32]. Barrier function in the lung is complicated and can be affected by both the virus itself and the immune response to the virus. In our research we wanted to understand whether individual proteins of influenza and SARS-CoV-2 were responsible, in part, for the breakdown of cell-cell barriers in the lung. We know the genetic sequence of influenza and SARS-CoV-2, so we inserted the genetic material into lung cells to have them make just one viral protein. This allows us to measure changes in barrier function and where tight junction proteins are in response to a given viral protein. This is a safe way to study viruses, as there are no live viruses involved, just one viral protein.

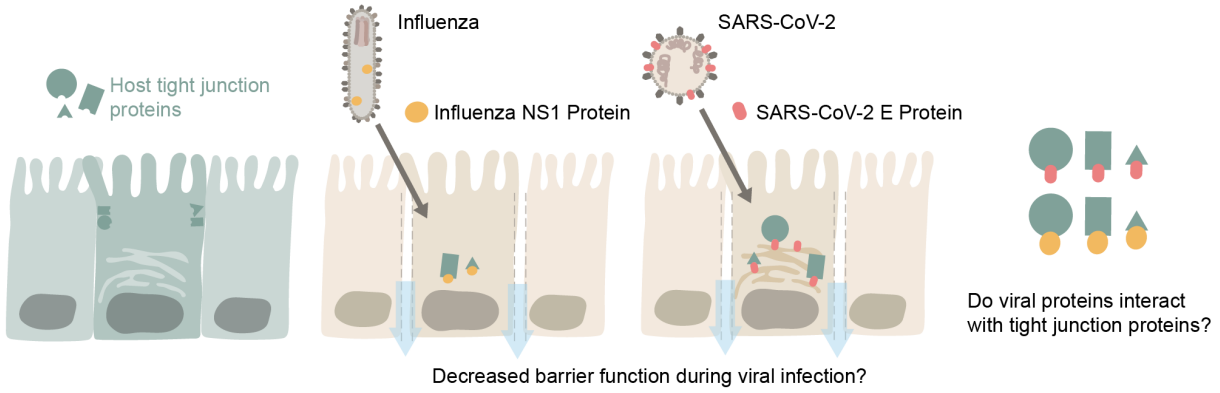

Figure 2 We asked the whether the influenza NS1 protein and SARS-CoV-2 E protein decrease barrier function by interacting with host cell tight junction proteins.

The viral protein of influenza that we are interested in is non-structural protein 1 (NS1). As may be obvious from the name, this protein is not required to form the structure of the physical virus. Instead, it interacts with lung cell proteins to disrupt normal lung cell behavior and prevent it from detecting it's infected with a virus[33]. There one part of the NS1 protein, a small end part known as a PDZ binding motif, that interacts with proteins at the tight junction[29,34–37]. There's something important to know about influenza: it mutates incredibly fast. That's why every year you have to get a new flu vaccine; every year scientists try to predict which strain will be most prominent and rush to make a vaccine to prevent infection. While we have sequencing data showing that NS1 has mutated each year, it has yet to be shown whether these mutations influence barrier function.

We looked at eight strains of influenza and expressed the NS1 protein in cells. Many strains of NS1 caused a decrease in barrier function and a change in tight junction localization. This preliminary work suggests that there is an evolutionary pressure for influenza to bind to tight junction proteins and disrupt barrier function; why else would so many strains have a similar end result? While we know that the different NS1s from different strains of influenza cause a breakdown of barriers, we don't know if they all interact with the same protein in the cell. Future work is needed to understand how these different NS1s break down barrier.

We took a similar approach when we started studying COVID-19. One protein of SARS-CoV-2 is the envelope protein (E protein). The E protein is critical for the structure of SARS-CoV-2, it forms an envelope in the membrane of the virus and is critical for the formation of the virus[38]. E protein of SARS has 96% sequence identity to the E protein of SARS-CoV-2, and just like the NS1 protein, the last bit of the E protein of SARS has been shown to interact with tight junction proteins[39,40]. We thought that maybe the E protein could also interact with tight junction proteins, and that this could help explain how barriers in the lung are disrupted (Figure 2).

To test this idea, we expressed the E protein in cells and the E protein with the last bit that we predicted would bind to tight junction proteins mutated away. We got a negative result; we found

that the last part of the E protein didn't influence barrier function. Our hypothesis was wrong. Even though we were wrong, we did see changes in the cells expressing the E protein compared to normal lung cells. When cells expressed the E protein they grew slower. So even though we were wrong about the last part of the E protein of SARS-CoV-2 breaking down barriers, it does seem that the E protein is interacting with proteins in lung cells to disrupt their behavior. Future directions include examining how the E protein changes cell growth rates and whether this impacts how the virus grows, spreads, and generally wreaks havoc in our bodies.

Controlling when proteins bind to the actin cytoskeleton

As we were studying actin binding of ZO-1 at the tight junction, we wanted a way to turn on actin binding in ZO-1. We wanted to control actin binding and look at how barrier function changes over time. This motivated us to engineer a protein switch that allows us turn on actin binding: a switchable actin binder. We quickly realized that a switchable actin binder can be used to study much more than the tight junction. This could be a widely applicable tool for scientists to use to turn on actin binding in live cells.

There is actin in every cell of our bodies, and what actin does in each cell is determined by which proteins bind to it (Figure 3A). In muscle cells, actin binding proteins bundle actin and molecular motors pull on actin in a coordinated way that leads to our muscle movement[41]. Every movement we make, including your eyes moving to read these words, is determined by when and where proteins bind to actin. This is true of nearly every cell type. As we showed, actin binding at the tight junction modulates barrier function in epithelial cells[42]. Actin binding determines cell migration[43]. Actin binding plays a critical role in our immune cells, and the cells that engulf and kill invading pathogens[44,45]. As of now, scientists have limited tools for controlling which proteins bind to actin in live cells. Our goal was to engineer a switchable actin binder and use this tool to answer the many questions about how actin binding alters cell behavior.

We first had to design a switchable actin binder and assess whether it worked. To design a switchable actin binder we designed a protein so that the actin binding was physically blocked by other parts of the protein, but would move away when we add a small molecule. We drew inspiration from proteins inside the cell that turn on actin binding. For example, ezrin doesn't bind to actin unless it's activated by another protein[46] or vinuclin[47], which doesn't bind actin unless it's physically stretched out to reveal an actin binding domain. For our design we used a protein domain from Bcl-xL and the BH3 motif[48–50]. BH3 binds tightly to BCLxL, and we thought that if we put an actin binding domain in between them they would physically block the actin binding domain from accessing actin. Inhibiting BH3 and BCLxL in cancer cells kills them, so scientists have identified many small molecules that interfere with this interaction that didn't kill regular, non-cancerous cells[49,51]. We designed the switchable actin binder with the idea that we could use the small molecules that inhibit Bcl-xL/BH3 binding, opening up the protein and allowing for actin binding. We tested many different configurations and actin binding motifs and measured whether

the switchable actin binder changes where it was in the cell from floating around in the cell to co-localized with the actin filaments. This strategy helped us identify a switchable actin binder candidate that could be incorporated into other proteins to induce actin binding. The winning configuration was Bcl-xL, the actin binding site of ZO-1 (ABS), and BH3 linked together as one protein (Figure 3B).

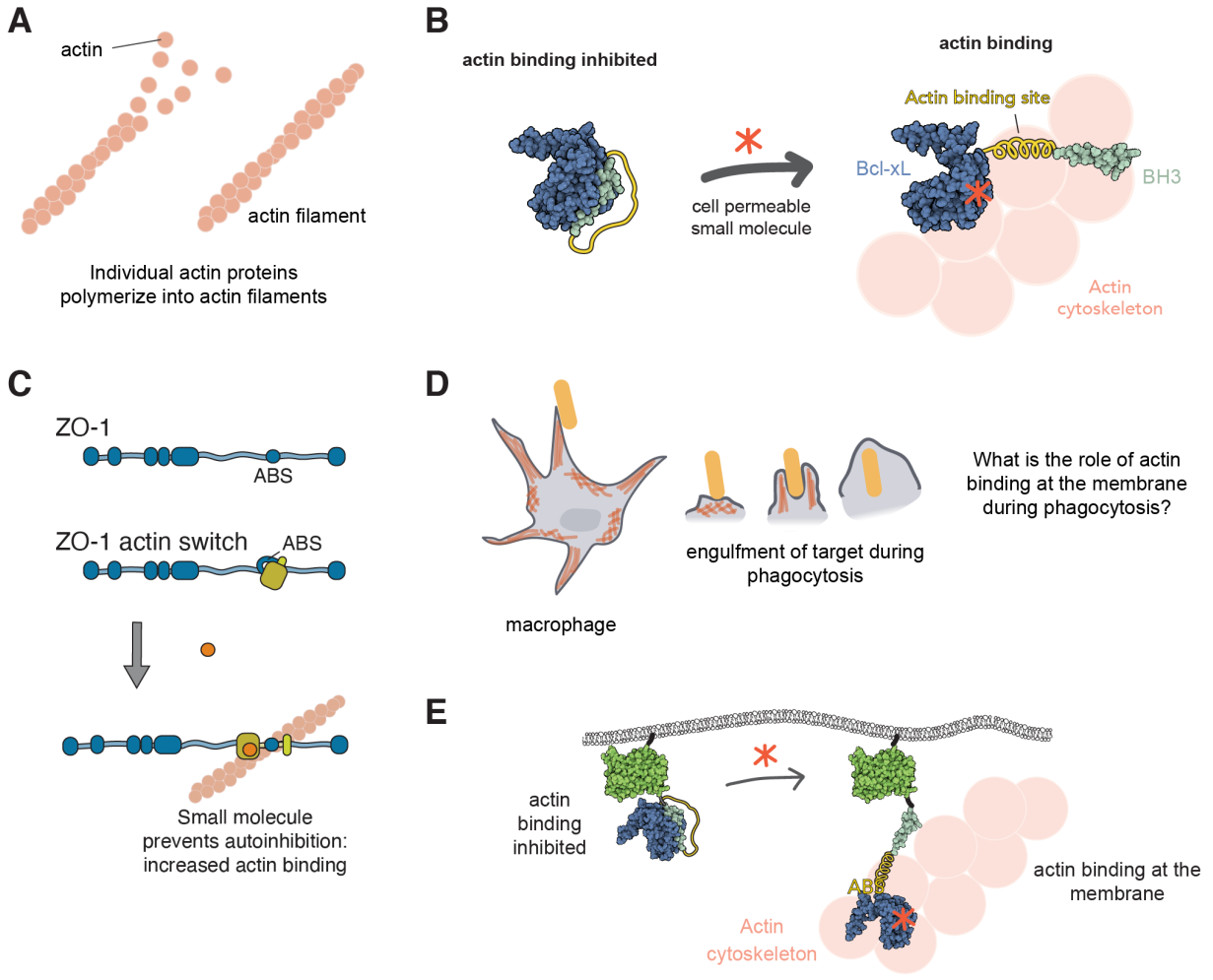

Figure 3 Development of a switchable actin binder to study actin binding at the tight junction and during macrophage phagocytosis.

A) Actin proteins polymerize into actin filaments.
B) We developed a switchable actin binder that allows us to control when, where, and how much a protein binds to actin.
C) We put the switchable actin binder into ZO-1 to control actin binding at the tight junction.
D) Macrophages are an immune cell that eat targets through a process called phagocytosis. Actin is known to be involved in many stages of phagocytosis.
E) We engineered the switchable actin binder to be in the cell membrane to study the role of actin binding at the membrane during phagocytosis.

Controlling actin binding at the tight junction

The first protein we added the switchable actin binder to was, you guessed it, ZO-1(Figure 3C). We found that incorporating the switchable actin binder into ZO-1, but not opening it up, reduced barrier function compared to ZO-1 with a normal actin binding site. This suggests we successfully blocked actin binding in ZO-1. When we added the small molecule to open up the switch in ZO-1 we restored barrier function to wildtype levels on the timescale of hours, with the caveat that the small molecule reduced barrier function in wildtype cells. The switchable actin binder allowed us to examine changing the strength of actin binding in live cells, and our results suggest that actin binding can alter barrier function relatively quickly, in just a few hours.

Controlling actin binding during macrophage phagocytosis

We next turned our attention to immune cells that eat bacteria, pathogens, and cells in our body. Macrophages (Greek for big eaters) are the immune cells that are responsible for engulfing and killing (eating) targets through a process called phagocytosis (Greek for eating cells)[44,45,52]. We know that actin is involved in many stages of phagocytosis and we wanted to know the role of actin binding to the membrane of cells on macrophage eating (Figure 3D). To study phagocytosis we engineered the switchable actin binder to be in the membrane (Figure 3E). We found that actin binding at the membrane decreased how many targets macrophages ate, but why?

Macrophages have these long, finger-like protrusions that wave around to find things to eat[53,54]. We found that the protrusions moved less when there was actin binding at the membrane. This implies that the macrophages explore a smaller area when there is actin binding at the membrane and find fewer things to eat. In addition to less macrophage movement, we wondered whether other stages of phagocytosis were influenced my actin binding to the membrane.

Macrophages decide whether or not to eat something based on whether receptors on the macrophage detect eat-me proteins on the target. In order to eat something, those receptors have to bind to eat-me proteins and cluster them together to activate the signaling pathways for phagocytosis[44,55-58]. If the macrophage protrusions come in contact with a pathogen, the receptors have to bind then move in the membrane to cluster together to signal that it's time to eat the pathogen. One theory is that if there is a lot of actin bound to the membrane, the receptors will keep bumping into the actin and not be able to cluster as quickly[59]. We hypothesized that if we bound actin to the membrane the macrophage receptors would cluster more slowly. Sure enough, our preliminary results suggest that this is the case. We found that while clustering could occur when actin was tethered to the membrane, it took longer. There is still more work to do to suss out how exactly receptor clustering is slowed down and how actin at the membrane might affect other stages of phagocytosis.

Overall, we developed a tunable, inducible, and movable actin binder that allows us to control when, where, and how much actin is bound in live cells and used this tool to study actin binding at tight junctions and during macrophage phagocytosis.

The whole kit and caboodle

My research led me through a winding road to learn about cell-cell barriers, how viruses break down cell-cell barriers, and how to control actin binding in cells. In Chapter 2, I will discuss my research into the molecular building blocks of cell-cell barriers and specifically into the role of actin binding at the tight junction. In Chapter 3, I turn my attention to how influenza and COVID-19 might break down cell-cell barriers. Lastly, in Chapter 4, I share my work developing a switchable actin binder which I used to control actin binding at cell-cell junctions and actin binding to the membrane during immune cell phagocytosis.

References

1. Sawada, N. Tight junction-related human diseases. *Pathol Int* **63**, 1–12 (2013).

2. Liang, G. H. & Weber, C. R. Molecular aspects of tight junction barrier function. *Curr Opin Pharmacol* **19**, 84–89 (2014).

3. Morita, K. & Miyachi, Y. Tight junctions in the skin. *J Dermatol Sci* **31**, 81–89 (2003).

4. Yokouchi, M. & Kubo, A. Maintenance of tight junction barrier integrity in cell turnover and skin diseases. *Exp Dermatol* **27**, 876–883 (2018).

5. Kirschner, N. & Brandner, J. M. Barriers and more: functions of tight junction proteins in the skin. *Ann Ny Acad Sci* **1257**, 158–166 (2012).

6. Hirase1, T. *et al.* Occludin as a possible determinant of tight junction permeability in endothelial cells. *Journal of Cell Science* (1997).

7. Morita, K., Sasaki, H., Furuse, M. & Tsukita, S. Endothelial Claudin: Claudin-5/TMVCF Constitutes Tight Junction Strands in Endothelial Cells. *The Journal of Cell Biology* (1999).

8. Kniesel, U. & Wolburg, H. Tight Junctions of the Blood–Brain Barrier. *Cell Mol Neurobiol* **20**, 57–76 (2000).

9. Buckley, A. & Turner, J. R. Cell Biology of Tight Junction Barrier Regulation and Mucosal Disease. *Csh Perspect Biol* **10**, a029314 (2018).

10. Itallie, C. M. V. & Anderson, J. M. Claudin interactions in and out of the tight junction. *Tissue Barriers* **1**, e25247 (2013).

11. Otani, T. & Furuse, M. Tight Junction Structure and Function Revisited. *Trends Cell Biol* **30**, 805–817 (2020).

12. Itallie, C. M. V. & Anderson, J. M. The Molecular Physiology of Tight Junction Pores. *Physiology* **19**, 331–338 (2004).

13. Zihni, C., Mills, C., Matter, K. & Balda, M. S. Tight junctions: from simple barriers to multifunctional molecular gates. *Nat Rev Mol Cell Bio* **17**, 564–580 (2016).

14. Stevenson, B. R., Siliciano, J. D., Mooseker, M. S. & Goodenough, D. A. Identification of ZO-I: A High Molecular Weight Polypeptide Associated with the Tight Junction (Zonula Occludens) in a Variety of Epithelia. *The Journal of Cell Biology* (1986).

15. Fanning, A. S., Jameson, B. J., Jesaitis, L. A. & Anderson, J. M. The Tight Junction Protein ZO-1 Establishes a Link between the Transmembrane Protein Occludin and the Actin Cytoskeleton. *THE JOURNAL OF BIOLOGICAL CHEMISTRY* (1998).

16. Haskins, J., Gu, L., Wittchen, E. S., Hibbard, J. & Stevenson, B. R. ZO-3, a Novel Member of the MAGUK Protein Family Found at the Tight Junction, Interacts with ZO-1 and Occludin. *J Cell Biology* **141**, 199–208 (1998).

17. Umeda, K. *et al.* ZO-1 and ZO-2 Independently Determine Where Claudins Are Polymerized in Tight-Junction Strand Formation. *Cell* **126**, 741–754 (2006).

18. Rottner, K., Faix, J., Bogdan, S., Linder, S. & Kerkhoff, E. Actin assembly mechanisms at a glance. *J Cell Sci* **130**, 3427–3435 (2017).

19. Inagaki, N. & Katsuno, H. Actin Waves: Origin of Cell Polarization and Migration? *Trends Cell Biol* **27**, 515–526 (2017).

20. Raftopoulou, M. & Hall, A. Cell migration: Rho GTPases lead the way. *Dev Biol* **265**, 23–32 (2004).

21. Hartsock, A. & Nelson, W. J. Adherens and tight junctions: Structure, function and connections to the actin cytoskeleton. *Biochimica Et Biophysica Acta Bba - Biomembr* **1778**, 660–669 (2008).

22. Coles, C. H. & Bradke, F. Coordinating Neuronal Actin–Microtubule Dynamics. *Curr Biol* **25**, R677–R691 (2015).

23. Myers, K. R. & Casanova, J. E. Regulation of actin cytoskeleton dynamics by Arf-family GTPases. *Trends Cell Biol* **18**, 184–192 (2008).

24. Maiers, J. L., Peng, X., Fanning, A. S. & DeMali, K. A. ZO-1 recruitment to α-catenin – a novel mechanism for coupling the assembly of tight junctions to adherens junctions. *J Cell Sci* **126**, 3904–3915 (2013).

25. Madara, J. L., Barenberg, D. & Carlson, S. Effects of Cytochalasin D on Occluding Junctions of Intestinal Absorptive Cells: Further Evidence That the Cytoskeleton May Influence Paracellular Permeability and Junctional Charge Selectivity. *The Journal of Cell Biology* (1986).

26. Matthews, J. B., Tally, K. J., Smith, J. A. & Awtrey, C. S. F-Actin Differentially Alters Epithelial Transport and Barrier Function. *J Surg Res* **56**, 505–509 (1994).

27. Itallie, C. M. V., Tietgens, A. J. & Anderson, J. M. Visualizing the dynamic coupling of claudin strands to the actin cytoskeleton through ZO-1. *Mol Biol Cell* **28**, 524–534 (2017).

28. Jinek, M. *et al.* A Programmable Dual-RNA–Guided DNA Endonuclease in Adaptive Bacterial Immunity. *Science* **337**, 816–821 (2012).

29. Javier, R. T. & Rice, A. P. Emerging Theme: Cellular PDZ Proteins as Common Targets of Pathogenic Viruses. *J Virol* **85**, 11544–11556 (2011).

30. Petersen, E. *et al.* Comparing SARS-CoV-2 with SARS-CoV and influenza pandemics. *Lancet Infect Dis* **20**, e238–e244 (2020).

31. Schaefer, I.-M. *et al.* In situ detection of SARS-CoV-2 in lungs and airways of patients with COVID-19. *Modern Pathol* 1–11 (2020) doi:10.1038/s41379-020-0595-z.

32. Bar-On, Y. M., Flamholz, A., Phillips, R. & Milo, R. SARS-CoV-2 (COVID-19) by the numbers. *Elife* **9**, e57309 (2020).

33. Hale, B. G., Randall, R. E., Ortín, J. & Jackson, D. The multifunctional NS1 protein of influenza A viruses. *J Gen Virol* **89**, 2359–2376 (2008).

34. Yu, J. *et al.* PDlim2 Selectively Interacts with the PDZ Binding Motif of Highly Pathogenic Avian H5N1 Influenza A Virus NS1. *Plos One* **6**, e19511 (2011).

35. Kumar, M., Liu, H. & Rice, A. P. Regulation of Interferon-β by MAGI-1 and Its Interaction with Influenza A Virus NS1 Protein with ESEV PBM. *Plos One* **7**, e41251 (2012).

36. Golebiewski, L., Liu, H., Javier, R. T. & Rice, A. P. The Avian Influenza Virus NS1 ESEV PDZ Binding Motif Associates with Dlg1 and Scribble To Disrupt Cellular Tight Junctions §. *J Virol* **85**, 10639–10648 (2011).

37. Liu, H. *et al.* The ESEV PDZ-Binding Motif of the Avian Influenza A Virus NS1 Protein Protects Infected Cells from Apoptosis by Directly Targeting Scribble ▿ . *J Virol* **84**, 11164–11174 (2010).

38. DeDiego, M. L. *et al.* Coronavirus virulence genes with main focus on SARS-CoV envelope gene. *Virus Res* **194**, 124–137 (2014).

39. Jimenez-Guardeño, J. M. *et al.* The PDZ-Binding Motif of Severe Acute Respiratory Syndrome Coronavirus Envelope Protein Is a Determinant of Viral Pathogenesis. *Plos Pathog* **10**, e1004320 (2014).

40. DeDiego, M. L. *et al.* Inhibition of NF-κB-Mediated Inflammation in Severe Acute Respiratory Syndrome Coronavirus-Infected Mice Increases Survival. *J Virol* **88**, 913–924 (2014).

41. Squire, J. Special Issue: The Actin-Myosin Interaction in Muscle: Background and Overview. *Int J Mol Sci* **20**, 5715 (2019).

42. Belardi, B. *et al.* A Weak Link with Actin Organizes Tight Junctions to Control Epithelial Permeability. *Dev Cell* (2020) doi:10.1016/j.devcel.2020.07.022.

43. Schaks, M., Giannone, G. & Rottner, K. Actin dynamics in cell migration. *Essays Biochem* **63**, 483–495 (2019).

44. Botelho, R. J. & Grinstein, S. Phagocytosis. *Curr Biol* **21**, R533–R538 (2011).

45. Flannagan, R. S., Jaumouillé, V. & Grinstein, S. The Cell Biology of Phagocytosis. *Annu Rev Pathology Mech Dis* **7**, 61–98 (2012).

46. Pelaseyed, T. *et al.* Ezrin activation by LOK phosphorylation involves a PIP2-dependent wedge mechanism. *Elife* **6**, e22759 (2017).

47. Atherton, P., Stutchbury, B., Jethwa, D. & Ballestrem, C. Mechanosensitive components of integrin adhesions: Role of vinculin. *Exp Cell Res* **343**, 21–27 (2016).

48. Oberstein, A., Jeffrey, P. D. & Shi, Y. Crystal Structure of the Bcl-XL-Beclin 1 Peptide Complex BECLIN 1 IS A NOVEL BH3-ONLY PROTEIN. *J Biol Chem* **282**, 13123–13132 (2007).

49. Maiuri, M. C. *et al.* Functional and physical interaction between Bcl-XL and a BH3-like domain in Beclin-1. *Embo J* **26**, 2527–2539 (2007).

50. Campbell, S. T., Carlson, K. J., Buchholz, C. J., Helmers, M. R. & Ghosh, I. Mapping the BH3 Binding Interface of Bcl-x L , Bcl-2, and Mcl-1 Using Split-Luciferase Reassembly. *Biochemistry-us* **54**, 2632–2643 (2015).

51. Shoemaker, A. R. *et al.* A Small-Molecule Inhibitor of Bcl-XL Potentiates the Activity of Cytotoxic Drugs In vitro and In vivo. *Cancer Res* **66**, 8731–8739 (2006).

52. Gordon, S. The macrophage: Past, present and future. *Eur J Immunol* **37**, S9–S17 (2007).

53. Flannagan, R. S., Harrison, R. E., Yip, C. M., Jaqaman, K. & Grinstein, S. Dynamic macrophage "probing" is required for the efficient capture of phagocytic targets. *J Cell Biology* **191**, 1205–1218 (2010).

54. Labernadie, A. *et al.* Protrusion force microscopy reveals oscillatory force generation and mechanosensing activity of human macrophage podosomes. *Nat Commun* **5**, 5343 (2014).

55. Joffe, A. M., Bakalar, M. H. & Fletcher, D. A. Macrophage phagocytosis assay with reconstituted target particles. *Nat Protoc* **15**, 2230–2246 (2020).

56. Aderem, A. & Underhill, D. M. MECHANISMS OF PHAGOCYTOSIS IN MACROPHAGES. *Annu Rev Immunol* **17**, 593–623 (1999).

57. Aderem, A. Phagocytosis and the Inflammatory Response. *J Infect Dis* **187**, S340-5 (2003).

58. Bakalar, M. H. *et al.* Size-Dependent Segregation Controls Macrophage Phagocytosis of Antibody-Opsonized Targets. *Cell* **174**, 131-142.e13 (2018).

59. Mylvaganam, S. M., Grinstein, S. & Freeman, S. A. Picket-fences in the plasma membrane: functions in immune cells and phagocytosis. *Semin Immunopathol* **40**, 605–615 (2018).

Chapter 2 – A weak link with actin organizes tight junctions to control epithelial permeability

Brian Belardi*, Tiama Hamkins-Indik*, Andrew R. Harris, Jeongmin Kim, Ke Xu, Daniel A. Fletcher
*co-first author

As published in *Developmental Cell*, September 2020.

Abstract

In vertebrates, epithelial permeability is regulated by the tight junction (TJ) formed by specialized adhesive membrane proteins, adaptor proteins, and the actin cytoskeleton. Despite the TJ's critical physiological role, a molecular-level understanding of how TJ assembly sets the permeability of epithelial tissue is lacking. Here, we identify a 28-amino acid sequence in the TJ adaptor protein ZO-1 that is responsible for actin binding and show that this interaction is essential for TJ permeability. In contrast to the strong interactions at the adherens junction, we find that the affinity between ZO-1 and actin is surprisingly weak, and we propose a model based on kinetic trapping to explain how affinity could affect TJ assembly. Finally, by tuning the affinity of ZO-1 to actin, we demonstrate that epithelial monolayers can be engineered with a spectrum of permeabilities, which points to a new target for treating transport disorders and improving drug delivery.

Introduction

In epithelial cells, the actin cytoskeleton plays numerous roles, ranging from structural to mechanical in nature. At the apical surface, cells make use of actin to assemble microvilli (Crawley et al., 2014), structures that increase the surface area of the membrane and expand the absorption potential of organs like the small intestine. On the basal side of polarized epithelia, focal adhesions rely on actin to orient and transmit forces between cells and extracellular matrix (Carragher and Frame, 2004). Actin filaments are also found at lateral contacts between epithelial cells, where they gird the cell in a belt-like arrangement (Miyoshi and Takai, 2008) and co-localize with two lateral junctions: the tight junction (TJ) and the adherens junction (AJ) (Fig. 1A).

The apical-most junction in vertebrate epithelia is the TJ, which is responsible for forming the vital barrier against paracellular flux, including at the blood-brain barrier and at the intestinal lining of the gut (Zihni et al., 2016). This is accomplished by selective pores generated by a class of adhesive membrane proteins known as the claudins (Furuse et al., 1998). In *trans*, claudins form extracellular channels between adjacent cells (Günzel and Yu, 2013; Suzuki et al., 2014), while in *cis*, claudins are thought to oligomerize to form polymeric strands within the same membrane

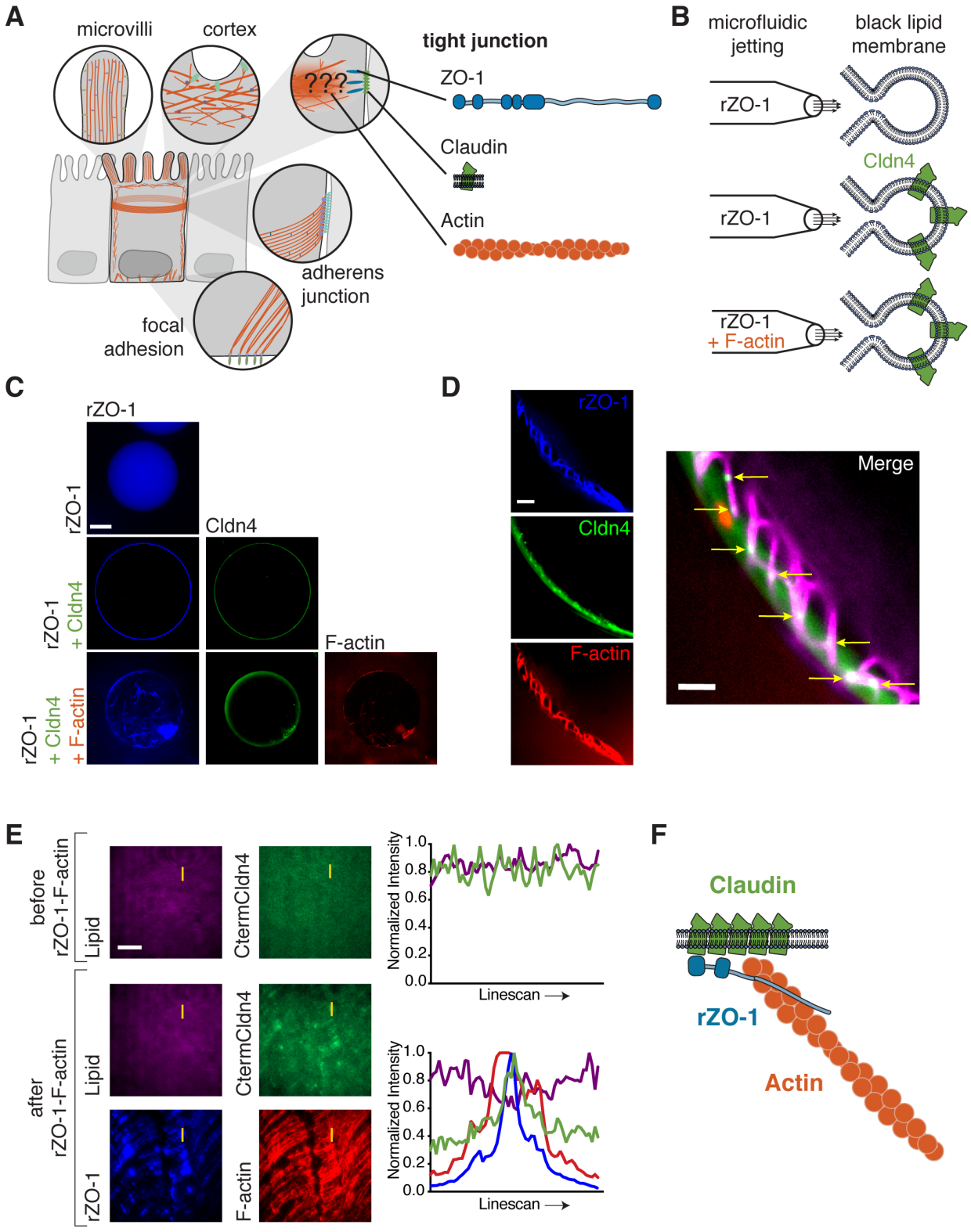

Figure 1. ZO-1 simultaneously engages actin and transmembrane claudins in vitro.

(A) Schematic of actin structures in polarized epithelial cells. The role of actin at TJs is still unresolved. Depicted are three TJ components that lie in and near the membrane: the plaque protein, ZO-1, which possesses binding motifs for claudins and F-actin; transmembrane claudins; and filamentous actin.

(B) GUVs were jetted with either rZO-1 (top), rZO-1 and Cldn4 (middle), or rZO-1, Cldn4, and F-actin (bottom).
(C) Fluorescent micrographs of jetted GUVs under the three conditions outlined in (B). Scale bar, 50 μm.
(D) Fluorescent micrographs of jetted GUVs containing rZO-1, Cldn4 and F-actin. Scale bar, 2.5 μm. The yellow arrows (right) indicate positions of enrichment of Cldn4 by ZO-1-F-actin meshes.
(E) Fluorescent micrographs of CtermCldn4 peptide tethered to DOPC-based supported lipids bilayers in the presence or absence of ZO-1-F-actin complexes and line scan (yellow line). Scale bar, 20 μm.
(F) rZO-1 directly links the actin cytoskeleton with claudin in vitro.
See also Figure S2.

(Gong et al., 2015; Irudayanathan et al., 2018; Koval, 2013; Piontek et al., 2007, 2011; Rossa et al., 2014; Sasaki et al., 2003; Zhao et al., 2018). In addition to the claudins, an abundant set of proteins including other membrane proteins, adaptors and actin have also been found to localize to the TJ in experiments based on fractionation, yeast two-hybrid screens, and proteomics (Mattagajasingh et al., 2000; Pulimeno et al., 2011; Van Itallie et al., 2013; Vogelmann and Nelson, 2005). Despite the extensive list of TJ-associated proteins, a mechanistic understanding of how key components assemble and interact with actin to establish a robust, yet malleable, paracellular barrier remains unresolved.

In contrast to TJs, a mechanistic understanding of actin's role within the AJ, which neighbors the TJ, has emerged over the last two decades. Bundles of actin filaments stabilize the AJ and lend integrity to epithelial sheets (Yonemura, 2011). At the molecular level, actin is connected to the membrane at the AJ indirectly through a protein hierarchy that extends perpendicular to the lipid bilayer, beginning with membrane proteins, which are linked to cytoplasmic adaptors that are coupled to cytoskeletal proteins (Bertocchi et al., 2017). One critical complex that spans this space is that between the adhesive transmembrane protein E-cadherin, the cytoplasmic adaptors α- and β-catenin, and filamentous actin (F-actin) (Yamada et al., 2005). Early work on α-catenin pointed to the necessity of actin association, as its actin-binding domain (ABD) was required for maintaining durable contacts between cells (Nagafuchi et al., 1994). More recently, work from several groups has shown that the interaction between α-catenin and F-actin is of high affinity (K_D ~ 400 nM) (Hansen et al., 2013) and is, notably, catch-bond-dependent (maximal lifetime at ~8 pN of force) (Buckley et al., 2014). These experiments point to a tensile model of AJ assembly, where forces due to formin-directed actomyosin contractility (Acharya et al., 2017; Kobielak et al., 2004) and *trans* interactions across cells lead to strong association between the catenin complex and actin, thereby stabilizing the AJ and integrating the cortices of individual cells into a resilient mechanical continuum.

TJs are often compared to AJs because of their biochemical similarities (Hartsock and Nelson, 2008). Akin to E-cadherin, transmembrane claudin proteins have a cytoplasmic binding sequence, a PDZ-binding sequence at the C-termini, which links TJ membrane proteins to cytoplasmic adaptors that in turn bind to F-actin. The main adaptors at the TJ are the PDZ-domain-containing proteins ZO-1 and ZO-2, which are large, multi-domain proteins that possess actin-binding activity through an unidentified motif in their long, C-terminal disordered regions (Fanning et al., 2002).

Despite mirroring molecular hierarchies, however, there are hints of significant differences between actin's function at AJs and TJs. For instance, parallel bundles of actin filaments that are part of the AJs are absent from TJs (Hull and Staehelin, 1979). Similarly, actin-based contractility does not appear to play the same role at the two junctions. Inhibition of actomyosin contractility disrupts the AJ, significantly reducing the area of E-cadherin-based junctions (Liu et al., 2010) and the overall tissue stiffness of epithelial monolayers (Harris et al., 2014). Conversely, we and others have found that inhibiting actomyosin contractility, either by treatment with blebbistatin or with MLCK and ROCK inhibitors, improves the ion barrier function of the TJ (Fig. S1) (Graham et al., 2019; Spadaro et al., 2017; Van Itallie et al., 2009; Yu et al., 2010). These experiments point to a fundamentally different role for actin at the TJ than for the neighboring AJ.

Here we describe how ZO-1 weakly couples the actin cytoskeleton to adhesive membrane proteins at the TJ to control the permeability of epithelial monolayers. This coupling is directed by a small, 28-amino acid actin-binding site (ABS) embedded in the middle of ZO-1's C-terminal disordered region. We find that ZO-1's ABS peptide, which represents a new actin-binding motif, is critical for TJ barrier function in epithelial cells. In contrast to the AJ, we show that low affinity association between ZO-1 and the actin cytoskeleton is critical for assembling TJs with robust barrier function, and we propose a kinetic trap model to explain the different role the actin cytoskeleton plays at TJs compared to AJs. By modulating the affinity of ZO-1 to F-actin, we were able to generate a series of epithelial cell lines with both increased and decreased permeabilities. Our data suggest that ZO-1's interaction with actin could be a new therapeutic target for efforts to address both delivering drugs past the blood-brain barrier (BBB) and for treating transport disorders, such as inflammatory bowel disease.

Results

Reconstitution of ZO-1 with claudin and F-actin forms co-localized structures in vitro

Previous work has found that three TJ proteins – membrane claudins, the ZO adaptor proteins and filamentous actin (F-actin) – interact and are indispensable for barrier function (Fanning et al., 1998; Itoh et al., 1999) (Fig. 1A). First, we sought to verify the binding of these proteins in vitro and observe how they self-organize, similar to how in vitro binding assays of AJ proteins showed how the catenins bound to the C-terminus of E-cadherin and to F-actin (Drees et al., 2005). To visualize complex formation at a membrane surface, we relied on a method we previously developed to embed the four-pass transmembrane claudins into the lipid bilayers of giant unilamellar vesicles (GUVs) (Belardi et al., 2019). This method is based on microfluidic jetting of black lipid membranes and gives rise to GUVs containing oriented claudin proteins, wherein claudin's C-terminal PDZ binding motif faces the lumen of vesicles. We took advantage of the microfluidic jetting procedure to load into the lumen of giant vesicles a recombinant, truncated form of ZO-1 that contains claudin- and F-actin-binding domains and regions (rZO-1, see Materials and Methods for details) (Fig. 1B). We found that rZO-1 localized exclusively to the

claudin-4 (Cldn4)-containing membrane, whereas in the absence of Cldn4, rZO-1 was strictly lumenal (Fig. 1C).

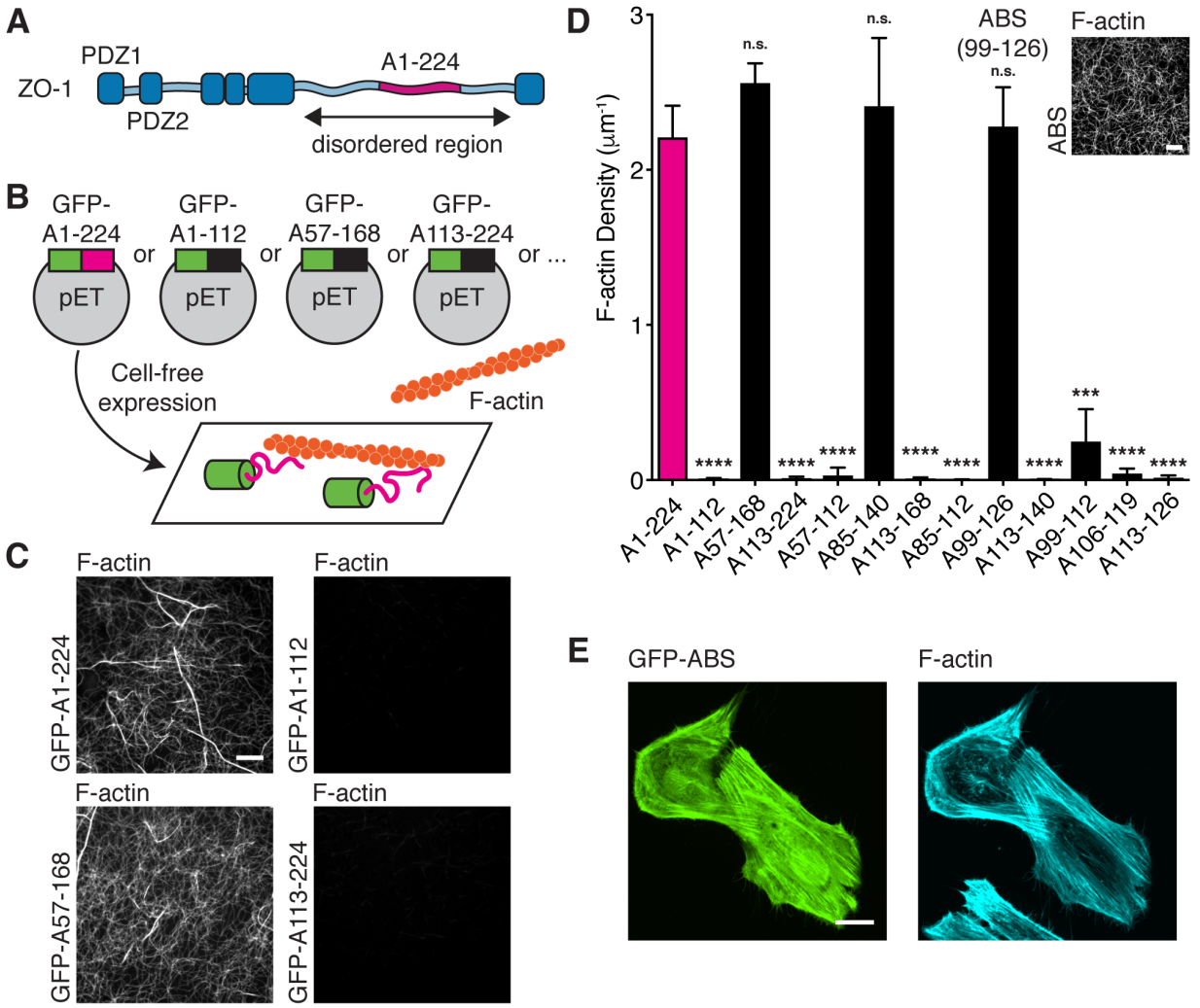

Figure 2. Identification of an ABS within ZO-1's C-terminal disordered region.

(A) Schematic of human ZO-1's primary sequence. A search for ZO-1's ABS was performed on a 224 amino acid portion (magenta) of ZO-1's long C-terminal disordered region.

(B) Schematic of cell-free, actin-binding assay. Segments of ZO-1 were fused to GFP and expressed using cell-free expression. F-actin binding was visualized using fluorescence microscopy.

(C) Fluorescent micrographs of F-actin binding assay after expressing different segments of ZO-1's disordered region. Scale bar, 10 μm.

(D) Quantification of F-actin density from cell-free actin-binding assay for various constructs encoding different portions of the disordered region. The magenta bar highlights the full 224 amino acid region. Bars represent mean ± SD, n=3, (p-values determined using a two-sample t-test with A1-224, *** $p<0.001$, **** $p<0.0001$, n.s. $p>0.05$). Inset: Fluorescent micrograph of F-actin binding assay after expressing ZO-1's ABS. Scale bar, 10 μm.

(E) Fluorescent micrographs of HeLa cells expressing GFP-ABS (left). Cells were fixed and stained for F-actin using AF647-phalloidin (right). Scale bar, 20 μm.

See also Figure S3.

Next, we loaded both rZO-1 and F-actin into the lumen of Cldn4-containing giant vesicles. In these vesicles, we observed that rZO-1 and F-actin formed an interconnected structure that appeared to template the enrichment of Cldn4 along the lipid bilayer at sites of co-localization with F-actin and rZO-1 (Fig. 1C and 1D). To further verify three-component complex formation, we turned to supported lipid bilayers (SLBs) and total internal reflection fluorescence (TIRF) microscopy. As a surrogate for full-length Cldn4, we

conjugated the C-terminal sequence of Cldn4, which contains the PDZ binding motif, to maleimide phospholipids in the SLB (Lin et al., 2014). After reaction, the Cldn4 peptide was imaged by TIRF and appeared homogenous on the membrane (Fig. 1E, top). To the Cldn4 peptide SLBs, we next added the rZO-1-F-actin mixture. Similar to the GUV results above, we observed a heterogeneous distribution after incubation (Fig. 1E, bottom), where enrichment of the Cldn4 peptide co-localized with rZO-1-F-actin meshes. We performed fluorescence recovery after photobleaching (FRAP) to determine if the mobility of the Cldn4 peptide was influenced by the presence of rZO-1 and F-actin, and we found that, indeed, its mobility was reduced and that the Cldn4 peptide's organization was templated by rZO-1-F-actin tracks (Fig. S2). Taken together, these results suggest that ZO-1 is capable of bridging F-actin and claudins simultaneously, forming co-localized structures (Fig. 1F).

ZO-1 binds to F-actin through a 28 amino acid motif within its C-terminal disordered region

How exactly human ZO-1 interacts with F-actin has remained unclear, beyond that it requires a segment in ZO-1's C-terminal disordered region (Fanning et al., 2002). So, we next turned our attention to identifying the specific site responsible for F-actin binding (Fig. 2A). To do this, we developed a simple, cell-free protein expression assay to rapidly screen sequences within ZO-1 for F-actin binding. In this assay, plasmids containing ZO-1 sequences are combined with bacterial cell extracts to initiate transcription and translation. These mixtures are then placed on a glass surface in order to immobilize expressed ZO-1 sequences. To this mixture, phalloidin-stabilized F-actin is added and fluorescence microscopy is used to visualize F-actin binding at the surface (Fig. 2B and 2C). We started with a segment of the C-terminal disordered region, known as the actin-binding region (ABR), to identify the critical residues for F-actin binding. A modified binary search was used, examining the N-terminal, C-terminal, or middle half of ZO-1 stretches. Doing so iteratively, we identified a 28-amino acid sequence within the ABR, which we refer to as the actin-binding site (ABS), that is the minimal sequence within ZO-1 capable of F-actin binding (Fig. 2D). In the context of ZO-1's primary sequence, the ABS resides in the central portion of the ABR of ZO-1 and, interestingly, has no homology to other actin-binding proteins in humans.

We performed an alanine scan of the ABS to identify amino acids that were indispensable for F-actin binding. Unsurprisingly, most of the 28 amino acids were important for F-actin binding, especially the positively-charged residues (Fig. S3A). However, two alanine mutant sequences, M1 and M6, had low and comparable binding of F-actin, respectively. To verify the binding

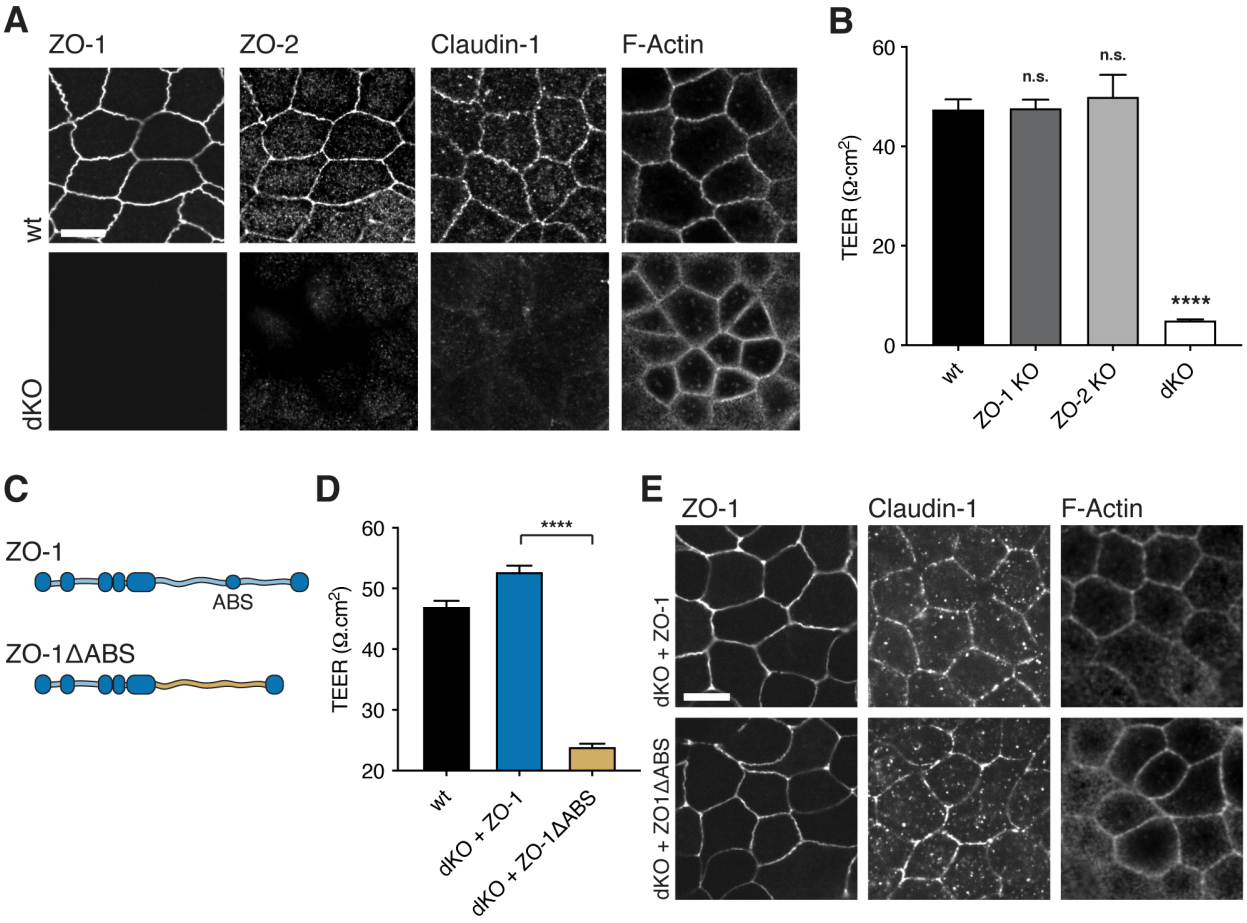

Figure 3. ZO-1's ABS is necessary for robust barrier function in dKO MDCK cells.

(A) Immunofluorescent micrographs of TJ proteins in wt and dKO cells. The images show lack of ZO-1 and ZO-2 in dKO cells. The localization of TJ proteins, e.g. Claudin-1 and F-actin, are altered in dKO cells. Scale bar, 10 μm.

(B) TEER measurements of wildtype (wt) MDCK II cells and of CRISPR/Cas9-generated ZO-1 and ZO-2 KO cells at day 4 of confluency. Bars represent mean ± SEM (p-values determined using a multi-comparison ANOVA between each of the means, **** $p<0.0001$, n.s. $p>0.05$). N values represent biological replicates, wt (N=6), ZO-1 KO (N=4), ZO-2 KO (N=3), dKO (N=7). Barrier function was abolished for cells lacking ZO-1 and ZO-2 (dKO).

(C) Schematic of ZO-1 constructs with and without ZO-1's ABS introduced into dKO cells.

(D) TEER measurements of wt and dKO cells expressing full-length ZO-1 and ZO-1ΔABS. Measurements are from day 4 of confluency. Bars represent mean ± SEM, n=4, (p-values determined using a two-sample t-test, **** $p<0.0001$).

(E) Immunofluorescent micrographs of ZO-1, Claudin-1, and F-actin in dKO cells expressing ZO-1 and ZO-1ΔABS. No difference in localization of TJ proteins was observed between the two cell lines. Scale bar, 10 μm.

See also Figure S4.

interaction in cells, we expressed a fluorescently-labeled minimal ABS (GFP-ABS) in HeLa cells, which provide distinct actin structures that can be used to characterize actin-binding domains (Harris et al., 2019). In this context, we found that the ABS decorated actin filaments in stress fiber structures as well as lamellipodia (Fig. 2E). To explore evolutionary conservation of the ABS, we aligned the site across ZO-1 homologs in various metazoans (Fig. S3B). We noted that vertebrates,

which all possess an apical tight junction, appeared to retain the site with a high degree of identity, whereas the ABS sequence is absent from aligned ABR regions in ZO-1 homologs in invertebrates, which lack apical tight junctions.

The 28-amino acid Actin Binding Site (ABS) of ZO-1 is required for barrier function

Our in vitro studies led us to ask whether ZO's ABS is necessary for physiological functions of the TJ, for instance the barrier function of epithelial cells. If so, then impaired barrier function should be observable after deletion of the ABS from ZO proteins. Using CRISPR/Cas9, we generated knock out cell lines of either ZO-1, ZO-2, or both ZO-1 and ZO-2 (dKO) in MDCK II cells, a cell line expressing the same claudin, Cldn4, used in the in vitro experiments (see Materials and Methods for details). By immunostaining, we

confirmed knockouts of the ZO proteins and found that proper localization of other TJ proteins, for example claudins, occludin, and cingulin, was disrupted in the dKO line but not in single KO cells (Fig. 3A and Fig. S4A and S4B) (Otani et al., 2019). We next measured barrier function of the different ZO knockouts by transepithelial electrical resistance (TEER) and a fluorescence Transwell apparent permeability assay. In both assays, we observed that barrier function was severely compromised in the dKO line but not in wildtype or in the single KO cells (Fig. 3B and Fig. S4E).

Next, we turned to the question of whether the 28-amino acid ABS contributed to ZO-1's ability to establish a paracellular barrier in epithelial cells. To test this, we first expressed full-length human ZO-1 in dKO cells. In this case, barrier function was fully restored upon ZO-1 expression (Fig. 3D). We then tested a ZO-1 construct that lacked the ABS (ΔABS) in the dKO. In the case of ΔABS, barrier function, as measured by both TEER and apparent permeability, was significantly impaired compared to the construct that possessed the native ABS (Fig. 3D and Fig. S4E). Both proteins appeared to traffic to the cell circumference normally by confocal microscopy, and immunostaining confirmed proper protein localization and density of other TJ proteins in both cell lines (Fig. 3E and Fig. S4D). Interestingly, actin localization to the cell circumference appeared unperturbed in the presence of ΔABS, suggesting other actin-binding partners that associate with ZO-1, such as Cingulin (D'Atri and Citi, 2001), may also be involved in recruiting actin to the TJ. These studies suggest that ZO-1 and F-actin, in concert, influence the establishment of an epithelial TJ with robust barrier function.

Replacing the ABS of ZO-1 with actin network regulators does not rescue barrier function

Having shown the importance of ZO-1's ABS on epithelial barrier function, we next asked what role the ABS might be playing in the organization of actin networks at the TJ. One possibility is that the ABS directly influences local actin network architecture at the TJ as has been shown for adaptor proteins at the AJ (Hansen et al., 2013). Several Rho family GTPases and their regulatory effectors, guanine nucleotide exchange factors (GEFs) and GTPase activating proteins (GAPs),

localize to the TJ, including Cdc42, RhoA (Quiros and Nusrat, 2014), p114RhoGEF (Terry et al., 2011), GEF H1 (Aijaz et al., 2005), Tuba (Otani et al., 2006), among others, suggesting that specific actin network architecture and dynamics are important for assembling TJs with robust barrier function.

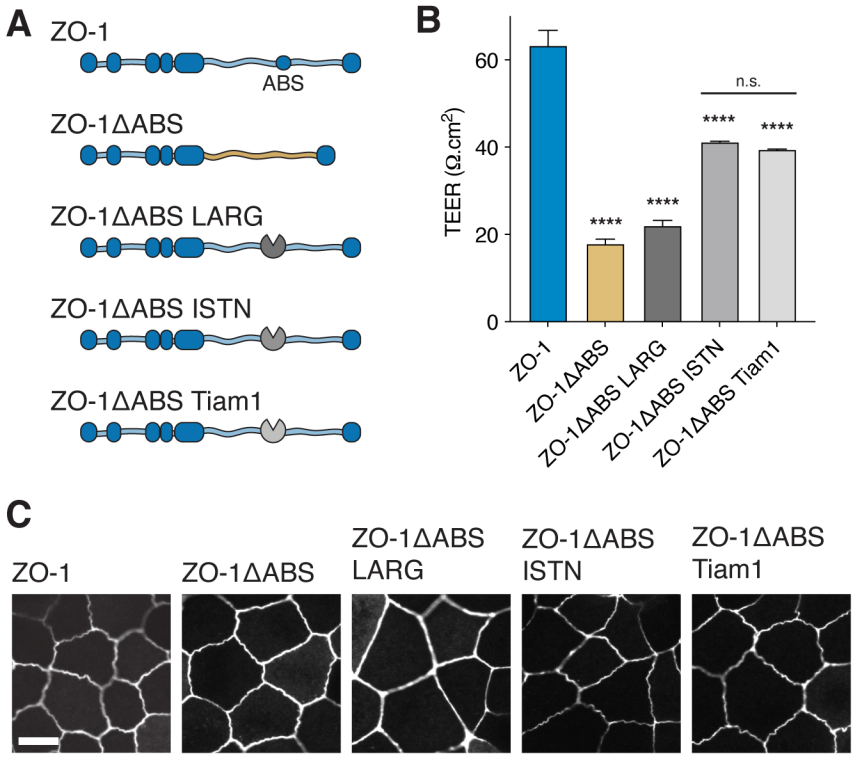

Figure 4. Engineering actin network structures at the TJ fails to restore barrier function of cells lacking ZO-1's ABS.

(A) Schematic of ZO-1 constructs introduced into dKO cells with the actin regulators, LARG, ISTN, and Tiam1, replacing the ABS.

(B) TEER measurements of dKO cells expressing ZO-1ΔABS GEF constructs. Measurements are from day 4 of confluency. Bars represent mean ± SEM, n=3, (p-values determined using a multiple comparison one-way ANOVA, p-values represent comparison with ZO-1, **** $p<0.0001$, n.s. $p>0.05$).

(C) Fluorescent micrographs of ZO-1ΔABS GEF constructs show localization to the TJ membrane. Scale bar, 10 μm.

To test whether the ABS might be partly responsible for actin organization at TJs, we replaced the ABS of ZO-1 with GEFs known to act on different Rho GTPases, which should alter local cytoskeletal architecture and dynamics (Fig. 4A). Specifically, we inserted the catalytic domains, DH or DH/PH domains, from three well-characterized GEFs – LARG, intersectin-1, and Tiam1 – into ZO-1. The GEF from LARG has previously been characterized to act on the GTPase RhoA and has been used ectopically to generate parallel actin bundles and contractility (Wagner and Glotzer, 2016), while the GEFs from intersectin-1 (ISTN) and Tiam1 act on Cdc42 and Rac1, respectively, which have also been used ectopically to engineer branched actin structures in cells (Beco et al., 2018; Zimmerman et al., 2017). By confocal microscopy, all three constructs localized

to the cell circumference in the dKO cell line (Fig. 4C). We observed slightly flatter TJs for the LARG construct, whereas both the ISTN and Tiam1 constructs generated TJs that were more tortuous than wildtype – consistent with the known activities of the three GEFs. We next used TEER to evaluate the effect of GEF insertion on barrier function. All three constructs failed to rescue barrier function in dKO cells compared to full-length ZO-1 (Fig. 4B), although each case achieved slightly elevated resistance values compared to the construct lacking an inserted GEF. Interestingly, both ISTN and Tiam1 constructs achieved higher TEER than the LARG construct, which might indicate a preference for branched actin structures at the TJ.

Barrier function is reduced when the ZO-1 ABS is replaced with a high-affinity actin-binding domain

Since insertion of the LARG, ISTN, and Tiam1 GEFs into ZO-1 lacked the ability to directly bind F-actin, we reasoned that the direct interface between ZO-1 and F-actin must be necessary for establishing a robust barrier in epithelial monolayers. If true, then replacing ZO-1's ABS with another actin-binding domain (ABD) should restore barrier function. To test this, we replaced ZO-1's ABS with an ABD from another junctional protein, α-catenin (Fig. 5A). As described above, α-catenin is part of the AJ and provides necessary contacts between the E-cadherin/catenin complex and F-actin. After confirming that the ZO-1 α -Catenin construct localized to the TJ (Fig. 5B), we measured TEER and apparent permeability to assay for barrier function. Interestingly, the construct did not rescue barrier function compared to full-length ZO-1 (Fig. 5C and Supplementary Fig. 6A), despite a slight improvement in resistance compared to the ZO-1 construct lacking ABS (□ABS). Although we did not observe any changes to the AJ of mature monolayers, it should be noted that the engineered ZO-1 containing α -Catenin's ABD may affect the nearby junction during the early stages of cell-cell adhesion.

The ABD from α -catenin is a 236-amino acid, five-helix bundle, which is a significant deviation in size and fold from ZO-1's ABS that could disrupt the ZO-1-F-actin interface. To address this concern, we replaced the ABS with an ABD of similar size, namely the short peptide Lifeact, which consists of 17 amino acids (Riedl et al., 2008). However, the ZO-1 Lifeact construct also failed to fully recover barrier function (Fig. 5C), although we noted an improvement in barrier function over the α -Catenin construct. Besides size and fold, another parameter that might have an effect on the proper assembly of TJ complexes is the affinity between binding partners.

Barrier function is rescued and can be enhanced when the ZO-1 ABS is replaced with low-affinity actin-binding domains

Both α -Catenin and Lifeact are examples of ABDs with high affinity (low K_D) toward F-actin. We measured the K_D for ZO-1's ABS and found that its affinity for F-actin was much weaker (~10 μM for both ABS and ABR, Fig. S5). To test whether weak association of ZO-1 with F-actin was an important feature of the TJ, we decided to replace the ABS with an ABD that has a weak affinity

for F-actin. Utrophin, a calponin homology (CH) domain-containing protein, has an ABD with a K_D of ~20 μM toward F-actin (Winder et al., 1995). After installing Utrophin's ABD in ZO-1 and measuring TEER and apparent permeability of an epithelial monolayer formed with the construct, we found that the ZO-1 containing the Utrophin ABD not only completely recovered barrier function compared to full-length ZO-1 but that the cell line expressing ZO-1 Utrophin led to enhanced barrier function in relation to wildtype ZO-1 (Fig. 5C and Fig. S6A). Other than modifying ZO-1's direct interaction with F-actin, one possible consequence of replacing ZO-1's ABS with other ABDs is that actin dynamics may be altered at the TJ, in turn augmenting barrier function. To examine this, we expressed mCherry-β-actin under a weak promoter in different ZO-1-expressing cell lines and used FRAP to assay for actin dynamics at the junction. We found no significant differences in junctional □-actin dynamics in these cell lines (Fig. S6B), further emphasizing that affinity between the ZO-1 constructs and F-actin, and not actin monomer turnover, is critical for affecting barrier function.

Next, we sought to evaluate how affinity differences between the ZO-1 constructs affected the constructs' spatial organization in epithelial monolayers. Each engineered form of ZO-1 localized to the cell circumference by confocal microscopy (Fig. 5B and 5H). However, confocal microscopy lacks the resolution necessary to image the spatial organization of ZO-1 within the dimensions of the tight junction. We, therefore, took advantage of a recent super-resolution 3D STORM microscopy technique (Kim et al., 2019), to image the ZO-1 constructs at sub-100 nm, 3-D resolution in epithelial monolayers (Fig. 5D-5F). Compared to wt ZO-1, we found that both ZO-1 lacking actin-binding, ΔABS, and ZO-1 α-Catenin had narrower height distributions (Fig. 5G). We also found that ZO-1 Utrophin, the construct with weak association to F-actin, possessed a wider height distribution relative to wt ZO-1 (Fig. 5G). We confirmed that ZO-1 distributions correlated with junctional length by transmission electron microscopy (TEM), e.g. narrower distributions resulted in shorter junctional lengths and wider distributions resulted in longer junctional lengths (Fig. S6C and S6D). Wider ZO-1 spatial distributions along the lateral membrane may provide more opportunities for claudin-claudin contacts across cells, therefore leading to the lower permeability of monolayers expressing wildtype ZO-1 or ZO-1 Utrophin.

Intrigued by this finding, we replaced the ABS of ZO-1 with an affinity series of other ABDs in order to better characterize the F-actin affinity-barrier function relationship for ZO-1. With this approach, we found that the relationship between ZO-1's affinity for F-actin and the ultimate permeability of the epithelial monolayer was defined by a bell-shaped curve, with a maximum at low affinity (~20 μM) and reduced barrier function at high and very low affinities (Fig. 5I and Table S2). In each case, proper localization of ZO-1 constructs was observed (Fig. 5H). Taken together, these studies show that the claudin-ZO-1-F-actin interface is necessary for achieving robust barrier function in epithelial monolayers. However, in contrast to the AJ where high affinity is important for junction integrity, these data demonstrate that a weak association between ZO-1 and F-actin is critical for assembling proper barrier function in epithelial cells. This insight enabled

us to engineer epithelial monolayers with either diminished or enhanced barrier function by modulating the affinity of ZO-1 for F-actin.

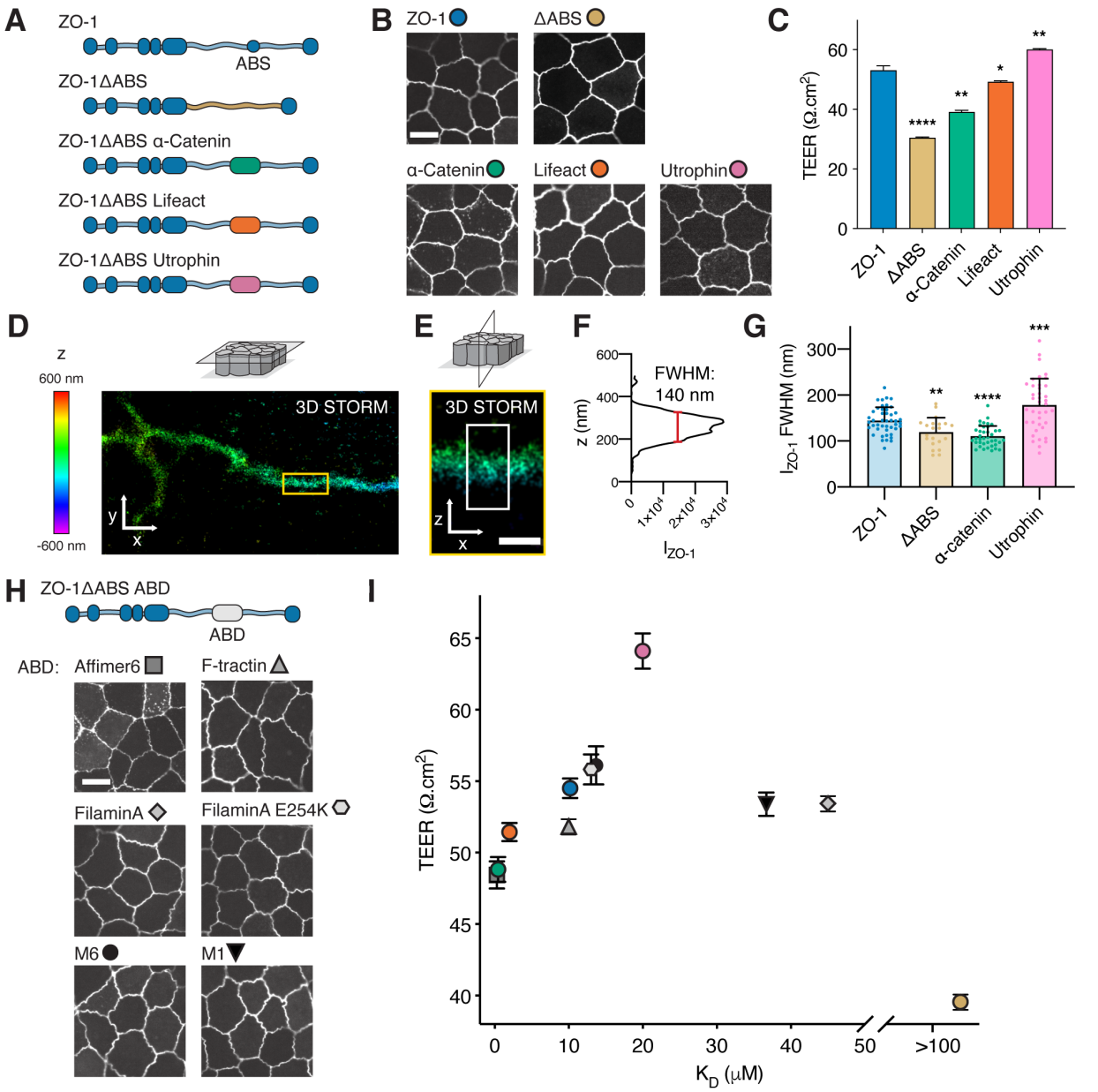

Figure 5. Weak association between ZO-1 and F-actin is required for robust epithelial barrier function.

(A) Schematic of ZO-1 constructs introduced into dKO cells with ectopic ABDs replacing the native ABS of ZO-1.

(B) Fluorescent micrographs of dKO cells from day 4 of confluency expressing ZO-1ΔABS with the ABDs from the AJ protein, α-Catenin, the short peptide, Lifeact, and the tandem calponin-homology domain protein, Utrophin. All constructs localized to the TJ. Scale bar, 10 μm.

(C) TEER measurements of dKO cells expressing ZO-1ΔABS with the ABDs from α-Catenin, Lifeact, and Utrophin. Measurements are from day 4 of confluency. Bars represent mean ± SEM, n=3, (p-values determined using a two-sample t-test for ZO-1 vs. ABD, * $p<0.05$, ** $p<0.01$, **** $p<0.0001$).

(D) Representative image of cell-cell junction using 3D STORM of dKO cells expressing ZO-1. Micrograph is a projection of anti-ZO-1 single molecules in the x-y plane color coded according to their z localization. Scale bar, 500 nm.
(E) Reconstructed micrograph of x-z projection of the yellow rectangle shown in (D). Scale bar, 250 nm.
(F) Fluorescence profile of ZO-1 (I_{zo1}) vs. z position after horizontal binning of the white box shown in (E). The full-width at half maximum (FWHM) was estimated from ZO-1's z distribution (red bar).
(G) Quantification of the I_{zo1}FWHM from super-resolution images of dKO cells expressing ZO-1 constructs with various ABDs. Bars represent mean ± SEM, (p-values determined using a two-sample t-test comparison with dKO + ZO-1, ** $p<0.01$, *** $p<0.001$, **** $p<0.0001$). Each symbol represents one cell-cell junction segment, ZO-1 (n=45), ΔABS (n=21), α-Catenin (n=39), Utrophin (n=39).
(H) Schematic of ZO-1 constructs introduced into dKO cells with ectopic ABDs replacing the native ABS of ZO-1 (top). Fluorescent micrographs of ZO-1ΔABS ABD constructs in dKO cells (bottom). All constructs localized to the TJ. Scale bar, 10 μm.
(I) TEER measurements of dKO cells expressing ZO-1ΔABS with ectopic ABDs replacing ZO-1's ABS plotted vs. the affinity of the ABD for F-actin (see Table S2). Measurements are from day 4 of confluency. Symbols represent mean ± SEM, n=3.
See also Figure S6.

Simulations show that low-affinity interactions between two polymers prevent kinetic trapping in misaligned configurations

How might weak association to F-actin be leveraged by TJs to assemble robust barrier function? One possibility might stem from a unique feature of claudins, which is their ability to form polymeric structures, or strands, in the plane of the membrane in cells (Gong et al., 2015; Irudayanathan et al., 2018; Koval, 2013; Piontek et al., 2007, 2011; Rossa et al., 2014; Sasaki et al., 2003; Zhao et al., 2018). These structures differ from transmembrane protein dimers or protein clusters in that each claudin monomer contains a front-to-back contact that repeats to generate a linear polymeric chain (Suzuki et al., 2014). Using structured illumination microscopy, recent work by van Itallie et al. noted a surprising arrangement of ectopically expressed claudin polymers in fibroblasts (Van Itallie et al., 2016). They found that in the presence of ZO-1, claudin polymers appeared to align with actin filaments, whereas in the absence of ZO-1, claudin polymers had no directional correlation with actin filaments. This observation led us to wonder whether the dynamics of aligning one polymer with another might be influenced by their interfacial affinity.

To examine this, we simulated fluctuating polymers (green) on a 2-D lattice, where static polymers (orange) were arranged in a grid pattern (Fig. 6A). Affinity between the two polymers was varied, and alignment of the two-polymer system was monitored over time. Figure 6B shows representative traces of alignment vs. time for a single fluctuating polymer with varying affinities. Under low affinity conditions, the fluctuating polymer reached a steady-state alignment in a short period of time (~100 τ where τ represents the time step) and oscillated around this alignment for the rest of the simulation. By contrast, under high affinity conditions, the fluctuating polymer remained in low alignment configurations for extended period of times (>10,000 τ) as the simulation evolved to higher alignments. We next compiled simulations from 100 different starting configurations. We found that increasing the affinity by an order of magnitude resulted in an average dwell time difference of over an order of magnitude (Fig. 6C), suggesting long periods of stalling for high affinity polymers before alignment is maximized. Figure 6D plots the normalized

average alignment at different numbers of time steps as a function of affinity. After 100 τ, the lowest affinity polymer had already reached ~97% of its equilibrium alignment, while the highest affinity had only reached ~65% of its steady-state alignment.

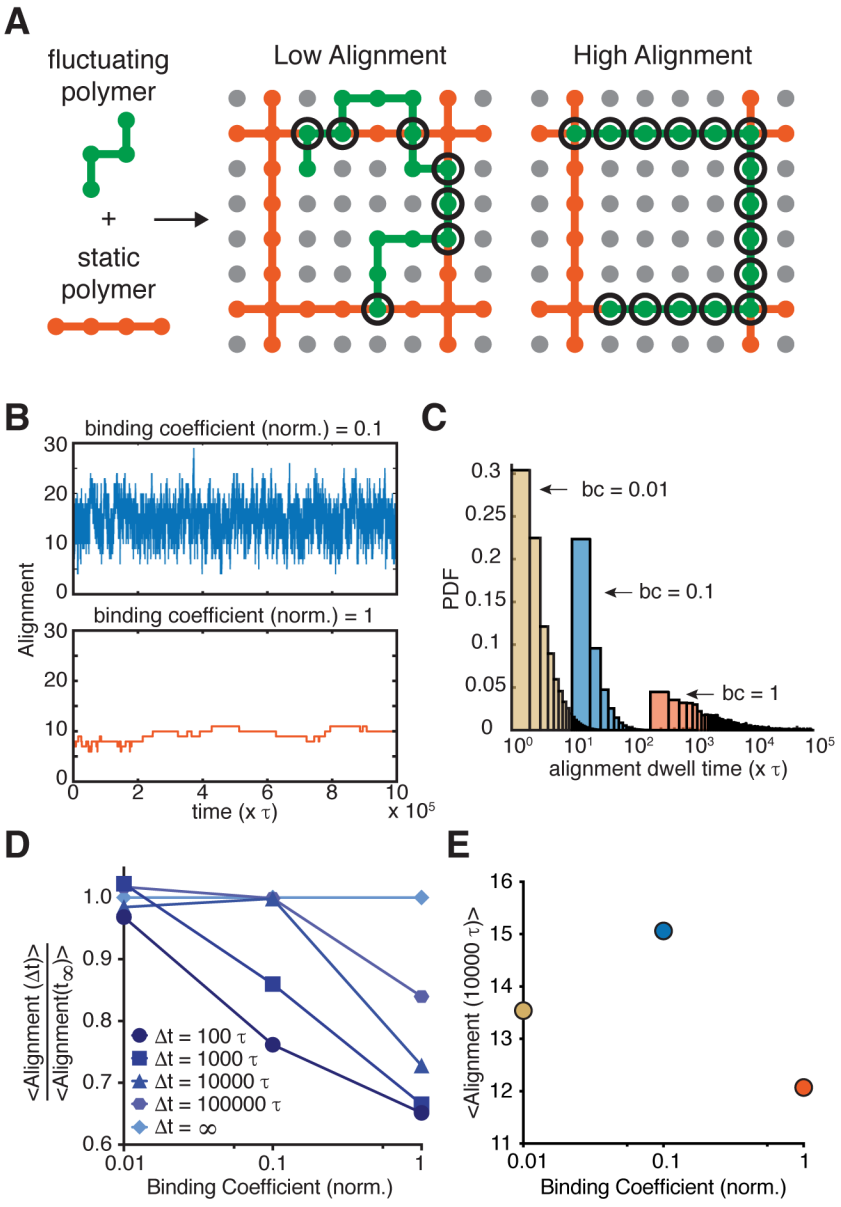

Figure 6. High affinity interaction between two polymeric species gives rise to kinetic traps.

(A) Schematic of lattice model indicating low and high alignment between a static polymer (orange) and a fluctuating polymer (green).

(B) Alignment traces of a single polymer fluctuating under two binding coefficients over time.

(C) Probability density function of alignment dwell times of fluctuating polymers under various binding coefficients (bc). Dwell time refers to the number of steps that polymers remain in individual alignment configurations.

(D) Normalized average alignments of fluctuating polymers under various binding coefficients at different time intervals. At short time intervals, fluctuating polymers with large binding coefficients are trapped at low

alignments, suggesting that a high affinity interaction to F-actin, a large persistence length polymer, at the TJ may kinetically trap claudins, a more flexible polymer, in unfavorable configurations.

(E) Average alignment of fluctuation polymers under various binding coefficients at 10,000 τ. At this time interval, kinetic trapping is convolved with the total number of contacts between the two polymers, resulting in a bell-shaped curve.

Collectively, these data point to a key feature of a two-polymer system – that the high affinity interaction of one polymer with another polymer will kinetically trap the system in sub-optimal configurations. Considering also that affinity affects the maximum level of alignment that can be achieved, Figure 6E presents non-normalized alignment after 10,000 τ showing that very low affinity, despite not being kinetically trapped, fails to reach high alignment, revealing a bell-shaped curve reminiscent of what we see experimentally. These results suggest that weak interactions between ZO-1 and F-actin may be critical for allowing the claudin polymer, which is much more flexible (Zhao et al., 2018) than F-actin (van Mameren et al., 2009), to achieve the alignment and organization necessary for achieving robust barrier function. Other factors, such as variations in fluctuating polymer length and flexibility, as well as differences in linear polymer density, geometry, and turnover, would be expected to alter the magnitude of alignment predicted by this model, providing the cell with additional ways to use kinetic trapping to tune TJ barrier function.

Discussion

The TJ and AJ are neighbors along the lateral surface of epithelial cells, and together have been hypothesized to work as a single sub-cellular structure called the apical junction complex (AJC) (Roignot et al., 2013). While a detailed understanding of TJ interactions with actin has remained incomplete, a picture of actin's function at the AJ has now come into focus (Bertocchi et al., 2017). Parallel actin bundles are present at the AJ (Hull and Staehelin, 1979), and actin-based contractility is critical for the strong lateral adhesions that maintain integrity across epithelial tissue (Harris et al., 2014).

Our work shows that the actin cytoskeleton functions fundamentally differently at the TJ. Disruption of actin-based contractility (Fig. S1) appears to be detrimental to the ion barrier properties of the TJ. More significantly, a weak, not strong, linkage between the actin cytoskeleton and claudins drives TJ organization and assembly – a stark contrast to the high-affinity F-actin association at AJs (Figure 7) (Hansen et al., 2013). This distinction extends to the molecular structures that interface with F-actin. We find that TJ assembly is directed by a small peptide embedded in the long, C-terminal disordered region of ZO-1, while the same interfaces at AJs are defined by an ABD with a five-helix fold. We also show that although actin association is critical at TJs, diminishes barrier function in epithelial monolayers. Taken together, our work suggests that the role for actin across epithelial junctions is not uniform.

How, then, might α-catenin's and other high-affinity actin-binding domains drive sub-optimal arrangement of TJs? Our Monte Carlo simulations provide one possible explanation. We found

that high affinity interactions between a two-polymer system leads to kinetic trapping, i.e. long-lived local minima rather than a global minimum along an energetic landscape. Kinetic traps in biology are not unprecedented. In fact, kinetic traps (in metastable states) have been directly observed in S-layer protein assembly (Shin et al., 2012) using atomic force microscopy and during the folding of proteins, including insulin (Hua et al., 1995). Thus, it's possible that the ZO-1 DABS α-Catenin ABD construct forms a kinetically trapped structure at the TJ. Our results suggest that the non-equilibrium dynamics of complex assembly, as opposed to equilibrium-based phenomena, might be critical for organizing the TJ, much as they have recently been shown to be important for carboxysome assembly (Rotskoff and Geissler, 2018). We imagine that TJs are also taking advantage of low-affinity interactions and dynamics to arrive at configurations that give rise to robust but malleable barrier function in epithelium.

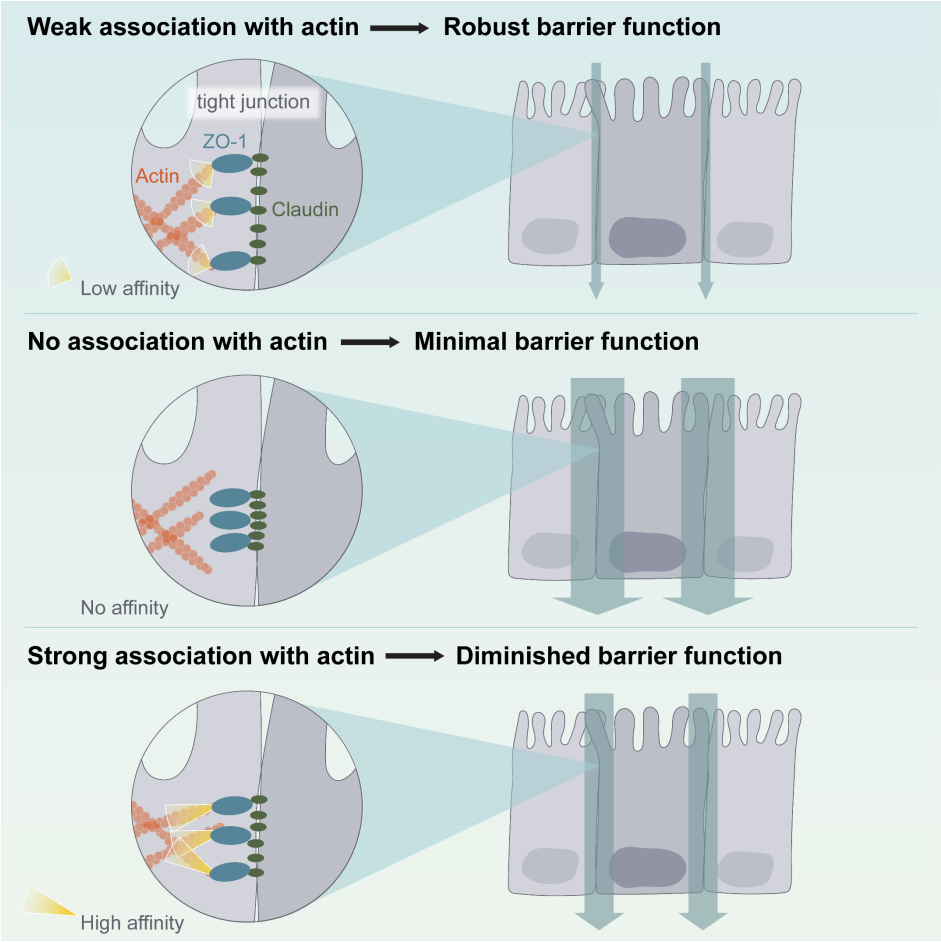

Figure 7. Summary schematic of findings

A different class of interaction, namely reversible, multivalent association, might also contribute to the dynamics at the TJ. Purified (Beutel et al., 2019) and non-junctional pools (Schwayer et al., 2019) of ZO-1 have recently been shown to exhibit phase separation behavior. Phase separated

systems are characterized by weak multivalent interactions that give rise to cellular biomolecular condensates with rapid internal exchange. Although the role of phase separation at mature TJs requires more work, multivalency with low-affinity interactions and rapid dynamics, a characteristic of membrane clusters as well as phase separated systems, may help the TJ to re-arrange readily and sample different configurations faster. Moreover, a multitude of ZO-1-ZO-1 associations would ensure continuous linkages between claudins and actin filaments as well as longevity, since displaced ZO-1 units would be replaced by other associated ZO-1 monomers. Dynamic interactions seem to play an outsized role in assembling a robust epithelial barrier, and, as such, we anticipate that low-affinity multivalency could also apply to other proteins at the TJ.

In conclusion, our findings suggest that a major function of F-actin in epithelial cells is to organize and stabilize claudin strands in the membrane through weak interactions with the adaptor protein ZO-1. In this capacity, F-actin at TJs acts not to apply strong forces to the junction, which is the case at AJs, but to template and align the transmembrane proteins responsible for forming intermolecular pores across epithelial cells. Our work also suggests that actin's templating role at the TJ could offer a new therapeutic target. We found that by modifying the affinity of ZO-1 to F-actin, the permeability of epithelial monolayers could be manipulated to exhibit either diminished or enhanced barrier function. The bioavailability of small molecule and protein therapeutics would benefit greatly from the ability to selectively modulate the paracellular flux between epithelial cells. By temporarily increasing the affinity of ZO-1 for F-actin or completely inhibiting F-actin association, drug delivery past epithelial monolayers, through the intestinal walls of the gut or through the BBB, could be improved. Moreover, patients with transport disorders characterized by leaky epithelium, for instance inflammatory bowel diseases, need treatments that specifically restore barrier function (Turner, 2009). This could also be accomplished by varying the affinity of ZO-1 to F-actin. One possible advantage of this strategy is that targeting the ZO-1-F-actin interface does not abolish barrier function. Consequently, a drug modulating ZO-1-F-actin association might lead to less toxicity and less side-effects than other general permeability enhancers, such as ultrasound treatment (Bors and Erdő, 2019) and sodium caprate administration (McCartney et al., 2016). Our work points to altering ZO-F-actin interactions as an exciting area of future investigation with the promise of fine-tuning barrier properties in the gut or at the BBB as a means therapeutic intervention.

Acknowledgements

We thank Sho Takatori and Jordi Silvestre-Ryan for advice and helpful discussions and Prof. Jianghui Hou and his laboratory (Washington University School of Medicine in St. Louis) for the generous gift of GFP-Cldn4. We thank Lienna Chan and Victoria Qian for their assistance with cell culture and experiment setup for revisions made to this manuscript. We also thank Eva Schmid for critical reading of the manuscript, and the staff, especially Danielle Jorgens and Reena Zalpuri, at the University of California, Berkeley Electron Microscope Laboratory for advice and assistance

in electron microscopy sample preparation and data collection. We acknowledge the assistance and support of the University of California, Berkeley Cell Culture Facility. Confocal laser scanning microscopy experiments were carried out at the CRL Molecular Imaging Center, supported by the Helen Wills Neuroscience Institute. We would like to thank Holly Aaron and Feather Ives for their microscopy training and assistance. This work was supported by grants from the NIH (R01GM114344), and the UCSF NSF Center for Cellular Construction (DBI-1548297). This work used the Vincent J. Proteomics/Mass Spectrometry Laboratory at UC Berkeley, supported in part by NIH S10 Instrumentation Grant S10RR025622. B.B. was supported by the NIH Ruth L. Kirschstein NRSA fellowship from the NIH (1F32GM115091). T.H-I was supported by an NSF-GRFP fellowship, Berkeley Stem Cell Center's NIH Stem Cell Biological Engineering Training Program (T32GM098218), and as a UC Berkeley Lloyd Scholar. A.R.H. was in receipt of an EMBO long-term fellowship 1075–2013 and an HFSP fellowship LT000712/2014. K.X. is a Chan Zuckerberg Biohub investigator and acknowledges support from the Bakar Fellows Award. D.A.F. is a Chan Zuckerberg Biohub Investigator.

Author contributions

Conceptualization, B.B., T.H-I., D.A.F.; Methodology, B.B., T.H-I., A.R.H., and J.K.; Investigation, B.B., T.H-I., and J.K.; Formal Analysis, B.B., T.H-I., and J.K.; Software, B.B.; Writing – Original Draft, B.B., T.H-I., and D.A.F.; Writing – Review & Editing, B.B., T.H-I., A.R.H., J.K., K.X., and D.A.F.; Funding Acquisition, D.A.F., K.X., B.B., and A.R.H.; Resources, D.A.F. and K.X.; Supervision, D.A.F.

Declaration of interests

The authors declare no competing interests.

Star methods

Resource Availability

Lead Contact

Further information and requests for resources and reagents should be directed to and will be fulfilled by the Lead Contact, Daniel Fletcher (fletch@berkeley.edu).

Materials Availability

Materials developed for this study are available on request to the corresponding authors.

Data and Code Availability

Data collected and computer codes developed for this study are available on request to the corresponding authors.

Experimental Model and Subject Details

Cell culture and cell lines

MDCK II cells were a gift from Keith Mostov (UCSF) and maintained at 37°C and 5% CO_2 in high glucose DMEM (4.5 g/l), supplemented with 10% fetal bovine serum (FBS) and penicillin-streptomycin (pen-strep). ZO-1 constructs were cloned using PCR and Gibson assembly into pHR backbone plasmids. Cell lines were created through lentivirus infection. Briefly, HEK293 cells were transfected with TransIT-293 (Mirus) according to manufacturer's instructions with three plasmids, pMD.2g, p8.91 and pHR with ZO-1 constructs (see Table S2 for amino acids details). Cells were grown for 2 days, after which media was collected and virus was concentrated with Lenti-X (Clontech) according to manufacturer's instructions. Virus was added to freshly passaged MDCK II cells, and cells were grown for two days before passaging and removing media. Cell lines created with fluorescently tagged proteins were sorted and normalized for expression using the UC Berkeley Flow Cytometry Facility (BD Bioscience Influx Sorter). Cell lines were confirmed with confocal imaging and immunoblot.

ZO-1, ZO-2, and double knockout (dKO) cell lines were created by first building a Cas9-expressing MDCK II cell line. Briefly, a lentiCas9-Blast (Addgene) plasmid was used to create stably expressing-Cas9 cell lines by selection under 5 ug/mL blasticidin for 7 days. Cas9 expression was confirmed with immunoblot. Three guide RNAs (gRNAs) for TJP1 were examined to create the ZO-1 KO (Table S1). The three pLenti-gRNA-puro plasmids were transduced into Cas9-expressing cells before selection in 10 μg/mL puromycin for 6 days. Knockout was initially confirmed with immunofluorescence imaging of ZO-1. Clonal cell lines were created by dilution plating, where a single cell suspension (5 cells/mL) was plated in a 96-well tissue culture dish. On day 7, each well was checked for a single colony, and on day 14, cells were passaged. Knockout was verified with immunofluorescence, immunoblot, and genomic sequencing (Fig. S4). dKO cells were created by following the protocol above with multiple TJP2 gRNAs (Table S1) and several TJP1 KO clones. After double knockout verification, a clone generated from gRNA 2 for TJP1 and gRNA 1 for TJP2 was used in subsequent experiments (Table S1).

Method Details

General methods

All of the chemical reagents were of analytical grade, obtained from commercial suppliers, and used without further purification, unless otherwise noted. Alexa Fluor 647 phalloidin was purchased from ThermoFisher. 1,2-diphytanoyl-*sn*-glycero-3-phophoscholine (DPhPC), 1,2-dioleoyl-*sn*-glycero-3-phosphocholine (DOPC), 1,2-dioleoyl-*sn*-glycero-3-phosphoethanolamine-N-[methoxy(polyethylene glycol)-2000], ammonium salt (DOPE-PEG), 1,2-dioleoyl-*sn*-glycero-3-phosphoethanolamine-N-[4-(p-maleimidophenyl)butyramide], sodium salt (DOPE-MPB) were

obtained from Avanti Polar Lipids, Inc. 1,2-Dioleoyl-*sn*-glycero-3-phosphoethanolamine labeled with Atto 390 (DOPE-Atto 390) and Lucifer yellow were purchased from Atto-tec and Sigma Aldrich, respectively.

Fluorescence imaging was carried out on a Ti Eclipse microscope (Nikon) equipped with a CSU-X spinning disk confocal module (Yokogawa) and a Zyla sCMOS camera (Andor). Fluorescence micrographs of giant vesicles or cells were acquired with either a 20x objective (Nikon, NA 0.45) or a 60x objective (Nikon, NA 1.49 TIRF). TIRF imaging was performed on the Ti Eclipse microscope (Nikon) using a 60x objective (Nikon, NA 1.49 TIRF) and an iXon Ultra EM-CCD camera (Andor).

Protein expression and purification

ZO-1 proteins used for in vitro reconstitution and co-sedimentation experiments were all prepared using insect cell expression. The rZO-1 construct consisted of an N-terminal RFP tag followed by amino acids 1-411 of the human ZO-1 gene, containing PDZ1 and PDZ2 domains, in frame with amino acids 1159-1382 of the human ZO-1 gene, followed by the Dual Strep purification tag. For co-sedimentation assays, ZO-1 ABR constructs consisted of an N-terminal EGFP tag followed by amino acids 1159-1382 of the human ZO-1 gene and a C-terminal Dual Strep purification tag. GFP-ABRM1 and GFP-ABRM6 constructs contained a stretch of four alanine mutations at different positions of the ABS sequence, amino acids 1-4 and 21-24 of the ABS, respectively. The ABS construct consisted of an N-terminal GST solubilization tag and thrombin cleavage site followed by amino acids 1257-1284 of the human ZO-1 gene (ABS) in frame with EGFP and a C-terminal 6xHis tag. For bacmid production, each sequence was cloned into the pFastBac HTA vector and transformed into DH10Bac bacterial cells. Transformed cells were grown on LB agar plates with kanamycin (50 μg/mL), gentamycin (7 μg/mL), tetracycline (10 μg/mL), IPTG (40 μg/mL), and Bluo-gal (100 μg/mL) and colonies that were white in color were picked for amplification and isolation of bacmid. PCR of bacmids confirmed the insertion of ZO-1 sequences. Sf-9 cells were transfected with isolated bacmids using Cellfectin (ThermoFisher), and after 4 days, supernatants containing baculovirus were collected and clarified by centrifugation at 1,000 x g for 5 min. Virus was then amplified by two rounds of Sf-9 cell infection and supernatant collection.

For expression, concentrated baculovirus was used to infect Sf-9 in a 1 L culture at 27 °C. After 2 days, cells were collected by centrifugation at 400 x g for 10 min and lysed into a lysis buffer containing 25 mM HEPES, pH 7.5, 150 mM NaCl, 1 mM EDTA, 1 mM TCEP supplemented with DNase I and protease inhibitors using a Dounce homogenizer. The lysate was clarified by centrifugation at 18,000 rpm at 4 °C. ZO-1 constructs were then purified using affinity chromatography. Briefly, clarified lysate was cycled over a Strep column (IBA Lifesciences) for 2 hr at 4 °C. The column was then washed with lysis buffer. For elution, lysis buffer containing 2.5 mM desthiobiotin was added to the column, and eluted proteins were further purified by size

exclusion chromatography using a Superdex 75 column (GE Healthcare) into a buffer containing 25 mM HEPES, pH 7.5, 150 mM NaCl, 1 mM TCEP.

Microfluidic jetting of giant unilamellar vesicles (GUVs)

GUVs were formed by placing a microfluidic jetting nozzle (Microfab Technologies, Inc., single jet microdispensing device with 25 μm orifice) filled with a 0.2 μM rZO-1, 10% OptiPrep (Sigma-Aldrich), 25 mM HEPES, pH 7.5, 150 mM NaCl solution in close proximity, <200 μm, to DPhPC planar bilayers with and without embedded GFP-Cldn4 (see Belardi et al., 2019). The rZO-1-containing solution ultimately constitutes the lumen of the jetted GUVs and has a matched osmolarity, but different density, compared to the outer buffer. Jetting was performed with and without AF647-phalloidin-stabilized F-actin (0.4 μM) included in the rZO-1-containing solution. The piezoelectric actuator of the nozzle was controlled by a waveform generator (Agilent) and an amplifier (Krohn-Hite) with pulse train envelops designed by a custom Matlab script. For jetting of GUVs, the actuator was triggered by an increasing parabolic envelop defined by 40 trapezoidal bursts at 15 kHz, 3 μs rise and fall times, a 30 μs hold time, and a maximum voltage of 15-30 V. Planar bilayer deformation and GUV formation were monitored using brightfield microscopy with a high-speed camera (Photron, 1024PCI). GUVs formed by microfluidic jetting sunk to the poly-L-lysine-coated coverglass due to the density mismatch between the interior of the GUVs and the surrounding buffer and were imaged using spinning disk confocal microscopy.

CtermCldn4 supported lipid bilayers

CtermCldn4-functionalized supported lipid bilayers (SLBs) were prepared in a similar manner to Lin et al. (Lin et al., 2014). Briefly, glass coverslips were RCA cleaned and treated with a 1 mg/mL solution of SUVs containing DOPC (97%), DOPE-MPB (2.5%), DOPE-PEG (1%) and DOPE-Atto 390 (0.1%) for 10 min to form SLBs. SLBs were washed five times with a volume of 200 μL of buffer containing 25 mM HEPES, pH 7.5, 150 mM NaCl. After washing, SLBs were blocked by treating with b-casein (Sigma Aldrich) for 10 min at room temperature. SLBs were washed again three times with a volume of 200 μL of buffer containing 25 mM HEPES, pH 7.5, 150 mM NaCl. DOPE-MPB lipids were then reacted with the terminal cysteine residue of a fluorescent CtermCldn4 peptide (300 nM, 5-FAM-Ahx-CPPRTDKPYSAKYSAARSAAASNYV, GenScript) for 1 hr at room temperature. Unreacted maleimide lipids were capped by treating SLBs with 2-mercaptoethanol for 10 min. SLBs were washed five times with a volume of 200 μL of buffer containing 25 mM HEPES, pH 7.5, 150 mM NaCl. Imaging of SLBs was performed using TIRF microscopy with a 60x objective before addition of rZO-1 and F-actin. AF647-phalloidin-stabilized F-actin (0.4 μM) was combined with rZO-1 (0.2 μM) for 30 min before addition to SLBs. rZO-1-F-actin complexes were incubated with SLBs for 30 min at room temperature and then washed three times with a volume of 200 μL of buffer containing 25 mM HEPES, pH 7.5, 150 mM NaCl. SLBs were again imaged using TIRF microscopy. Fluorescence recovery after photobleaching (FRAP) of fluorescent CtermCldn4 was performed by narrowing a field stop in

the excitation path and illuminating the sample at high power for 10 s. The field stop was then opened and a time-lapse acquisition (every 20 s) was performed.

Cell free expression and in vitro actin-binding assay

To express a range of GFP-tagged ZO-1 segments, cell-free protein expression was performed by first cloning appropriate sequences of ZO-1 into a pET28a expression vector. Expression of GFP fusions of ZO-1 segments was commenced by combining 3.5 μL of bacterial extract (Biotech Rabbit), 4 μL of reaction buffer (Biotech Rabbit), 2 μL of plasmid solution (final mass, 1 μg of DNA), and 0.5 μL of a 20 mM IPTG solution and placing the mixture at 37 °C for 1 hr. A laser-cut imaging chamber (acrylic wells UV-cured to 1.5 glass coverslip) was cleaned by sonicating the glass in the presence of deionized water, EtOH, and 3M NaOH solutions, sequentially. After washing with deionized water, the cell-free expression mixture was applied to chambers to immobilize the expressed fluorescent constructs. To this mixture, AF647-phalloidin-stabilized F-actin was added to a final concentration of 0.5 μM. After 45 min, each chamber was imaged using fluorescence microscopy without washing.

ABS alignment

To align the ABS site across species, ZO-1 homologs were identified by a protein BLAST (NCBI) search: human (Uniprot Q07157), mouse (Uniprot P39447), rat (Uniprot A0A0G2K2P5), dog (Uniprot O97758), frog (Uniprot A0A1L8GT63), zebrafish (Uniprot A0A2R8QMK9), chicken (Uniprot A0A1D5NWX9), fruit fly (Uniprot A0A0B4K6Y7), roundworm (Uniprot Q8I103), sea urchin (Uniprot W4ZFF8), sea squirt (Uniprot A0A3Q0JQ32), lancelet (Uniprot C3YKF2), acorn worm (NCBI ProteinID XP_006813237.1), brachiopod (Uniprot A0A2R2MJX0), pacific oyster (NCBI XP_011435800.2), leech (Uniprot T1FAR7), flatworm (Uniprot G4VGU1), hydra (Uniprot Q9BKL2), and placozoan (Uniprot B3S7T9). No ZO-1 homologs were found in the ctenophore and the porifera clades. A local alignment of the human ZO-1 ABR was performed (Water, EMBL) for each ZO-1 homolog. With the homologous ABR sequences in hand, we then performed a second local alignment (Water, EMBL) with the 28-amino acid ABS sequence.

Co-sedimentation actin-binding assay

F-actin was prepared by polymerizing β-actin at 68 μM for 1.5 hr at room temperature. Various concentrations of F-actin were then combined with a constant concentration of GFP-tagged ZO-1 constructs (0.5 μM) in Buffer F. Sub-stoichiometric concentrations of ZO-1 constructs were used in all experiments, such that the assumption of $[\text{F-actin}]_{\text{total}} \approx [\text{F-actin}]_{\text{free}}$ was valid. After incubation at room temperature for 30 min, F-actin was pelleted at 150,000 x g for 60 min at 4 °C. The supernatants were then collected, and unbound ZO-1 construct fluorescence intensity was analyzed using a fluorimeter (Biotek Instruments, Inc.). Bound fractions were fitted with the following equation $I = \frac{[F-actin]}{(k_D+[F-actin])}$, where I is the bound fraction, [F-actin] is the F-actin concentration and k_D is the dissociation constant.

Barrier assays

Cells were plated on 24-well Transwell inserts (polyester (PE), 0.4 μm pore size (Corning)) coated with 30 μg/mL Collagen I (Cellmatrix) at a cell density of 3.33E4 cells/cm^2. Transepithelial electrical resistance measurements (TEER) was performed using the ENDOHM6 cup chamber (WPI) with EVOM2 (WPI) in cell culture media. For transport measurements, phenol red-free media (4.5 g/L glucose, (-) L-glut, (-) Sodium Pyruvate, (-) phenol red DMEM supplemented with 10% FBS, pen-strep, and GlutaMax) with 10 μM of Lucifer yellow was added to Transwell insert. After 3 hours of incubation, media was collected from the basal culture well and fluorescence was measured using a fluorescence plate reader (Biotek Instruments, Inc.). Apparent permeability (P_{app}) was calculated as $P_{app} = \frac{V_r * C_1}{A * C_o * dt}$, where V_r is the volume of the basal well, C_1 is the concentration measured in the basal well, A is the area of the transwell insert, C_o is the concentration of Lucifer yellow added to the insert, and dt is the incubation time.

Immunostaining and imaging

Cells were plated on a 2.1 μg/mL collagen I gel (Cellmatrix), pH 7.4, in a glass-bottom cell culture dish at a cell density of 3.33E4 cells/cm^2 and grown for 2 or 4 days. Fixation methods were optimized for each antibody used. Cells were either fixed in 1% of 4% PFA at room temperature for 20 minutes or in 100% EtOH or 100% MeOH at -20° C for 30 min. Cells fixed in PFA were first permeabilized with 0.2% (v/v) Triton X-100 at room temperature for 10 minutes. To block, fixed cells were incubated in 5% (w/v) BSA in PBS at room temperature for 2 hours. Cells were then incubated with primary antibodies in a 1% (w/v) BSA in PBS solution at 4° C, overnight. Secondary antibodies were applied in a 1% BSA in PBS solution at room temperature for 1 hour. Three PBS washes were done after each antibody incubation step. Cells were incubated in Hoechst for 10 minutes at room temperature. Cells were imaged on a Ti Eclipse microscope (NIKON) using a 60x 1.49 NA objective and an iXon Ultra EMCCD (Andor). For live cell imaging, cells were plated identically, but not fixed, and imaged on the same microscope.

Immunoblot

Cells were plated in a 6-well plate at a cell density of 3.33E4 cells/cm^2 and grown for 2 or 4 days. Cells were lysed in RIPA buffer (1% (v/v) Triton X-100, 0.1% (w/v) SDS, 1% (w/v) deoxycholate) with protease inhibitors (Thermo Fisher) on ice for 30 minutes. Lysate was spun at 13,000 rpm for 15 minutes at 4° C. A BCA assay (Thermo Fisher) was performed according to manufacturer's instructions to determine protein concentration. All samples were diluted to the same protein concentration. Loading buffer was added to lysate, and samples were run on a 4-20% polyacrylamide gel (Bio-Rad) and at 200 V for 35 minutes. Gel was transferred using iBlot (Thermo Fisher) according to manufacturer's instructions at 20 V for 5 min. Ponceau S was incubated for 10 minutes at room temperature to visualize total protein. The blot was blocked in 2% (w/v) BSA in PBS with 0.1% Tween-20 (PBS-T) for 1 hour at room temperature. Primary antibody was administered in 1% (w/v) BSA overnight on a shaker at 4° C, and secondary was administered in 1% (w/v) BSA for 1 hour on a shaker at room temperature. Three, 10-minute PBS-

T washes were performed after each antibody incubation. The blot was visualized on a ChemiDoc (BioRad).

PCR of genomic DNA

Control and MDCK II cell lines were plated in a 6-well plate and grown to confluency. Genomic DNA was isolated using PureLink® Genomic DNA Mini Kit (Thermo Fisher) according to manufacturer's instructions. PCR of ZO-1 was run on an agarose gel to confirm a single band, and the amplified segment was sequenced by the UC Berkeley DNA Sequencing Facility. PCR and sequencing were used to confirm knockout cell lines as well as insertion of ZO-1 and other constructs.

FRAP of β-actin

Cells were plated on a 2.1 μg/mL collagen I gel (Cellmatrix), pH 7.4, in a glass-bottom cell culture dish at a cell density of 3.33E4 cells/cm^2. After culture for 4 days, medium was exchanged for Liebowitz-15 Medium, supplemented with 10% fetal bovine serum (FBS), GlutaMAX, and penicillin-streptomycin (pen-strep) and allowed to equilibrate at room temperature for 30 minutes before imaging. Scanning confocal light microscopy was performed (Zeiss LSM-880 NLO Airyscan) with a 40X/NA 1.0 water-immersion objective and a pinhole set to 0.7 AU. Bleaching and imaging of mCherry-β-actin was performed with a 561 nm DPSS laser and detection was gated between 570 nm and 695 nm. Imaging and bleaching at the TJ was performed by first focusing the sample on ZO-1 fusion proteins with a 488 argon laser. Then, bleaching and imaging of mCherry-β-actin was executed to image actin recovery at the TJ. For bleaching, a region of interest was defined, and the 561 nm BPSS laser was set to maximum laser power with a scan speed of 2 and two iterations. After bleaching, images were taken every 5 seconds to monitor fluorescence recovery.

Images were opened as a time series in ImageJ and registered using the descriptor-based series registration (2d/3d + t) plugin. The ROI manager was used to create reference and background regions. Mean fluorescence of bleached areas was normalized to pre-bleach intensity and normalized to fluorescence of actin at the tight junction far from the bleach location to account for photobleaching due to imaging. Full-scale normalization was used to correct for differences in bleaching efficiency.

3D STORM imaging of ZO-1

For super-resolution optical imaging of ZO-1 by STORM (stochastic optical reconstruction microscopy), dKO MDCK II cells stably expressing ZO-1 constructs with various ABDs were cultured on #1.5H glass coverslips (22 mm × 22 mm). Plating was performed on a 2.1 μg/mL collagen I gel (Cellmatrix), pH 7.4, at a cell density of 3.3×10^4 cells/cm^2, and cells were grown for 4 days. Cells were washed three times with PBS (1x) and then fixed with 4% PFA at room temperature for 10 min. Next, cells were permeabilized with 2% (v/v) Triton X-100 at room

temperature for 10 minutes and subsequently washed twice with PBS (1x). Samples were then blocked with 5% (w/v) BSA in PBS at room temperature for 2 hours. Cells were then incubated with an anti-ZO-1 antibody (Thermo Fisher) in a 5% (w/v) BSA in PBS solution at room temperature for 45 min. Next, cells were washed three times with PBS (1x). An anti-mouse IgG Alexa Fluor 647 antibody was applied in a 5% BSA in PBS solution at room temperature for 30 min. Five PBS (1x) washes were performed after the secondary antibody step. The cells were then fixed again with 4% PFA for 10 min and washed three times with PBS (1x). The cell-mounted coverslips were washed sequentially with 10%, 25% and 50% (w/v) sucrose in PBS for 5 min each and mounted on a large #1.5H coverslip (24 mm × 60 mm) with a STORM imaging buffer containing 52% (w/v) sucrose, 100 mM cysteamine, 5% glucose, 0.8 mg/ml glucose oxidase and 40 μg/ml catalase in Tris-HCl (pH 7.5), and sealed prior to imaging. Sucrose was used to increase the buffer's refractive index to ~1.406 for a 1.35-NA silicone oil immersion objective (UPLSAPO100XS, Olympus). The prepared sample was loaded on a home-built STORM microscope capable of both epi-illumination and oblique light-sheet illumination (Kim et al., 2019). TJs were imaged through the large coverslip under the wide-field illumination of 647-nm laser light (MPB Communications), from which the TJ was aligned to lie on the oblique light sheet (~1.2 μm thick at beam waist) for STORM imaging with minimal background fluorescence. STORM data were acquired at ~50 frames/s over ~40,000 frames per TJ section under the 647-nm sheet illumination (~20 kW/cm^2) together with 405-nm activation light (0-10 W/cm^2). Three-dimensional STORM was enabled with a cylindrical lens (LJ1653RM-A, Thorlabs) placed right in front of an Andor iXon Ultra 888 electron-multiplying charge-coupled device (EMCCD) camera (Huang et al., 2008). The raw STORM data were processed by the Insight3 software (Dr. Bo Huang, University of California at San Francisco) and 3D super-resolution images of ZO-1 were reconstructed (Fig. 5D and 5E). To quantify the distribution of ZO-1, a 250-nm-long section of the 3D TJ image (marked as the white box in Fig. 5E) was binned in the x direction to produce a 1D intensity cross-section in the TJ length direction (Fig. 5F), from which the full width at half minimum (FWHM) was estimated as a measure of TJ length. The ZO-1 FWHM was measured at several locations within one TJ section and over separate TJ sections for statistical significance.

TEM

For transmission electron microscopy (TEM), cells were plated on 24-well Transwell inserts (polyester (PE), 0.4 μm pore size (Corning)) coated with 30 ng/mL Collagen I (Cellmatrix) at a cell density of 3.33E4 cells/cm^2 and grown for 4 days. Cells were fixed for 1.5 hours at room temperature in 2.5% glutaraldehyde and paraformaldehyde (EMS) in 0.1 M sodium cacodylate buffer, pH 7.2, and then washed three times with sodium cacodylate buffer for 15 min. After fixation, membranes were cut out of Transwell inserts for handling and kept hydrated. Membranes with cells were then incubated in 1% osmium tetroxide in sodium cacodylate buffer for 30 minutes on ice in the dark, followed by three washes in sodium cacodylate buffer for 15 min. Samples were dehydrated using progressively higher percentages of ice cold EtOH (35%, 50%, 70%, 80%, 90%, 100%, 100%), each incubation was performed for 7 minutes. For TEM, after dehydration in EtOH,

cells were infiltrated with resin with progressively higher percentages of resin (25%, 50%, 75%, 100%, 100%), each incubation was performed for 15 minutes. Samples were cut and layered into molds and cured at 60° C for two days. Sections, 70-90 nm thin, were cut on either a Reichert-Jung Ultracut E (Leica) or Leica EM UC6 (Leica) and collected onto 50 mesh copper grids, then post-stained with 2% aqueous uranyl acetate and lead citrate for 5-7 minutes in each. Images were collected on an FEI Tecnai12 transmission electron microscope (FEI, Hillsboro, OR).

Simulations

Monte Carlo polymer simulations

A custom Matlab (Mathworks) script was developed to run dynamic simulations of 2-D polymeric species on a 2-D lattice. Polymer dynamics were modeled using the slithering snake algorithm (Wall and Mandel, 1975), which is well-suited to studying polymer fluctuations in crowded environments, e.g. cell membranes (Itzhak et al., 2016). Briefly, linear, static polymers were placed on a 100x100 lattice every 5 lattice sites apart in both the x and y directions. A second polymeric species with an odd-number of monomers was placed on the gird in a random configuration. A set of randomly orientated polymers with a constant number of contacts with the static polymers was created. The randomly oriented polymeric species was then initialized to perform a slithering snake movement. Either end of the polymer was chosen at random as the head of the polymer and allowed to sample adjacent lattice sites by comparing the transition probability to a random number. If a move is accepted, the head moves to the new lattice site and the rest of polymer follows. The transition probability depends on the number of contact sites and the effective affinity between the fluctuating polymer and the linear, static polymer. If the move position is already occupied, the head and tail of the polymer are switched, and the same procedure is repeated. We performed simulations of 100 initial starting conditions at three different polymer-polymer affinities. Data are displayed for polymer lengths of 39 monomers. The results are consistent for larger and smaller fluctuating polymers, however at lengths much smaller than the bounding static polymer squares, kinetic trapping is negligible.

Supplemental figures

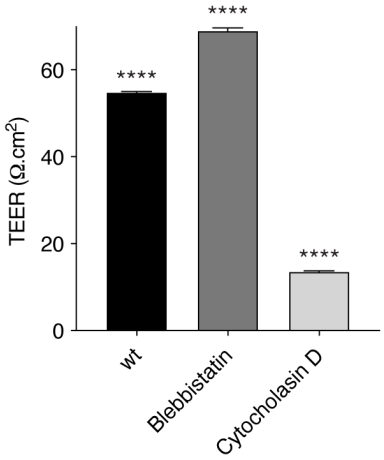

Figure S1. Actin contractility is detrimental to epithelial barrier function, Related to Figure 1.
TEER measurements of wt MDCK II cells treated with DMSO, 100 μM blebbistatin, or 10 μM cytochalasin D for 3 hr. Measurements are from day 4 of confluency. Bars represent mean ± SEM, n=4, (p-values determined using a multiple comparison one-way ANOVA, p-values represent comparison all samples, **** $p<0.0001$)

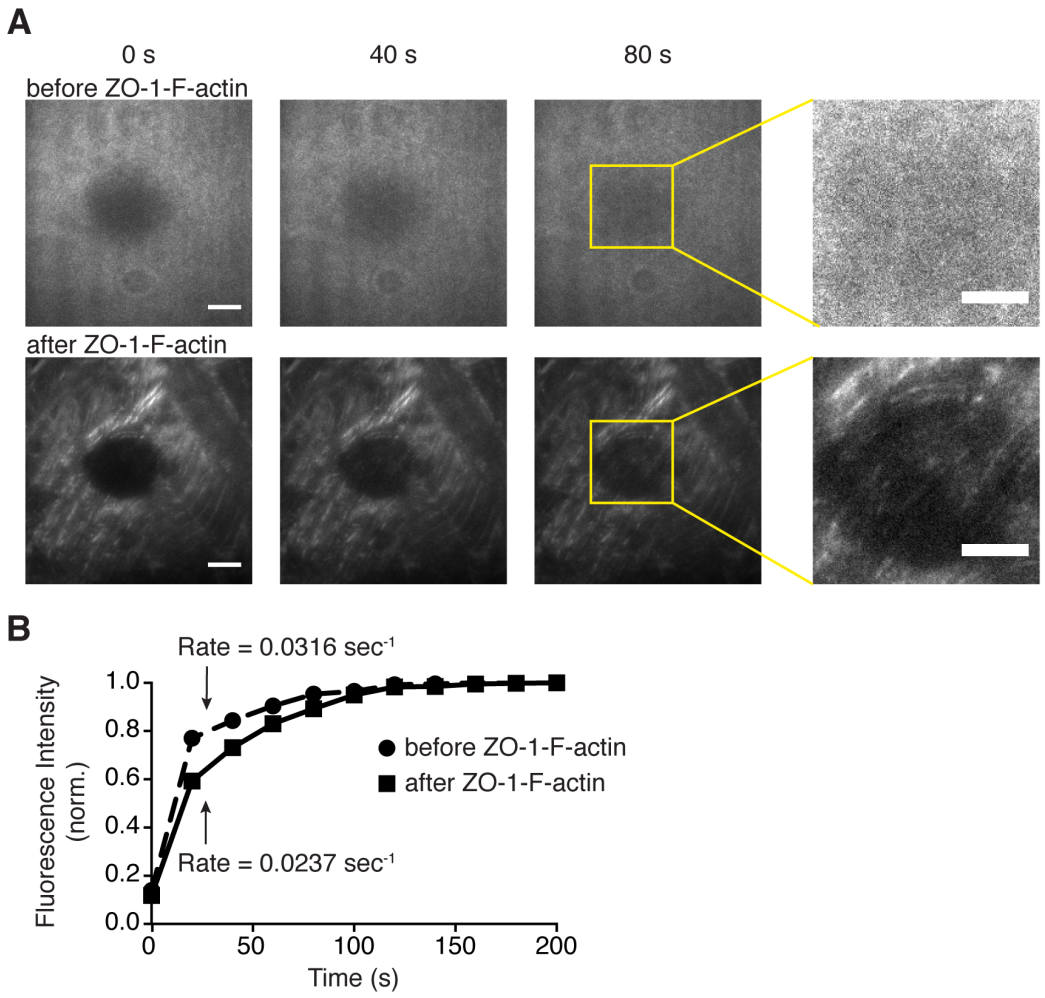

Figure S2. ZO-1-F-actin complexes template CtermCldn4 peptide recovery on a supported lipid bilayer, Related to Figure 1.

(A) Fluorescent micrographs of CtermCldn4 peptide recovery after photobleaching on an SLB with and without ZO-1-F-actin complexes. CtermCldn4 recovery is heterogeneously templated along ZO-1-F-actin complexes in the bleached area (right). Scale bar, 20 μm (left) and 5 μm (right).

(B) Quantification of CtermCldn4 fluorescence intensity in bleached region over time. Squares represent mean, n=3.

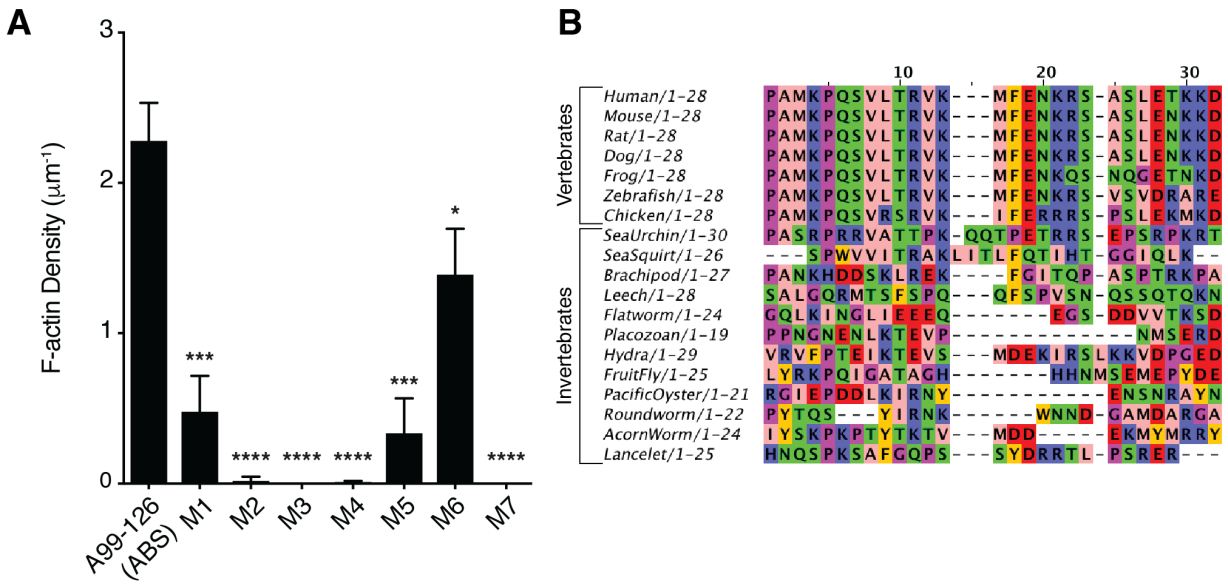

Figure S3. ABS alignment and mutational analysis, Related to Figure 2.

(A) Quantification of F-actin binding assay for ABS mutations. M1-M7 represent sequences of ABS where a string of four successive amino acids are mutated to alanine residues. Bars represent mean ± SD, n=3, (p-values determined using a two-sample t-test with A99-126, * $p<0.05$, *** $p<0.001$, **** $p<0.0001$).

(B) ABS sequence alignment across metazoans. Sequence homology is high for vertebrates.

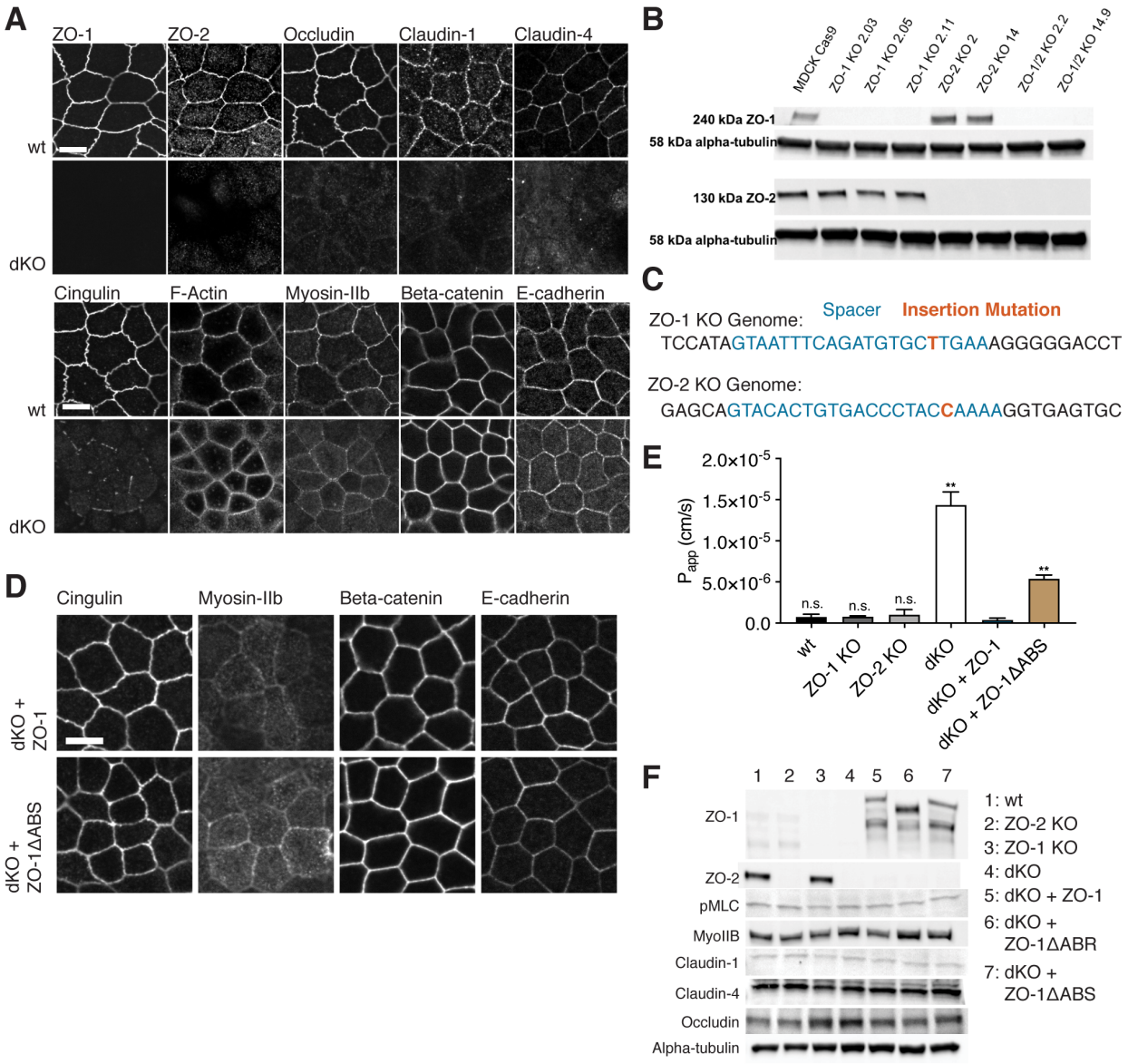

Figure S4. ZO-1ΔABS expression restores TJ protein localization but not barrier function compared to wt ZO-1 in dKO cells, Related to Figure 3.

(A) Immunofluorescent micrographs of TJ and AJ proteins in dKO and wt cells. Scale bar, 10 μm.
(B) Western blots of wt and KO clones showing knockout of ZO proteins.
(C) Genomic sequences of ZO-1 and ZO-2 loci in dKO cells.
(D) Immunofluorescent micrographs of junctional proteins in dKO cells expressing either ZO-1 or ZO-1ΔABS. Scale bar, 10 μm.
(E) Apparent permeability (Papp) measurements of wt, KO, dKO and dKO cells expressing ZO-1 and ZO-1ΔABS are consistent with TEER results. Bars represent mean ± SEM, n=3, (p-values determined using a two-sample t-test comparison with dKO + ZO-1, ** $p<0.01$, n.s. $p>0.05$).
(F) Western blot analysis of wt, ZO-1 KO, ZO-2 KO, dKO, and dKO cells expressing ZO-1 and ZO-1ΔABS.

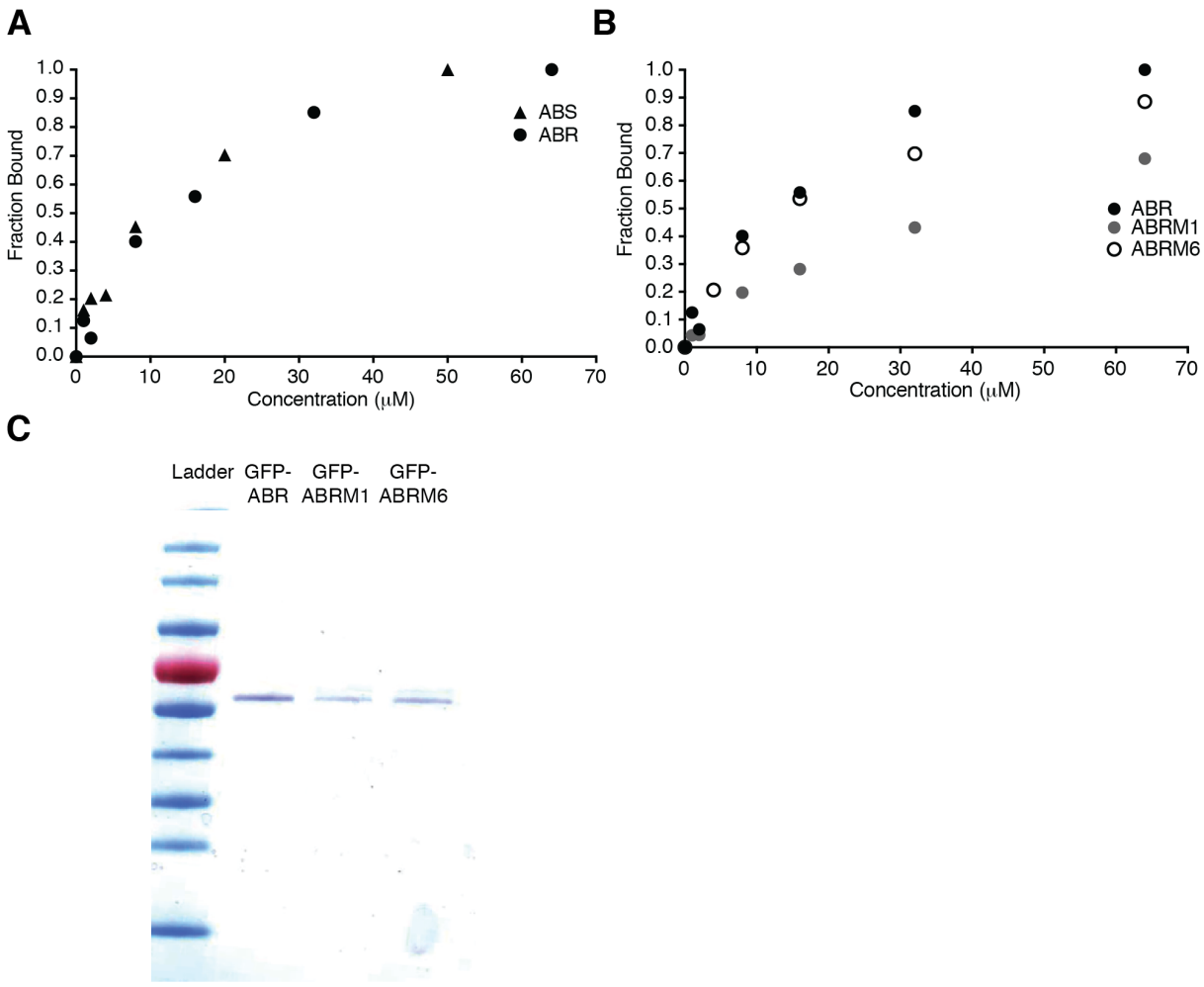

Figure S5. Binding curves of ZO-1's ABS and ABR toward F-actin, Related to Figure 5.

(A) F-actin binding curves for ZO-1's ABS and ABR. Both show similar affinity for F-actin. Circles and triangles represent mean, n=4.

(B) F-actin binding curves for ZO-1's ABR (KD = 10.2 μM) and the ABR mutants, M1 (KD = 36.7 μM) and M6 (KD = 13.7 μM) (see SI Fig. 3 for more details). Circles represent mean, n=4.

(C) SDS-PAGE gel of purified ZO-1 constructs: ABR, ABRM1, and ABRM6.

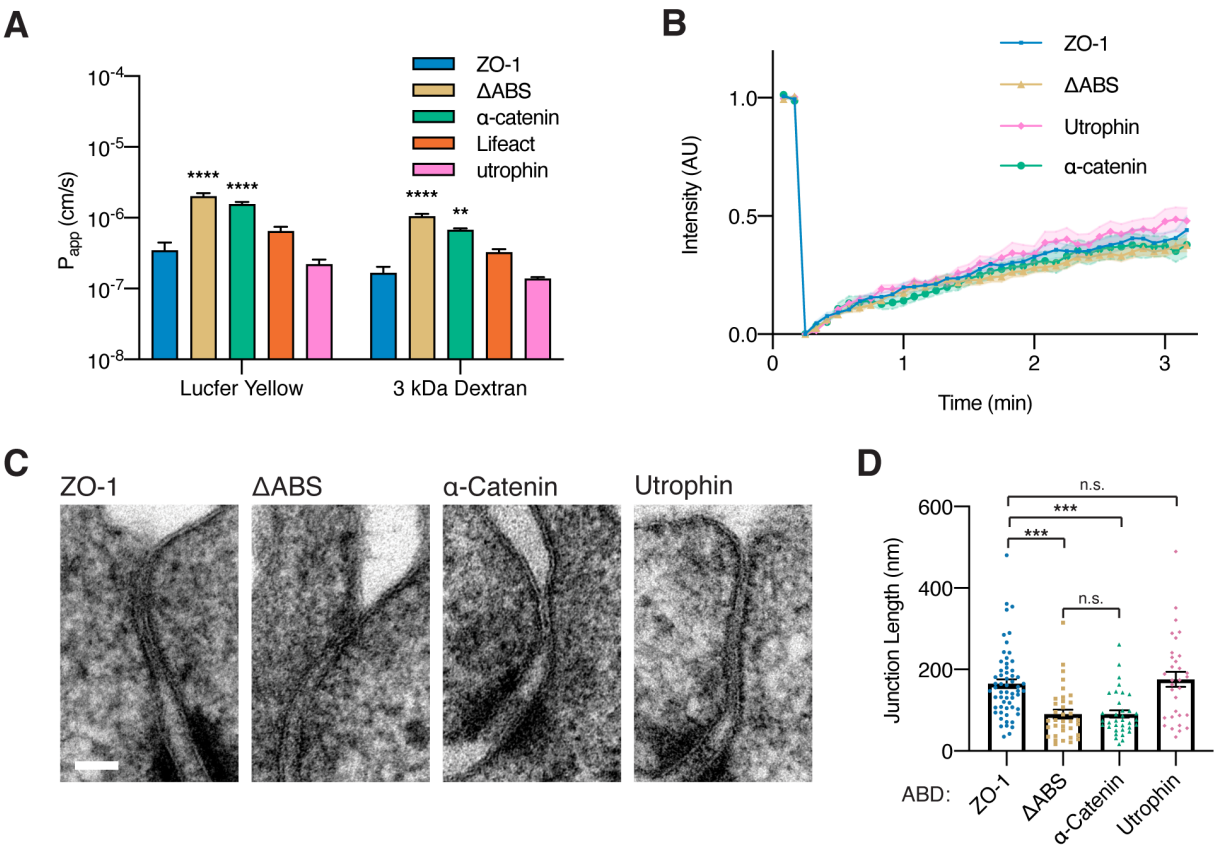

Figure S6. Engineering ZO-1's ABD alters permeability and junctional length but not actin dynamics at the TJ, Related to Figure 5.

(A) Apparent permeability (Papp) measurements of dKO cells expressing ZO-1 constructs with various ABDs. Bars represent mean ± SEM, n=3, (p-values determined using a two-sample t-test comparison with dKO + ZO-1, ** $p<0.01$, **** $p>0.0001$). Papp measurements are consistent with TEER results.

(B) Quantification of β-actin fluorescence intensity in bleached regions over time for dKO cells expressing both ZO-1 with various ABDs and mCherry-β-actin. Symbols represent the mean, n=3, and the shading indicates the SEM.

(C) Representative TEM images of dKO cells expressing ZO-1 constructs with various ABDs. Scale bar, 50 nm.

(D) Quantification of TJ length from TEM images of dKO cells expressing ZO-1 constructs with various ABDs. Bars represent mean ± SEM, (p-values determined using a multi-comparison one-way ANOVA with a Brown-Forsythe test, *** $p<0.001$, n.s. $p>0.05$). Each symbol represents one cell-cell junction, ZO-1 (n=59), ΔABS (n=35), α-Catenin (n=35), Utrophin (n=32).

Supplemental table title and legends

Name	Sequence	Genomic regions
gRNA ZO-1	GTAATTTCAGATGTGCTGAA	CanFam3.1: Chr3: 39059138:39059157
gRNA ZO-2	GTACACTGTGACCCTACAAAA	CanFam3.1: Chr1: 88163622:88163642

Table S1. Guide RNA (gRNA) used for CRISPR/Cas9 knockout of ZO-1 and ZO-2.

Name	Backbone	Protein	Actin binding Domain (ABD) Amino Acid Sequence	Measured Affinity (K_D, μM)	Citation
pHR ZO-1	pHR	TFP-YFP-ZO-1 (human ZO-1 AA1-1748)		10.2	
pHR ZO-1ΔABS	pHR	TFP-YFP-ZO-1ΔABS (human ZO-1 AA1-1748, ΔAA1257-1284)			This paper
pHR ZO-1ΔABS LARG	pHR	TFP-YFP-ZO-1ΔABS (human ZO-1 AA1-1748, ΔAA1257-1284) LARG GEF			Wagner et al. (2016)
pHR ZO-1ΔABS ISTN	pHR	TFP-YFP-ZO-1ΔABS (human ZO-1 AA1-1748, ΔAA1257-1284) ISTN GEF			Beco et al. (2018); Zimmerman et al. (2017)
pHR ZO-1ΔABS Tiam1	pHR	TFP-YFP-ZO-1ΔABS (human ZO-1 AA1-1748, ΔAA1257-1284) Tiam1 GEF			Beco et al. (2018); Zimmerman et al. (2017)
pHR ZO-1 ΔABS α-Catenin	pHR	TFP-YFP-ZO-1ΔABS (human ZO-1 AA1-1748, ΔAA1257-1284) α-Catenin ABD	AIMAQLPQEQKAKIAEQVASFQEEKSKLDAEVSK WDDSGNDIIVLAKQMCMIMMEMTDFTRGKGPLK NTSDVISAAKKIAEAGSRMDKLGRTIADHCPDSA CKQDLLAYLQRIALYCHQLNICSKVKAEVQNLGG ELVVSGVDSAMSLIQAAKNLMNAVVQTVKASYVA STKYQKSQGMASLNLPAVSWKMKAPEKKPLVKR EKQDETQTKIKRASQKKHVNPVQALSEFKAMDSI	~0.450	Hansen et al. (2013)
pHR ZO-1 ΔABS Lifeact	pHR	TFP-YFP-ZO-1ΔABS (human ZO-1 AA1-1748, ΔAA1257-1284) Lifeact ABD	MGVADLIKKFESISKEE	~2.00	Riedl et al. (2008)
pHR ZO-1 ΔABS Utrophin	pHR	TFP-YFP-ZO-1ΔABS (human ZO-1 AA1-1748, ΔAA1257-1284) Utrophin ABD	MAKYGEHEASPDNGQNEFSDIIKSRSDEHNDVQ KKTFTKWINARFSKSGKPPINDMFTDLKDGRKLL DLLEGLTGTSLPKERGSTRVHALNNVNRVLQVLH QNNVELVNIGGTDIVDGNHKLTLGLLWSIILHWQV KDVMKDVMSDLQQTNSEKILLSWVRQTTRPYSQ VNVLNFTTSWTDGLAFNAVLHRHKPDLFSWDKV VKMSPIERLEHAFSKAQTYLGIEKLLDPEDVAVRL PDKKSIIMYLTSLFEVLPQQVTID	~20.0	Winder et al. (1995)
pHR ZO-1 ΔABS Affimer6	pHR	TFP-YFP-ZO-1ΔABS (human ZO-1 AA1-1748,	Sequence was a kind gift from Michelle Peckham	~0.300	Lopata et al. (2018)

		ΔAA1257-1284) Affimer6			
pHR ZO-1 ΔABS F-tractin	pHR	TFP-YFP-ZO-1ΔABS (human ZO-1 AA1-1748, ΔAA1257-1284) F-tractin	GMARPRGAGPCSPGLERAPRRSVGELRLLFEARCAAVAAAAAAG	~10.0	Brehm et al. (2004)
pHR ZO-1 ΔABS Filamin A	pHR	TFP-YFP-ZO-1ΔABS (human ZO-1 AA1-1748, ΔAA1257-1284) Filamin A ABD	MSSSHSRAGQSAAGAAPGGGVDTRDAEMPATEKDLAEDAPWKKIQQNTFTRWCNEHLKCVSKRIANLQTDLSDGLRLIALLEVLSQKKMHRKHNQRPTFRQMQLENVSVALEFLDRESIKLVSIDSKAIVDGNLKLILGLIWTLILHYSISMPMWDEEEDEEAKKQTPKQRLLGWIQNKLPQLPITNFSRDWQSGRALGALVDSCAPGLCPDWDSWDASKPVTNAREAMQQADDWLGIPQVITPEEIVDPNVDEHSVMTYLSQFPKAKLKPGAPLRPK	~45.0	Clark et al. (2009)
pHR ZO-1 ΔABS Filamin A E254K	pHR	TFP-YFP-ZO-1ΔABS (human ZO-1 AA1-1748, ΔAA1257-1284) Filamin A ABD E254K	MSSSHSRAGQSAAGAAPGGGVDTRDAEMPATEKDLAEDAPWKKIQQNTFTRWCNEHLKCVSKRIANLQTDLSDGLRLIALLEVLSQKKMHRKHNQRPTFRQMQLENVSVALEFLDRESIKLVSIDSKAIVDGNLKLILGLIWTLILHYSISMPMWDEEEDEEAKKQTPKQRLLGWIQNKLPQLPITNFSRDWQSGRALGALVDSCAPGLCPDWDSWDASKPVTNAREAMQQADDWLGIPQVITPEEIVDPNVDKHSVMTYLSQFPKAKLKPGAPLRPK	~13.0	Clark et al. (2009)
pHR ZO-1 ΔABS ABSM1	pHR	TFP-YFP-ZO-1ΔABS (human ZO-1 AA1-1748, ΔAA1257-1284) ABSM1	ABSM1: AAAAPQSVLTRVKMFENKRSASLETKKD	36.7	This paper
pHR ZO-1 ΔABS ABSM6	pHR	TFP-YFP-ZO-1ΔABS (human ZO-1 AA1-1748, ΔAA1257-1284) ABSM6	ABSM6: PAMKPQSVLTRVKMFENKRSAAAATKKD	13.7	This paper
pHR PhosNull ZO-1	pHR	TFP-YFP-ZO-1 (human ZO-1 AA1-1748) AA1159-1382 mutations: Ser, Thr --> Ala, Tyr --> Phe			
pHR PhosSerThr ZO-1	pHR	TFP-YFP-ZO-1 (human ZO-1 AA1-1748) AA1159-1382 mutations: Ser, Thr --> Asp			
pHR PhosAll ZO-1	pHR	TFP-YFP-ZO-1 (human ZO-1 AA1-1748) AA1159-1382 mutations: Ser,			

		Thr --> Asp, Tyr --> Asp			
rZO-1	pFastBac HTA	RFP-rZO-1-2xStrepTag (human ZO-1 AA1-411, 1159-1382)			
EGFP-ABS	pFastBac HTA	EGFP-ABS-2xStrepTag	PAMKPQSVLTRVKMFENKRSASLETKKD		
EGFP-ABR	pFastBac HTA	EGFP-ABR-2xStrepTag	EQPAPGYDTHGRLRPEAQPHPSAGPKPAESKQ YFEQYSRSYEQVPPQGFTSRAGHFEPLHGAAAV PPLIPSSQHKPEALPSNTKPLPPPPTQTEEEEDP AMKPQSVLTRVKMFENKRSASLETKKDVNDTGS FKPPEVASKPSGAPIIGPKPTSQNQFSEHDKTLY RIPEPQKPQLKPPEDIVRSNHYDPEEDEEYYRKQ LSYFDRRSFENKPPAHIAASHLSE		Fanning et al. (2002)
EGFP-ABSM1	pFastBac HTA	EGFP-ABRM1-2xStrepTag			
EGFP-ABSM6	pFastBac HTA	EGFP-ABRM6-2xStrepTag			
GFP-ABR A1-224	pET28a	GFP-ABR A1-224			
GFP-ABR A1-112	pET28a	GFP-ABR A1-112			
GFP-ABR A57-168	pET28a	GFP-ABR A57-168			
GFP-ABR A113-224	pET28a	GFP-ABR A113-224			
GFP-ABR A57-112	pET28a	GFP-ABR A57-112			
GFP-ABR A85-140	pET28a	GFP-ABR A85-140			
GFP-ABR A113-168	pET28a	GFP-ABR A113-168			
GFP-ABR A85-112	pET28a	GFP-ABR A85-112			
GFP-ABR A99-126	pET28a	GFP-ABR A99-126			
GFP-ABR A113-140	pET28a	GFP-ABR A113-140			
GFP-ABR A99-112	pET28a	GFP-ABR A99-112			
GFP-ABR A106-119	pET28a	GFP-ABR A106-119			
GFP-ABR A113-126	pET28a	GFP-ABR A113-126			

Table S2. Plasmids used with amino acid sequences of actin-binding domains.

References

Acharya, B.R., Wu, S.K., Lieu, Z.Z., Parton, R.G., Grill, S.W., Bershadsky, A.D., Gomez, G.A., and Yap, A.S. (2017). Mammalian Diaphanous 1 Mediates a Pathway for E-cadherin to Stabilize Epithelial Barriers through Junctional Contractility. Cell Rep. *18*, 2854–2867.

Aijaz, S., D'Atri, F., Citi, S., Balda, M.S., and Matter, K. (2005). Binding of GEF-H1 to the tight junction-associated adaptor cingulin results in inhibition of Rho signaling and G1/S phase transition. Dev. Cell *8*, 777–786.

Beco, S. de, Vaidžiulytė, K., Manzi, J., Dalier, F., Federico, F. di, Cornilleau, G., Dahan, M., and Coppey, M. (2018). Optogenetic dissection of Rac1 and Cdc42 gradient shaping. Nat. Commun. *9*, 1–13.

Belardi, B., Son, S., Vahey, M.D., Wang, J., Hou, J., and Fletcher, D.A. (2019). Claudin-4 reconstituted in unilamellar vesicles is sufficient to form tight interfaces that partition membrane proteins. J. Cell. Sci. *132*, jcs221556.

Bertocchi, C., Wang, Y., Ravasio, A., Hara, Y., Wu, Y., Sailov, T., Baird, M.A., Davidson, M.W., Zaidel-Bar, R., Toyama, Y., et al. (2017). Nanoscale architecture of cadherin-based cell adhesions. Nat. Cell Biol. *19*, 28–37.

Beutel, O., Maraspini, R., Pombo-Garcia, K., Martin-Lemaitre, C., and Honigmann, A. (2019). Phase Separation of Zonula Occludens Proteins Drives Formation of Tight Junctions. Cell, 923-936.

Bors, L.A., and Erdő, F. (2019). Overcoming the Blood–Brain Barrier. Challenges and Tricks for CNS Drug Delivery. Scientia Pharmaceutica *87*, 6.

Brehm, M.A., Schreiber, I., Bertsch, U., Wegner, A., and Mayr, G.W. (2004). Identification of the actin-binding domain of Ins(1,4,5)P3 3-kinase isoform B (IP3K-B). Biochem. J. *382*, 353–362.

Buckley, C.D., Tan, J., Anderson, K.L., Hanein, D., Volkmann, N., Weis, W.I., Nelson, W.J., and Dunn, A.R. (2014). The minimal cadherin-catenin complex binds to actin filaments under force. Science *346*, 1254211.

Carragher, N.O., and Frame, M.C. (2004). Focal adhesion and actin dynamics: a place where kinases and proteases meet to promote invasion. Trends Cell Biol. *14*, 241–249.

Clark, A.R., Sawyer, G.M., Robertson, S.P., and Sutherland-Smith, A.J. (2009). Skeletal dysplasias due to filamin A mutations result from a gain-of-function mechanism distinct from allelic neurological disorders. Hum. Mol. Genet. *18*, 4791–4800.

Crawley, S.W., Mooseker, M.S., and Tyska, M.J. (2014). Shaping the intestinal brush border. J. Cell Biol. *207*, 441–451.

D'Atri, F., Citi, S. (2001). Cingulin Interacts With F-actin in Vitro. FEBS Lett. *507*, 21-24.

Drees, F., Pokutta, S., Yamada, S., Nelson, W.J., and Weis, W.I. (2005). α-Catenin Is a Molecular Switch that Binds E-Cadherin-β-Catenin and Regulates Actin-Filament Assembly. Cell *123*, 903–915.

Fanning, A.S., Jameson, B.J., Jesaitis, L.A., and Anderson, J.M. (1998). The tight junction protein ZO-1 establishes a link between the transmembrane protein occludin and the actin cytoskeleton. J. Biol. Chem. *273*, 29745–29753.

Fanning, A.S., Ma, T.Y., and Anderson, J.M. (2002). Isolation and functional characterization of the actin binding region in the tight junction protein ZO-1. FASEB J. *16*, 1835–1837.

Furuse, M., Sasaki, H., Fujimoto, K., and Tsukita, S. (1998). A single gene product, claudin-1 or -2, reconstitutes tight junction strands and recruits occludin in fibroblasts. J. Cell Biol. *143*, 391–401.

Gong, Y., Renigunta, V., Zhou, Y., Sunq, A., Wang, J., Yang, J., Renigunta, A., Baker, L.A., and Hou, J. (2015). Biochemical and biophysical analyses of tight junction permeability made of claudin-16 and claudin-19 dimerization. Mol. Biol. Cell *26*, 4333–4346.

Graham, W.V., He, W., Marchiando, A.M., Zha, J., Singh, G., Li, H.-S., Biswas, A., Ong, M.L.D.M., Jiang, Z.-H., Choi, W., et al. (2019). Intracellular MLCK1 diversion reverses barrier loss to restore mucosal homeostasis. Nat. Med. *25*, 690–700.

Günzel, D., and Yu, A.S.L. (2013). Claudins and the Modulation of Tight Junction Permeability. Physiol. Rev. *93*, 525–569.

Hansen, S.D., Kwiatkowski, A.V., Ouyang, C.-Y., Liu, H., Pokutta, S., Watkins, S.C., Volkmann, N., Hanein, D., Weis, W.I., Mullins, R.D., et al. (2013). αE-catenin actin-binding domain alters actin filament conformation and regulates binding of nucleation and disassembly factors. Mol. Biol. Cell *24*, 3710–3720.

Harris, A.R., Daeden, A., and Charras, G.T. (2014). Formation of adherens junctions leads to the emergence of a tissue-level tension in epithelial monolayers. J. Cell Sci. *127*, 2507–2517.

Harris, A.R., Belardi, B., Jreij, P., Wei, K., Bausch, A., and Fletcher, D.A. (2019). Steric Regulation of Tandem Calponin Homology Domain Actin-Binding Affinity. BioRxiv 598359.

Hartsock, A., and Nelson, W.J. (2008). Adherens and Tight Junctions: Structure, Function and Connections to the Actin Cytoskeleton. Biochim. Biophys. Acta *1778*, 660–669.

Howarth, A.G., Singer, K.L., and Stevenson, B.R. (1994). Analysis of the distribution and phosphorylation state of ZO-1 in MDCK and nonepithelial cells. J. Membr. Biol. *137*, 261–270.

Hua, Q.X., Gozani, S.N., Chance, R.E., Hoffmann, J.A., Frank, B.H., and Weiss, M.A. (1995). Structure of a protein in a kinetic trap. Nat. Struct. Biol. *2*, 129–138.

Huang, B., Wang, W., Bates, M., and Zhuang, X. (2008). Three-dimensional Super-Resolution Imaging by Stochastic Optical Reconstruction Microscopy. Science. *319*, 810-813.

Hull, B.E., and Staehelin, L.A. (1979). The terminal web. A reevaluation of its structure and function. J. Cell Biol. *81*, 67–82.

Irudayanathan, F.J., Wang, X., Wang, N., Willsey, S.R., Seddon, I.A., and Nangia, S. (2018). Self-Assembly Simulations of Classic Claudins-Insights into the Pore Structure, Selectivity, and Higher Order Complexes. J. Phys. Chem. B *122*, 7463–7474.

Itoh, M., Furuse, M., Morita, K., Kubota, K., Saitou, M., and Tsukita, S. (1999). Direct Binding of Three Tight Junction-Associated Maguks, Zo-1, Zo-2, and Zo-3, with the Cooh Termini of Claudins. J. Cell Biol. *147*, 1351–1363.

Itzhak, D.N., Tyanova, S., Cox, J., and Borner, G.H. (2016). Global, quantitative and dynamic mapping of protein subcellular localization. eLife *5*, e16950.

Kim, J., Wojcik, M., Wang, Y., Moon, S., Zin, E.A., Marnani, N., Newman, Z.L., Flannery, J.G., Xu, K., and Zhang, X. (2019). Oblique-plane Single-Molecule Localization Microscopy for Tissues and Small Intact Animals. Nat. Methods. *16*, 853-857.

Kobielak, A., Pasolli, H.A., and Fuchs, E. (2004). Mammalian formin-1 participates in adherens junctions and polymerization of linear actin cables. Nat. Cell Biol. *6*, 21–30.

Koval, M. (2013). Differential pathways of claudin oligomerization and integration into tight junctions. Tissue Barriers *1*, e24518.

Lin, W.-C., Iversen, L., Tu, H.-L., Rhodes, C., Christensen, S.M., Iwig, J.S., Hansen, S.D., Huang, W.Y.C., and Groves, J.T. (2014). H-Ras forms dimers on membrane surfaces via a protein–protein interface. Proc. Natl. Acad. Sci. U.S.A. *111*, 2996–3001.

Liu, Z., Tan, J.L., Cohen, D.M., Yang, M.T., Sniadecki, N.J., Ruiz, S.A., Nelson, C.M., and Chen, C.S. (2010). Mechanical tugging force regulates the size of cell–cell junctions. Proc. Natl. Acad. Sci. U.S.A. *107*, 9944–9949.

Lopata, A., Hughes, R., Tiede, C., Heissler, S.M., Sellers, J.R., Knight, P.J., Tomlinson, D., and Peckham, M. (2018). Affimer proteins for F-actin: novel affinity reagents that label F-actin in live and fixed cells. Sci. Rep. *8*, 1–15.

Mattagajasingh, S.N., Huang, S.C., Hartenstein, J.S., and Benz, E.J. (2000). Characterization of the interaction between protein 4.1R and ZO-2. A possible link between the tight junction and the actin cytoskeleton. J. Biol. Chem. *275*, 30573–30585.

McCartney, F., Gleeson, J.P., and Brayden, D.J. (2016). Safety concerns over the use of intestinal permeation enhancers: A mini-review. Tissue Barriers *4*.

Miyoshi, J., and Takai, Y. (2008). Structural and functional associations of apical junctions with cytoskeleton. Biochim. Biophys. Acta, Biomembr. *1778*, 670–691.

Nagafuchi, A., Ishihara, S., and Tsukita, S. (1994). The roles of catenins in the cadherin-mediated cell adhesion: functional analysis of E-cadherin-alpha catenin fusion molecules. J. Cell Biol. *127*, 235–245.

Otani, T., Ichii, T., Aono, S., and Takeichi, M. (2006). Cdc42 GEF Tuba regulates the junctional configuration of simple epithelial cells. J. Cell Biol. *175*, 135–146.

Otani, T., Nguyen, T.P., Tokuda, S., Sugihara, K., Sugawara, T., Furuse, K., Miura, T., Ebnet, K., and Furuse, M. (2019). Claudins and JAM-A coordinately regulate tight junction formation and epithelial polarity. J. Cell Biol. jcb.201812157.

Piontek, J., Winkler, L., Wolburg, H., Müller, S.L., Zuleger, N., Piehl, C., Wiesner, B., Krause, G., and Blasig, I.E. (2007). Formation of tight junction: determinants of homophilic interaction between classic claudins. FASEB J. *22*, 146–158.

Piontek, J., Fritzsche, S., Cording, J., Richter, S., Hartwig, J., Walter, M., Yu, D., Turner, J.R., Gehring, C., Rahn, H.-P., et al. (2011). Elucidating the principles of the molecular organization of heteropolymeric tight junction strands. Cell. Mol. Life Sci. *68*, 3903–3918.

Pulimeno, P., Paschoud, S., and Citi, S. (2011). A role for ZO-1 and PLEKHA7 in recruiting paracingulin to tight and adherens junctions of epithelial cells. J. Biol. Chem. *286*, 16743–16750.

Quiros, M., and Nusrat, A. (2014). RhoGTPases, actomyosin signaling and regulation of the epithelial Apical Junctional Complex. Semin. Cell Dev. Biol. *36*, 194–203.

Riedl, J., Crevenna, A.H., Kessenbrock, K., Yu, J.H., Neukirchen, D., Bista, M., Bradke, F., Jenne, D., Holak, T.A., Werb, Z., et al. (2008). Lifeact: a versatile marker to visualize F-actin. Nat. Methods *5*, 605–607.

Roignot, J., Peng, X., and Mostov, K. (2013). Polarity in Mammalian Epithelial Morphogenesis. Cold Spring Harbor Perspect. Biol. *5*, a013789.

Rossa, J., Ploeger, C., Vorreiter, F., Saleh, T., Protze, J., Günzel, D., Wolburg, H., Krause, G., and Piontek, J. (2014). Claudin-3 and Claudin-5 Protein Folding and Assembly into the Tight Junction Are Controlled by Non-conserved Residues in the Transmembrane 3 (TM3) and Extracellular Loop 2 (ECL2) Segments. J. Biol. Chem. *289*, 7641–7653.

Rotskoff, G.M., and Geissler, P.L. (2018). Robust nonequilibrium pathways to microcompartment assembly. Proc. Natl. Acad. Sci. U.S.A. *115*, 6341–6346.

Sasaki, H., Matsui, C., Furuse, K., Mimori-Kiyosue, Y., Furuse, M., and Tsukita, S. (2003). Dynamic behavior of paired claudin strands within apposing plasma membranes. Proc. Natl. Acad. Sci. U.S.A. *100*, 3971–3976.

Schwayer, C., Shamipour, S., Pranjic-Ferscha, K., Schauer, A., Balda, M., Tada, M., Matter, K., and Heisenberg, C-P. (2019). Mechanosensation of Tight Junctions Depends on ZO-1 Phase Separation and Flow. Cell *179*, 937-952.

Shin, S.-H., Chung, S., Sanii, B., Comolli, L.R., Bertozzi, C.R., and Yoreo, J.J.D. (2012). Direct observation of kinetic traps associated with structural transformations leading to multiple pathways of S-layer assembly. Proc. Natl. Acad. Sci. U.S.A. *109*, 12968–12973.

Spadaro, D., Le, S., Laroche, T., Mean, I., Jond, L., Yan, J., and Citi, S. (2017). Tension-Dependent Stretching Activates ZO-1 to Control the Junctional Localization of Its Interactors. Curr. Biol. *27*, 3783-3795.e8.

Stevenson, B.R., Anderson, J.M., Braun, I.D., and Mooseker, M.S. (1989). Phosphorylation of the tight-junction protein ZO-1 in two strains of Madin-Darby canine kidney cells which differ in transepithelial resistance. Biochem. J. *263*, 597–599.

Suzuki, H., Nishizawa, T., Tani, K., Yamazaki, Y., Tamura, A., Ishitani, R., Dohmae, N., Tsukita, S., Nureki, O., and Fujiyoshi, Y. (2014). Crystal structure of a claudin provides insight into the architecture of tight junctions. Science *344*, 304–307.

Terry, S.J., Zihni, C., Elbediwy, A., Vitiello, E., Leefa Chong San, I.V., Balda, M.S., and Matter, K. (2011). Spatially restricted activation of RhoA signalling at epithelial junctions by p114RhoGEF drives junction formation and morphogenesis. Nat. Cell Biol. *13*, 159–166.

Turner, J.R. (2009). Intestinal mucosal barrier function in health and disease. Nat. Rev. Immunol. *9*, 799–809.

Van Itallie, C.M., Fanning, A.S., Bridges, A., and Anderson, J.M. (2009). ZO-1 Stabilizes the Tight Junction Solute Barrier through Coupling to the Perijunctional Cytoskeleton. Mol. Biol. Cell *20*, 3930–3940.

Van Itallie, C.M., Aponte, A., Tietgens, A.J., Gucek, M., Fredriksson, K., and Anderson, J.M. (2013). The N and C termini of ZO-1 are surrounded by distinct proteins and functional protein networks. J. Biol. Chem. *288*, 13775–13788.

Van Itallie, C.M., Tietgens, A.J., and Anderson, J.M. (2016). Visualizing the dynamic coupling of claudin strands to the actin cytoskeleton through ZO-1. Mol. Biol. Cell *28*, 524–534.

Van Mameren, J., Vermeulen, K.C., Gittes, F., and Schmidt, C. (2009). Leveraging single protein polymers to measure flexural rigidity. J. Phys. Chem. B *113*, 3837-3844.

Vogelmann, R., and Nelson, W.J. (2005). Fractionation of the Epithelial Apical Junctional Complex: Reassessment of Protein Distributions in Different Substructures. Mol. Biol. Cell *16*, 701–716.

Wagner, E., and Glotzer, M. (2016). Local RhoA activation induces cytokinetic furrows independent of spindle position and cell cycle stage. J. Cell Biol. *213*, 641–649.

Wall, F.T., and Mandel, F. (1975). Macromolecular dimensions obtained by an efficient Monte Carlo method without sample attrition. J. Chem. Phys. *63*, 4592–4595.

Winder, S.J., Hemmings, L., Maciver, S.K., Bolton, S.J., Tinsley, J.M., Davies, K.E., Critchley, D.R., and Kendrick-Jones, J. (1995). Utrophin actin binding domain: analysis of actin binding and cellular targeting. J. Cell Sci. *108*, 63–71.

Yamada, S., Pokutta, S., Drees, F., Weis, W.I., and Nelson, W.J. (2005). Deconstructing the Cadherin-Catenin-Actin Complex. Cell *123*, 889–901.

Yonemura, S. (2011). Cadherin–actin interactions at adherens junctions. Curr. Opin. Cell Biol. *23*, 515–522.

Yu, D., Marchiando, A.M., Weber, C.R., Raleigh, D.R., Wang, Y., Shen, L., and Turner, J.R. (2010). MLCK-dependent exchange and actin binding region-dependent anchoring of ZO-1 regulate tight junction barrier function. Proc. Natl. Acad. Sci. U.S.A. *107*, 8237–8241.

Zhao, J., Krystofiak, E.S., Ballesteros, A., Cui, R., Itallie, C.M.V., Anderson, J.M., Fenollar-Ferrer, C., and Kachar, B. (2018). Multiple claudin–claudin cis interfaces are required for tight junction strand formation and inherent flexibility. Commun. Biol. *1*, 1–15.

Zihni, C., Mills, C., Matter, K., and Balda, M.S. (2016). Tight junctions: from simple barriers to multifunctional molecular gates. Nat. Rev. Mol. Cell Biol. *17*, 564–580.

Zimmerman, S.P., Asokan, S.B., Kuhlman, B., and Bear, J.E. (2017). Cells lay their own tracks – optogenetic Cdc42 activation stimulates fibronectin deposition supporting directed migration. J. Cell Sci. *130*, 2971–2983.

Chapter 3 – Disruption of epithelial barrier function by Influenza and SARS-CoV-2

Tiama Hamkins-Indik, Amanda Meriwether, Lienna Chan, Vikki Qian, Roni Weissman, Daniel A. Fletcher

This work is unpublished.

Abstract

The current SARS-CoV-2, the virus responsible for COVID-19, outbreak has created a devastating global health crisis that has been exacerbated by limited treatment options. Similarly, last year there were 39-56 million flu cases and 24,000-62,000 flu deaths in the USA. We investigated the SARS-CoV-2 E protein and the influenza NS1 protein as a potential molecular determinants and therapeutic target for one major symptom of both COVID-19 and influenza– breakdown of epithelial barrier function. Viruses are known to dysregulate epithelial barriers by targeting tight junctions. As the apical most cell-cell junction in epithelial cells, tight junctions regulate paracellular transport of ions, proteins, and immune cells. To achieve this function, tight junctions are organized by proteins containing PDZ domains. The PDZ domains bind to PDZ binding motifs (PBM) at the C-terminus of other proteins. Four amino acids in the PBM confer specificity to the PDZ-PBM interaction, allowing the PDZ-PBM interactions to act as modular building bricks for protein organization and signaling. To test the importance of the E protein PBM and NS1 protein PBM on epithelial barrier function, we built ectopic expression cell culture models and measured tight junction protein localization and barrier function. We found that the PBM of NS1 from different strains of influenza had a variable effect on barrier function. Most PBMs significantly decreased barrier function, despite variable amino acid sequence. Alternatively, we found that the PBM of the E protein of SARS-CoV-2 was not a determinant in barrier function, though expression of the E protein did result in reduced barrier function in lung epithelial cells.

Introduction

Each year influenza spreads globally, and last year there were 39-56 million flu cases and 24,000-62,000 flu deaths in the USA[1]. The ongoing SARS-CoV-2 outbreak has created a devastating global health crisis[2]. New therapeutic options are urgently needed, and basic studies of host-pathogen interactions have the potential to provide key insights into identifying and developing potential therapeutics. In this study we examine how individual proteins of influenza and SARS-CoV-2 influence epithelial barrier function. Influenza and SARS-CoV-2 infections cause overlapping symptoms, including the breakdown of cell-cell barriers resulting in cell infiltrates in the lung and lung edema, the accumulation of fluid in the lung which limits oxygen diffusion[3]. However, the mechanisms of how SARS-CoV-2 and influenza cause the breakdown of cell barriers is not fully understood.

Tight junctions are targeted by viruses to disrupt epithelial barrier function

Viruses target host proteins for degradation, sequestration, or downregulation ultimately resulting in a breakdown in cell-cell barriers by inducing apoptosis, inciting the release of cytokines, or directly targeting tight junction proteins (Figure 1A). Tight junctions are the apical most cell-cell junction in epithelial cells and are responsible for regulating paracellular transport of ions, proteins, and immune cells through epithelial cell[4]. Tight junctions also transduce signals to regulate cell polarization, proliferation, gene expression, and differentiation[5–7]. Many viruses have evolved to target tight junction proteins to break down cell-cell barriers, alter cell polarity, or affect signaling pathways in the cell[8]. Some viruses, such as HIV[9] and West Nile Virus[10], target tight junction proteins directly to pass between cells, enter the bloodstream, and spread infection. Others, such as Influenza A Virus[11] and SARS[12] are known to disrupt barrier function by targeting tight junction proteins involved in cell polarization and other cell signaling pathways. Breakdown of cell barrier function can be linked with clinical symptoms such as diarrhea, fluid buildup in the abdomen, and pulmonary edema[13].

PDZ-containing proteins are essential for tight junction formation and epithelial barrier function

PDZ domains are abundant protein interaction modules that bind to short PDZ binding motifs (PBM) at the C-terminus of other proteins. The last four amino acids at the C-terminus of the PBM confer specificity for PDZ binding partners, allowing for modular building bricks for protein organization and signaling[14,15]. PDZ domain-containing proteins such as the ZO-family, PATJ, PALS1, and MUPP1 regulate and organize the tight junction[16]. Many viruses have evolutionarily conserved PBMs including influenza, HIV, HPV, and SARS, which hijack existing host cell signaling pathways at the tight junction resulting in host cell changes, including altering barrier function, changing cell polarity, and inducing oncogenicity[8].

Could a PDZ binding motif (PBM) of influenza cause epithelial barrier function disruption?

Previous studies have shown that PBM of the NS1 protein of avian influenza A plays a role in regulating barrier function[17–20]. Interestingly, when all four residues the PBM of NS1 were mutated to alanine, barrier function was not reduced[20]. Notably, Scribble, Dlg1, MAGI-1, MAGI-2, and MAGI-3 were shown to interact with the PBM of NS1[20]. However, these studies are limited to examining the avian strain of influenza A. We sought better understand whether different strains on human influenza also disrupt barrier function and which PBMs, which vary by a single residue to all four, could be responsible.

Could a PDZ binding motif (PBM) of SARS-CoV-2 cause epithelial barrier function disruption?

We hypothesized that the PDZ binding motif (PBM) of the E protein is responsible, in part, for the loss of epithelial barrier function in SARS-CoV-2 infected cells. The E protein PBM of SARS-CoV, the virus responsible for the SARS outbreak, is important for viral pathogenicity. Notably, the E protein of SARS-CoV-2 shares 96% homology with and has the same PBM as the E protein

of SARS-CoV. SARS and COVID-19 also present similar symptoms, further suggesting similar pathways of disease progression. Previous studies of the E protein of SARS-CoV found that it plays a crucial role in cytokine production, barrier function, viral load, apical-basal polarity, and the ultimate survival of the host[12]. It has been shown that mice infected with the SARS virus die after ten days and have severe lung edema with cell infiltrates. However, genetically modifying the E protein to either delete the PBM and six preceding residues or mutate the last four amino acids to glycines results in 100% mouse survival after ten days. Additionally, these mice had mild or no lung edema with fewer cell infiltrates. Deleting the SARS E protein PBM reduced inflammatory cytokine expression, potentially limiting over-activation of the immune system. Furthermore, the viral titer in organs of infected mice was significantly reduced when the PBM of the E protein was removed. Additionally, ectopic expression of the SARS E protein in epithelial cells significantly changed barrier function and disrupted apical-basal polarity[21]. This data suggests that the PBM of the E protein of SARS-CoV plays a role in the pathogenicity of the virus, potentially through multiple pathways and binding partners targeting inflammatory cytokine production, barrier function, and polarity.

Blocking a PBM pathway may have therapeutic potential

Researchers identified PALS1 and syntenin as PDZ binding partners of the SARS-CoV E protein PBM[12,21]. PALS1 and syntenin target two different pathways: PALS1 interacts with PATJ and CRB3 to form the crumb complex, and syntenin activates p38 mitogen-activated protein kinase (MAPK). Both pathways ultimately lead to disruption of barrier function. To interfere with E protein-mediated activation of p38 MAPK, mice infected with wild type virus were administered SB 203580, a specific inhibitor of p38 MAPK activation. 80% of mice survived ten days post infection under this treatment, compared to 0% of mice who survived without drug treatment. Identifying drugs that interfere with players in PBM-mediated pathways thus seems promising.

Results

To examine how SARS-CoV-2 and influenza influence epithelial barrier function, we established an experimental system that is safe in BSL2 facilities. We built ectopic expression models, where an individual viral protein in expressed in relevant cell lines, this allows us to study how expression of one viral protein affects the cell without the risk of working with live virus. For our studies we focused on the E protein of SARS-CoV and SARS-CoV-2 and the NS1 protein of influenza.

The NS1 protein of influenza

To study the NS1 protein of influenza we fused a fluorescent tag, eGFP, onto the N-terminus of the protein with a linker (Figure 1B). As discussed, influenza mutates very quickly and we were interested in examining strain to strain differences. We were interested in focusing only on how the PBM of NS1 affects barrier function, so we used the protein sequence of NS1 from A/Puerto Rico/8/1934 H1N1 strain and only changed the last four amino acids to those of other strains as

well as a mutated PBM (mutPBM) to all alanine to disrupt any PDZ binding (Figure 1B). This strategy ensures that any stain to strain variability in NS1 is limited to just the effects of the PBM.

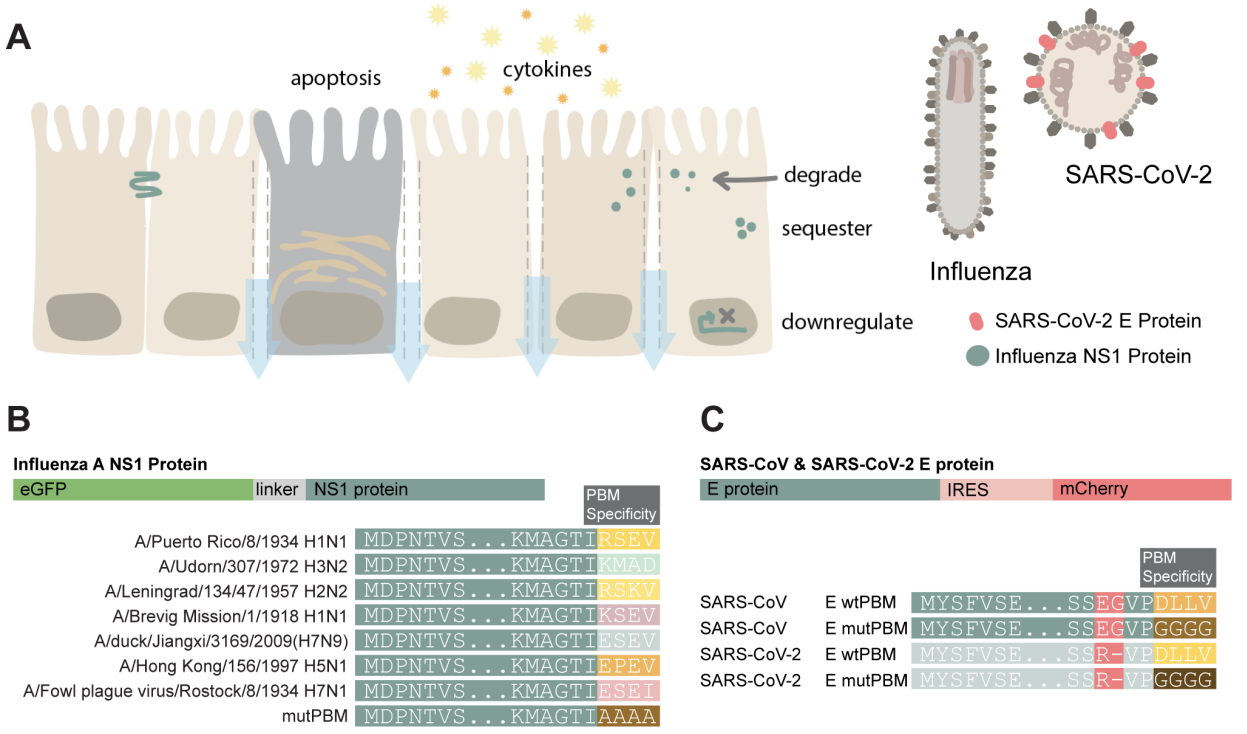

Figure 1. Constructs for expressing the Influenza A NS1 protein with PDZ-binding-motifs (PBMs) from various strains, and the SARS-CoV-2 E protein.

A) Viruses target host proteins for degradation, sequestration, or downregulation ultimately resulting in a breakdown in cell-cell barriers, in this study we examine two viruses: influenza and SARS-CoV-2.

B) Construct design for expressing Influenza A NS1 protein with PDZ-binding-motifs (PBMs) from various strains of influenza.

C) Construct design for SARS-CoV and SARS-CoV-2 E proteins with their native PBM (DLLV) and with glycine mutates (GGGG).

One critical aspect of barrier function is examining the localization and expression of tight junction proteins. We built MDCK II, canine kidney epithelial cells, expressing GFP-NS1 with various PBMs and sorted the cells for expressing cells. After expanding cells, we plated cells for immunofluorescence imaging, barrier function, western blot, and flow analysis. We found that cells drifted, though the strain of the PBM impacted how much the cells drifted (Supplemental Figure 1). ZO-1 and ZO-2 are adapter proteins at the tight junction that are responsible for, among other roles, organizing transmembrane tight junction proteins. We previously showed that knocking out both ZO-1 and ZO-2 results in tight junction proteins are no longer localized to cell-cell junctions and a corresponding dramatic decrease in barrier function[22]. We also examined a change in localization of two tight junction proteins, occludin, a transmembrane protein, and cingulin, another adapter protein at the tight junction. In wildtype MDCK II cells ZO-1, ZO-2, occludin, and cingulin colocalize and are enriched at the cell-cell junction, outlining cells (Figure 2A). In mixed populations of cells expressing GFP-NS1 and wt MDCK II, there is a clear

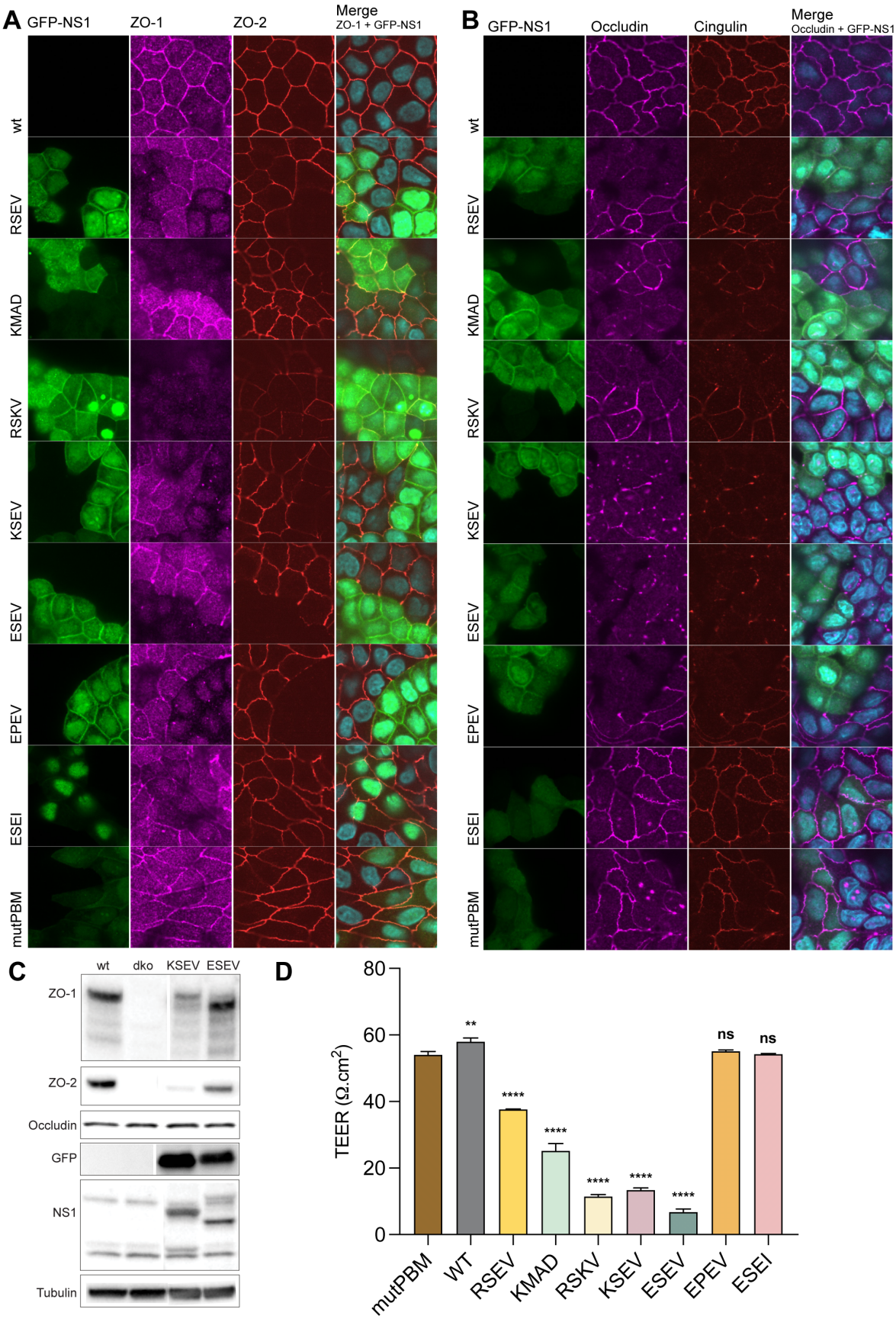
A
GFP-NS1
ZO-1
ZO-2
Merge
ZO-1 + GFP-NS1
wt
RSEV
KMAD
RSKV
KSEV
ESEV
EPEV
ESEI
mutPBM
B
GFP-NS1
Occludin
Cingulin
Merge
Occludin + GFP-NS1
C
wt
dko
KSEV
ESEV
ZO-1
ZO-2
Occludin
GFP
NS1
Tubulin
D
TEER (Ω.cm²)
80
60
40
20
0
**
****
****
****
****
****
ns
ns
mutPBM
WT
RSEV
KMAD
RSKV
KSEV
ESEV
EPEV
ESEI

Figure 2. Influenza NS1 protein with PBMs from multiple strains alter localization and quantity of tight junction proteins and reduce barrier function.

A) Micrographs of MDCK II cells expressing influenza NS1 protein with PBMs from different strains after four days of growth showing GFP-NS1 (green), ZO-1 (magenta), ZO-2 (red).
B) Micrographs of MDCK II cells expressing influenza NS1 protein with PBMs from different strains after four days of growth showing GFP-NS1 (green), occludin (magenta), cingulin (red).
C) Western blot of MDCK II cells expressing influenza NS1 protein with PBMs from different strains after four days of growth probed for ZO-1, ZO-2, occludin, GFP, NS1, and tubulin.
D) Barrier function measure with TEER of MDCK II cells expressing influenza NS1 protein with PBMs from different strains after four days of growth. ANOVA showing p-values for comparison with mutPBM, ** $p < 0.01$, **** $p < 0.0001$

distinction between cells expressing GFP-NS1 and the wt MDCK II cells. In cells expressing GFP-NS1 with PBMs from various influenza A strains we found that, to varying extent, ZO-1, ZO-2, occludin, and cingulin are less enriched at cell-cell junctions. In GFP-NS1 mutPBM cells, however, ZO-1, ZO-2, occludin, and cingulin localization appears as in wt MDCK II, with all highly enriched at the cell-cell junctions (Figure 2B). This implies that the PBM of NS1 modulates tight junction protein localization. Furthermore, there seems to be some variability in the extent of how ZO-1 and ZO-2 are removed from the cell-cell junctions, depending on which strain of the PBM is expressed.

For cell lines that had a large proportion of GFP positive cells (Supplemental Figure 1), PBMs KSEV and ESEV, we used a western blot to probe for changes in protein expression. We found reduced expression of ZO-1 and ZO-2 in these cell lines, though occludin expression remained unchanged. We further found that bands of NS1 as identified with an anti-NS1 antibody were two different lengths, implying that the PBM may regulate NS1 itself, perhaps driving a yet to be discovered cleavage event to alter the protein size (Figure 2C).

Lastly, we measured barrier function using transepithelial electrical resistance (TEER) and with a fluorescent molecule permeability assay (data not shown) of our cells expressing GFP-NS1 with different PBMs. We found that the PBM differentially altered barrier function, with some PBMs reducing barrier function to a greater extent than others (Figure 2D). When NS1 is expressed with a mutated PBM (mutPBM), there is a slight but statistically significant decrease in barrier function from cells expressing wildtype NS1. We found that PBMs from many strains (RSEV, KMAD, RSKV, KSEV, ESEV) significantly decreased barrier function in comparison to NS1-mutPBM (Figure 2D). We sorted all cells for the same expression level then expanded for three passages. Despite the identical treatment of these cells, cells with different PBMs drifted to varying degrees (Supplemental Figure 1). In addition to the PBM blocking tight junction PDZ proteins, the PBM may be affecting barrier function measurements by driving extrusion or changes in proliferation to alter the percentage of cells expressing NS1.

The E protein of SARS-CoV-2

To study the E protein of SARS-CoV and SARS-CoV-2 we built an expression system where the untagged protein is expressed with a fluorescent reporter, mCherry (Figure 1C). We found that adding an N-terminal tag onto the E protein disrupted expected localization which is reported to be localized to the ERGIC complex[23] to diffuse in the cytoplasm (Supplemental Figure 2). As localization of the E protein may be important for sequestering or degrading PDZ binding partners we opted to express the E protein without a fluorescent tag. SARS-CoV and SARS-CoV-2 have nearly identical sequence identity, and the same PBM. However, a deletion in the amino acid sequence may play a role in affinity, though not specificity, of PDZ domain binding. As such, we expressed the SARS-CoV and SARS-CoV-2 E protein with wildtype PBM (wtPBM) and with a mutated PBM to gycines (mutPBM) (Figure 1C).

The E protein of SARS-CoV (SARS) and SARS-CoV-2 (nCoV) was expressed in identical numbers of A549 cells, a human lung carcinoma cell line. We observed morphology differences in this cell line, where wildtype (wt) A549 formed a dense cell layer, while cells expressing the E protein were fewer in number and more spread out (Figure 3A). While the E protein had an effect on morphology, we did not observe any differences due to the PBM of the E protein (SARS and nCoV). We quantified the number of cells, and found that cells expressing the E protein were significantly fewer for SARS E-GGGG, nCoV E, and nCoV E-GGGG. We did not see a significant change in cell number between wtPBM and mutPBM for both SARS and nCoV (Figure 3B). Time lapse images of newly transduced A549 cells (data not shown) revealed that expression of the E protein reduced the number of actively dividing cells, and no apoptotic cells were observed. This implies that the E protein alters proliferation rates to influence final cell number.

While overall cell number was not affected by different PBMs we did find different numbers of cells expressing our reporter to be influenced by PBM in A549 (Figure 3C). The A549 cells were expressing the E protein with a mCherry reporter, therefore after transduction we could compare the number of cells expressing mCherry and infer which cells were expressing the E protein. We found that for nCoV E protein, a mutated PBM (E-GGGG), increased the percentage of mCherry positive cells. These studies bear repeating to add more statistical significance. When we used another cell culture model, MDCK II, a canine kidney epithelial cell line, we found no different in the percentage of cells that were mCherry positive (Figure 3D).

We measured barrier function with TEER and found that expression of the E protein from both SARS and nCoV significantly reduced barrier function in A549 cells after growth for 5 days. However, the PBM of the E protein of SARS and nCoV did not significantly change barrier function (Figure 3E). This implies that the PBM is not responsible for the decrease in barrier function observed in A549. Expression of the E protein of SARS and nCoV in MDCK II did not alter barrier function (Figure 3F). This data suggests that the E protein interacts with host proteins

that are only expressed in A549; which could be due to cell type (kidney vs. lung) or species (human vs. canine).

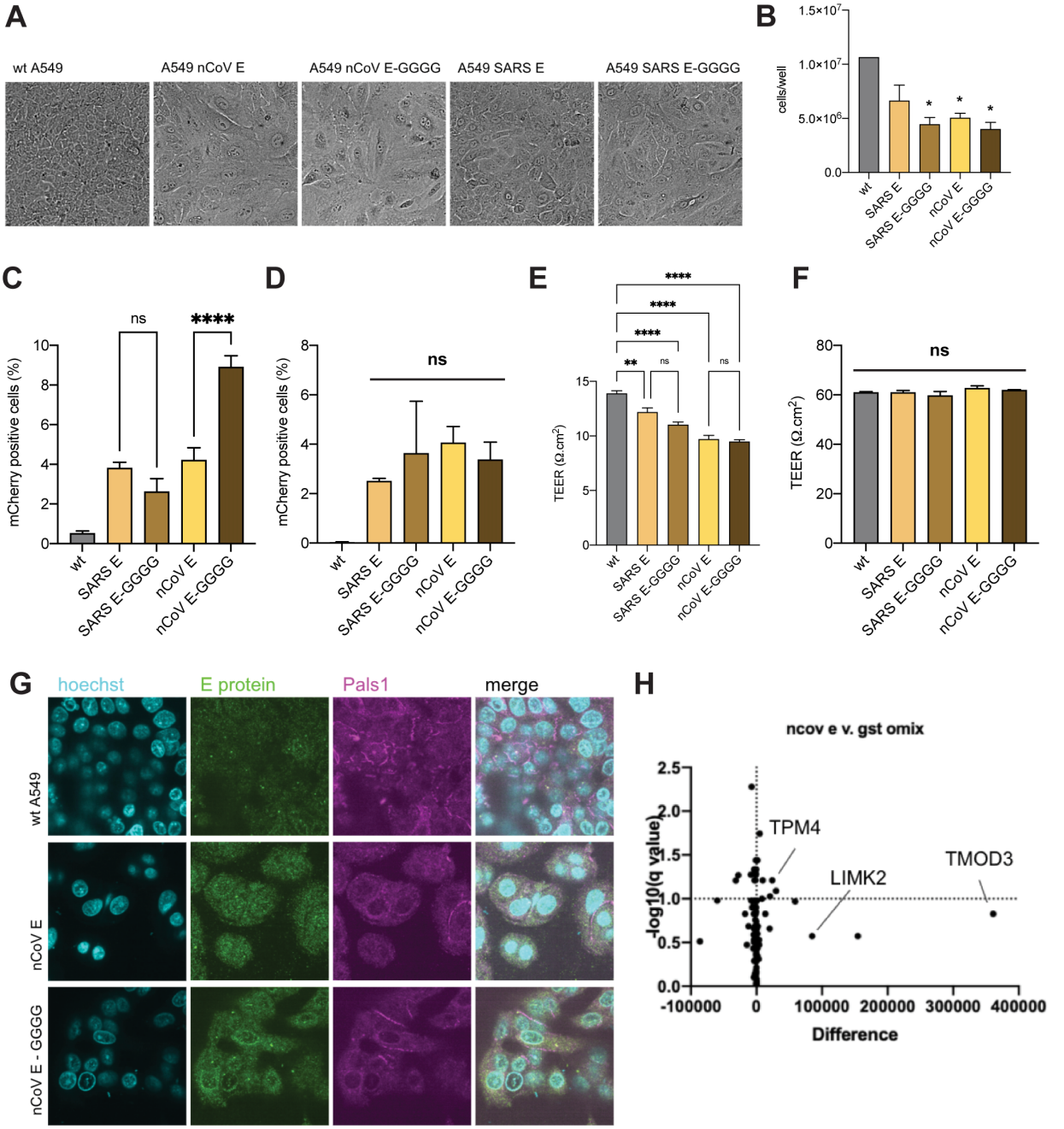

Figure 3. SARS-CoV-2 (nCoV) and SARS-CoV (SARS) E protein alters cell number and barrier function, though not in PBM-dependent manner.

A) Micrographs of A549 cells 7 days after lentiviral transduction with SARS-CoV E protein (SARS E and SARS E-GGGG) and SARS-CoV-2 E protein (nCoV E and nCoV E-GGGG).

B) Quantification of cell number 7 days after plating A549 cells expressing SARS-CoV E protein (SARS E and SARS E-GGGG) and SARS-CoV-2 E protein (nCoV E and nCoV E-GGGG). ANOVA showing p-values for comparison with wt A549, * $p < 0.05$.

C) Quantification of mCherry positive cells 7 days after plating A549 cells expressing SARS-CoV E protein (SARS E and SARS E-GGGG) and SARS-CoV-2 E protein (nCoV E and nCoV E-GGGG) with an mCherry reporter. ANOVA showing p-values for comparison with wt A549, **** $p < 0.0001$.
D) Quantification of mCherry positive cells 7 days after plating MDCK II cells expressing SARS-CoV E protein (SARS E and SARS E-GGGG) and SARS-CoV-2 E protein (nCoV E and nCoV E-GGGG) with an mCherry reporter. ANOVA showing p-values for comparison with wt MDCK II.
E) Barrier function measured with TEER after 4 days of growth of A549 cells expressing SARS-CoV E protein (SARS E and SARS E-GGGG) and SARS-CoV-2 E protein (nCoV E and nCoV E-GGGG). ANOVA showing p-values for comparison with wt A549.
F) Barrier function measured with TEER after 4 days of growth of MDCK II cells expressing SARS-CoV E protein (SARS E and SARS E-GGGG) and SARS-CoV-2 E protein (nCoV E and nCoV E-GGGG). ANOVA showing p-values for comparison with wt MDCK II.
G) Micrograph of of A549 cells expressing SARS-CoV E protein (SARS E and SARS E-GGGG) and SARS-CoV-2 E protein (nCoV E and nCoV E-GGGG) after 4 days, DAPI (blue), E protein (green), PALS1 (magenta).
H) Proteins identified from a pull-down using the last 10 amino-acids of SARS-CoV-2 (nCoV) fused to GST as bait with the lysate of A549 cells.

Previous studies have found that the SARS E protein bind to PALS1 through it PBM. We therefore used immunofluorescent (IF) imaging to detect changes in localization of PALS1 in A549 expressing the E protein. Our imaging results were inconclusive; we could not say whether PALS1 at cell-cell junctions is reduced in cells expressing the E protein of nCoV (Figure 3G).

Lastly, we performed a pull down to identify binders of the SARS and nCoV E protein PBM. To accomplish this, we purified a bait where we fused the last ten amino acids of the E protein to GST with a linker, previous studies have used the last 10 amino acids of a PBM to identify PDZ binding partners[24]. We incubated our PBM bait with cell lysate form A549 to pulldown PDZ binders and used mass spectrometry to identify proteins. Potential binders are plotted against their q value error from a GST control bait (no PBM). While we identified some binders of interest, this study showed no binders that we only identified in the PBM pull down, suggesting that the PBM may simply be altering the ability of the GST to pull down non-specific binders (Figure 3H).

Discussion

Influenza NS1 PBMs as a potential target for treating viral infection

Our work adds to the body of work on how viruses use PBMs to target host proteins. Our work shows how multiple strains of a single virus, influenza, can result in the same functional output: barrier function. The various strains of NS1 PBMs interact with PDZ domains that drive ZO-1, ZO-2, cingulin, and occludin from cell-cell junctions and ultimately affect barrier function. Future work will include looking at the molecular mechanisms of how the various PBMs can target the same pathway. Are the PBMs binding to the same target protein? Are they binding to different host proteins that all affect barrier function? Pull down assays, especially with mass spectrometry, could be used to identify PDZ domain binding partners. PBMs are tricky to target with therapeutics, as they are wide ranging and are hard to make specific to only the viral PBM. That

said, there are PBM based therapeutics that have made it to clinical trials[25]. We see potential for building a screen based on the various PBMs of influenza to block interactions with host proteins, though with fast-mutating influenza, therapeutics may quickly be obsolete. Alternatively, if the molecular pathways that influenza targets to breakdown cell-cell barriers is known and is already a drug target, already existing therapeutics could be repurposed to help treat the symptoms of severe influenza.

SARS-CoV-2 E protein as a target for further study

The results from our studies on the E protein of SARS-CoV and SARS-CoV-2 are far less conclusive. The PBM of the E protein itself does not influence barrier function. Given that SARS-CoV infectivity seems to be dependent on the PBM[12,21], it is worth continuing the study of the SARS-CoV-2 E protein PBM to see which host proteins it interacts with, and identify which pathways it is acting through. We found that expression of the E protein alone reduced proliferation rates in A549 cells. This suggests that the E protein is interacting with host proteins to alter cell behavior. In our studies, A549 cells proliferation rate is not dependent on the E protein PBM, therefore other binding motifs and domains of the E protein should be explored to determine how the E protein reduces proliferation. In the long term, proliferation rates can affect barrier function; if cells cannot divide to replace normal turnover in the lung, the reduced cell number can result in lower barrier function. This could explain, at least in part, how the E protein reduces barrier function in A549 cells. Understanding that the E protein PBM does not drive changes in barrier function also leads to questions of how the barrier is affected during infection. Is it due to cytokine response? Are proliferation results affected driving a decrease in barrier function? Are there other SARS-CoV-2 proteins that interact with host proteins to alter barrier function?

Ectopic expression limitations

Our studies show the value of using ectopic expression models of viral proteins individually to be able to tease out the effects on one protein on cell function. As we showed with our SARS-CoV-2 studies, the choice of cell line is critical for understanding our results. Further exploration of relevant human cell lines and primary human cell lines may be necessary to understand viral protein interactions with host proteins only expressed in certain cell types. This approach should be combined with full virus infection to better understand the role of a given protein in the context of infection. For the influenza NS1 protein, we plan on making PBM mutations in a reverse genetics engineered influenza virus, and measure changes in viral titer and barrier function.

Viral evolution

Barrier function is crucial for understanding the symptoms of influenza and SARS-CoV-2, and we are interested in uncovering future therapeutic targets. We are also interested why so many viruses evolved to disrupt tight junction proteins. What is the evolutionary advantage for viruses to disrupt barrier function? We know that some viruses break down barriers to spread though the blood stream, but could there be a propagation advantage for virus replicating in cells with reduced

barrier function? We have already built cells without tight junction proteins ZO-1 and ZO-2, and we can examine whether not having a tight junction or barrier function alters virus fitness, by measuring viral titer from cells with and without tight junctions. In other words, does decreasing barrier function increase viral fitness?

Conclusions

We show that the PBM from various strains of the NS1 protein of influenza can all impact barrier function, despite having different PBM specificity. This opens the door to further research into which pathways are targeted by influenza. We also show that the E protein of SARS-CoV-2 may cause a change in barrier function, though this effect may be cell-type specific. Our studies lay the groundwork for understanding how influenza and SARS-CoV-2 viral proteins may interact with host proteins to breakdown cell-cell junctions affecting overall epithelial barrier function.

Methods

Generations of constructs

eGFP-Influenza NS1 (A/Puerto Rico/8/1934 H1N1) constructs were cloned using PCR and Gibson assembly into a pHR backbone for lentivirus production. The last four amino acids, which confer specificity of the PBM, of NS1 were modified to PBMs from other strains of influenza, as well as mutPBM (AAAA) using PCR and Gibson assembly. SARS-CoV-2 (The GenBank sequence for SARS-CoV-2 isolate 2019-nCoV/USA-WA1/2020, accession MN985325) and SARS-CoV(NC_004718) E protein sequences were cloned with an IRES and mCherry reporter into pHR backbone using PCR and Gibson assembly. For GST-PBM constructs for affinity pull down and mass spectrometry linked GST with a flexible linker (GGGGS) to the final 10 amino acids of the E protein from SARS-CoV and SARS-CoV-2 using PCR and Gibson assembly into a pet28a backbone. All DNA oligos were ordered from IDT.

Cell culture and cell lines

MDCK II cells were a gift from Keith Mostov (UCSF) and maintained at 37°C and 5% CO_2 in high glucose DMEM (4.5 g/l), supplemented with 10% fetal bovine serum (FBS) and penicillin-streptomycin (pen-strep). Similarly, A549 cells were maintained at 37°C and 5% CO_2 in high glucose DMEM (4.5 g/l), supplemented with 10% FBS, and pen-strep. NS1 and E protein constructs were cloned using PCR and Gibson assembly into pHR backbone plasmids. Cell lines were created through lentivirus infection. Briefly, HEK293 cells were transfected with TransIT-293 (Mirus) according to manufacturer's instructions with three plasmids, pMD.2g, p8.91 and pHR with viral protein constructs. Cells were grown for 2 days, after which media was collected and virus was concentrated with Lenti-X (Clontech) according to manufacturer's instructions. Lentivirus was added to freshly passaged MDCK II cells, and cells were grown for two days before passaging and removing media. For E protein constructs with neomycin resistance, cells were selected in high glucose DMEM (4.5 g/l), supplemented with 10% FBS, pen-strep, and 500 ug/mL G418. NS1 cell lines created with fluorescently tagged proteins were sorted and normalized for

expression using the UC Berkeley Flow Cytometry Facility (BD Bioscience Influx Sorter). Cell lines were confirmed with confocal imaging.

Immunostaining and imaging

Cells were plated on a 2.1 μg/mL collagen I gel (Cellmatrix), pH 7.4, in a glass-bottom cell culture dish at a cell density of 3.33E4 cells/cm^2 and grown for 2 or 4 days. Fixation methods were optimized for each antibody used. Cells were either fixed in 1% of 4% PFA at room temperature for 20 minutes or in 100% EtOH or 100% MeOH at -20° C for 30 min. Cells fixed in PFA were first permeabilized with 0.2% (v/v) Triton X-100 at room temperature for 10 minutes. To block, fixed cells were incubated in 5% (w/v) BSA in PBS at room temperature for 1 hour. Cells were then incubated with primary antibodies in a 1% (w/v) BSA in PBS solution at room temperature for 1 hour. Secondary antibodies were applied in a 1% BSA in PBS solution at room temperature for 1 hour. Three PBS washes were done after each antibody incubation step. Cells were incubated in Hoechst for 10 minutes at room temperature. Cells were imaged on a Ti Eclipse microscope (NIKON) using a 60x 1.49 NA objective and an iXon Ultra EMCCD (Andor). For live cell imaging, cells were plated identically, but not fixed, and imaged on the same microscope.

Immunoblot

Cells were plated in a 6-well plate at a cell density of 3.33E4 cells/cm^2 and grown 4 days. Cells were lysed in RIPA buffer (1% (v/v) Triton X-100, 0.1% (w/v) SDS, 1% (w/v) deoxycholate) with protease inhibitors (Thermo Fisher) on ice for 30 minutes. Lysate was spun at 13,000 rpm for 15 minutes at 4° C. A BCA assay (Thermo Fisher) was performed according to manufacturer's instructions to determine protein concentration. All samples were diluted to the same protein concentration. Loading buffer was added to lysate, and samples were run on a 4-20% polyacrylamide gel (Bio-Rad) and at 200 V for 35 minutes. Gel was transferred using iBlot (Thermo Fisher) according to manufacturer's instructions at 20 V for 5 min. Ponceau S was incubated for 10 minutes at room temperature to visualize total protein. The blot was blocked in 2% (w/v) BSA in PBS with 0.1% Tween-20 (PBS-T) for 1 hour at room temperature. Primary antibody was administered in 1% (w/v) BSA overnight on a shaker at 4° C, and secondary was administered in 1% (w/v) BSA for 1 hour on a shaker at room temperature. Three, 10-minute PBS-T washes were performed after each antibody incubation. The blot was visualized on a ChemiDoc (BioRad).

Barrier assays

Cells were plated on 24-well Transwell inserts (polyester (PE), 0.4 μm pore size (Corning)) coated with 30 μg/mL Collagen I (Cellmatrix) at a cell density of 3.33E4 cells/cm^2. Transepithelial electrical resistance measurements (TEER) was performed using the ENDOHM6 cup chamber (WPI) with EVOM2 (WPI) in cell culture media.

Flow cytometry

Cell lines created with fluorescently tagged proteins or fluorescent reporters were measured with ThermoFisher Attune NxT Acoustic Focusing Cytometer and analysis was done in FlowJo software.

GST-PBM purification

GST-PBM constructs were expressed in Rosetta and induced with IPTG for 4 hours at 37C. Cells were resuspended in lysis buffer (25 mM HEPES pH 7.2, 150 mM NaCl, 1 mM DTT, 1x PMSF) and lysed by sonication. Cell debris was pelleted and the supernatant was bound onto glutathione resin (GBiosciences). Resin was washed with 10 column volumes of wash buffer (25 mM HEPES pH 7.2, 150 mM NaCl, 1 mM DTT) and protein was eluted with elution buffer (25 mM HEPES pH 7.2, 150 mM NaCl, 1 mM DTT, 30mM glutathione). Protein was desalted into storage buffer (25 mM HEPES pH 7.2, 150 mM NaCl, 1 mM DTT, 10% glycerol) and flash frozen.

Affinity purification

A549 were grown to confluency in a 150 mm2 dish, and lysed in 50mM HEPES pH7.4, 150mM NaCl, 1mM MgCl2, 1% Triton-x-100, protease inhibitor cocktail I (Calbiochem) for 10 minutes on ice, before being spun at 14,000 rpm for 10 min at 4 C. Cell lysate was was pre-cleaned by incubating with glutathione beads for 2 hours at 4 C. Pre-cleaned cell lysate was incubated with GST-PBM proteins for 2 hours at 4 C before 3 washes.

Mass spectrometry

On bead trypsin digestion was performed as reported[24], before desalt and clean-up with C18 Omix tips. Samples were resuspended 50% acetonitrile, 0.1% acetic acid. In-solution liquid chromatography and mass spectrometry were performed according to standard procedures by the Vincent J. Coates Proteomics/Mass Spectroscopy laboratory (UC Berkeley).

Acknowledgements

This work used the Vincent J. Proteomics/Mass Spectrometry Laboratory at UC Berkeley, supported in part by NIH S10 Instrumentation Grant S10RR025622.

Supplemental Figures

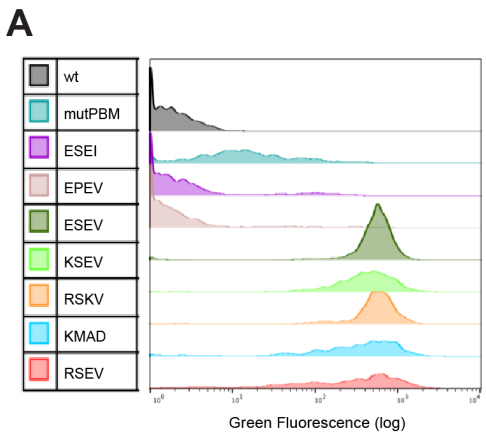

Supplemental Figure 1. Cell expression drift after expression of GFP-NS1 with various PBMs

A) Flow cytometry data of GFP expression of MDCK II cells expressing GFP-tagged influenza NS1 protein with PBMs from different strains.

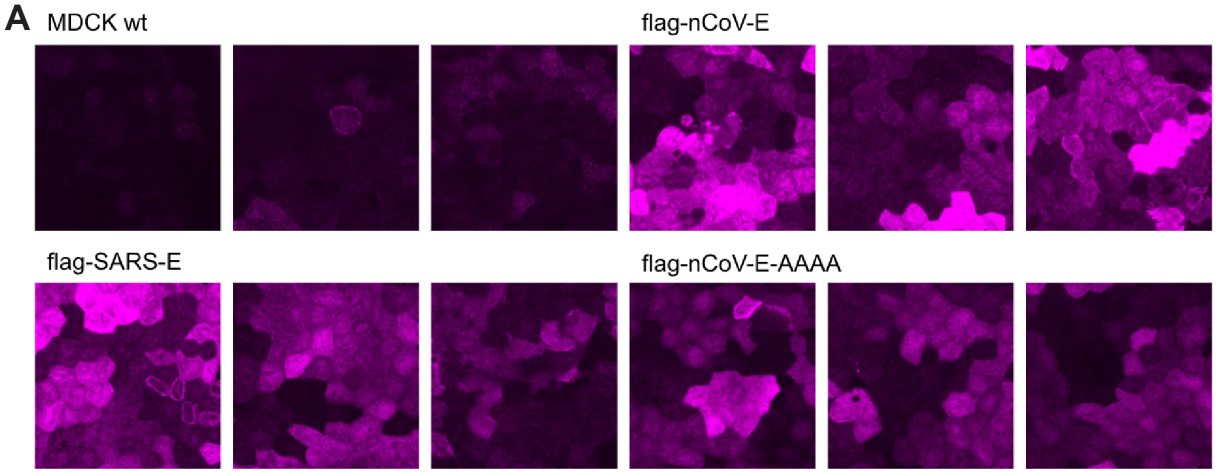

Supplemental Figure 2. Flag-tag E protein is diffuse in cytoplasm.

A) Micrographs of A549 cells expressing flag-tagged SARS-CoV E protein (SARS E and SARS E-GGGG) and flag-tagged SARS-CoV-2 E protein (nCoV E and nCoV E-GGGG).

References

1. 2019-2020 U.S. Flu Season: Preliminary In-Season Burden Estimates | CDC. https://www.cdc.gov/flu/about/burden/preliminary-in-season-estimates.htm (n.d.).

2. Sohrabi, C. *et al.* World Health Organization declares Global Emergency: A review of the 2019 Novel Coronavirus (COVID-19). *Int J Surg* **76**, 71–76 (2020).

3. Martines, R. B. *et al.* Early Release - Pathology and Pathogenesis of SARS-CoV-2 Associated with Fatal Coronavirus Disease, United States - Volume 26, Number 9—September 2020 - Emerging Infectious Diseases journal - CDC. *Emerg Infect Dis* **26**, 2005–2015 (2020).

4. González-Mariscal, L., Betanzos, A., Nava, P. & Jaramillo, B. E. Tight junction proteins. *Prog Biophysics Mol Biology* **81**, 1–44 (2003).

5. Zihni, C., Mills, C., Matter, K. & Balda, M. S. Tight junctions: from simple barriers to multifunctional molecular gates. *Nat Rev Mol Cell Bio* **17**, 564–580 (2016).

6. Georgiadis, A. *et al.* The Tight Junction Associated Signalling Proteins ZO-1 and ZONAB Regulate Retinal Pigment Epithelium Homeostasis in Mice. *Plos One* **5**, e15730 (2010).

7. Tsukita, S., Furuse, M. & Itoh, M. Structural and signalling molecules come together at tight junctions. *Curr Opin Cell Biol* **11**, 628–633 (1999).

8. Torres-Flores, J. M. & Arias, C. F. Tight Junctions Go Viral! *Viruses* **7**, 5145–5154 (2015).

9. Dallasta, L. M. *et al.* Blood-Brain Barrier Tight Junction Disruption in Human Immunodeficiency Virus-1 Encephalitis. *Am J Pathology* **155**, 1915–1927 (1999).

10. Verma, S. *et al.* West Nile virus infection modulates human brain microvascular endothelial cells tight junction proteins and cell adhesion molecules: Transmigration across the in vitro blood-brain barrier. *Virology* **385**, 425–433 (2009).

11. Jackson, D., Hossain, Md. J., Hickman, D., Perez, D. R. & Lamb, R. A. A new influenza virus virulence determinant: The NS1 protein four C-terminal residues modulate pathogenicity. *Proc National Acad Sci* **105**, 4381–4386 (2008).

12. Jimenez-Guardeño, J. M. *et al.* The PDZ-Binding Motif of Severe Acute Respiratory Syndrome Coronavirus Envelope Protein Is a Determinant of Viral Pathogenesis. *Plos Pathog* **10**, e1004320 (2014).

13. Guttman, J. A. & Finlay, B. B. Tight junctions as targets of infectious agents. *Biochimica Et Biophysica Acta Bba - Biomembr* **1788**, 832–841 (2009).

14. Saras, J. & Heldin, C.-H. PDZ domains bind carboxy-terminal sequences of target proteins. *Trends Biochem Sci* **21**, 455–458 (1996).

15. Nourry, C., Grant, S. G. N. & Borg, J.-P. PDZ Domain Proteins: Plug and Play! *Sci Signal* **2003**, re7–re7 (2003).

16. Itallie, C. M. V. & Anderson, J. M. Architecture of tight junctions and principles of molecular composition. *Semin Cell Dev Biol* **36**, 157–165 (2014).

17. Yu, J. *et al.* PDlim2 Selectively Interacts with the PDZ Binding Motif of Highly Pathogenic Avian H5N1 Influenza A Virus NS1. *Plos One* **6**, e19511 (2011).

18. Kumar, M., Liu, H. & Rice, A. P. Regulation of Interferon-β by MAGI-1 and Its Interaction with Influenza A Virus NS1 Protein with ESEV PBM. *Plos One* **7**, e41251 (2012).

19. Golebiewski, L., Liu, H., Javier, R. T. & Rice, A. P. The Avian Influenza Virus NS1 ESEV PDZ Binding Motif Associates with Dlg1 and Scribble To Disrupt Cellular Tight Junctions §. *J Virol* **85**, 10639–10648 (2011).

20. Liu, H. *et al.* The ESEV PDZ-Binding Motif of the Avian Influenza A Virus NS1 Protein Protects Infected Cells from Apoptosis by Directly Targeting Scribble ▿ . *J Virol* **84**, 11164–11174 (2010).

21. Teoh, K.-T. *et al.* The SARS Coronavirus E Protein Interacts with PALS1 and Alters Tight Junction Formation and Epithelial Morphogenesis. *Molecular Biology of the Cell* (2010).

22. Belardi, B. *et al.* A Weak Link with Actin Organizes Tight Junctions to Control Epithelial Permeability. *Dev Cell* (2020) doi:10.1016/j.devcel.2020.07.022.

23. Nieto-Torres, J. L. *et al.* Subcellular location and topology of severe acute respiratory syndrome coronavirus envelope protein. *Virology* **415**, 69–82 (2011).

24. Thomas, M., Myers, M. P., Massimi, P., Guarnaccia, C. & Banks, L. Analysis of Multiple HPV E6 PDZ Interactions Defines Type-Specific PDZ Fingerprints That Predict Oncogenic Potential. *Plos Pathog* **12**, e1005766 (2016).

25. Christensen, N. R. *et al.* PDZ Domains as Drug Targets. *Adv Ther* **2**, 1800143 (2019).

Chapter 4 – Developing a switchable actin binder

Tiama Hamkins-Indik, Brian Belardi, Marija Podolski, Kathy Wei, Daniel A. Fletcher

This work is unpublished.

Abstract

The actin cytoskeleton plays a critical role in diverse cell processes, including formation of tight junctions between epithelial cells and phagocytosis of target particles by immune cells. Regulation of these distinct processes within the shared cytoplasm of a cell requires a broad set of actin-binding proteins that organize actin filaments into specific structures through tethering, crosslinking, and nucleating activities. We developed a switchable actin binder that binds to actin only when a cell-permeable small molecule is administered and used it to investigate actin tethering in live cells. The switch is comprised of three fused protein domains – an actin-binding motif and two flanking domains that heterodimerize to block actin binding. For the actin-binding motif, we chose the actin binding site (ABS) of ZO-1 and sandwiched it between truncated Bcl-xL and the modified peptide, BH3, whose binding can be disrupted by the small molecule A-1155463. We confirmed that when the switchable actin binder is expressed in cells and the small molecule is administered, the switchable actin binder colocalizes with actin. Furthermore, we show that the switchable actin binder is tunable; with increasing concentration of the small molecule, there is increasing colocalization of the switchable actin binder with actin. To demonstrate functionality of the probe, we engineered ZO-1, an adapter protein that links actin filaments with tight junction proteins, by replacing the ABS of ZO-1 with the switchable actin binder. We found that when actin binding was inhibited in ZO-1, epithelial barrier function was reduced based on measurements of trans-epithelial electrical resistance. By administering A-1155463 to open the switchable actin binder within ZO-1, barrier function significantly increased. As a second demonstration of the switchable actin binder, we incorporated a CAAX motif that localized the switch to the plasma membrane and expressed it in macrophages. We found that when A-1155463 was administered, phagocytosis of antibody-coated targets decreased, filopodia were suppressed, and Fc receptor enrichment at the target site required more time. As indicated by these results, a switchable actin binder that controls when, where, and how much actin binding occurs in live cells has the potential to be a useful and versatile tool for investigating the role of actin networks in cells.

Introduction

Actin is controlled by the proteins that bind to it

The actin cytoskeleton provides mechanical structure in the cell and is composed of polymerized actin proteins. Actin is regulated by actin binding proteins in the cell, which control where, how, and when actin structures form. These structures include the mesh-like cellular cortex and bundled stress fibers[1–3]. Actin structures play a role in many cell processes like vesicular trafficking[4],

endocytosis[5,6], migration[7], cell-cell junctions[8–14], and phagocytosis[15–17], to name a few. A critical part of most actin processes is that they are dynamic. Actin polymerizes, depolymerizes, is stabilized by actin binding proteins, and is bound and unbound to proteins throughout the cell. Changes in when a protein binds to actin can have far reaching consequences. Vinculin, which when under force, binds more to actin in the cell, stabilizing the cell-cell junction, the adherens junction[18]. Ezrin similarly acts as a switchable actin binder and can be phosphorylated to open an actin-binding domain, which allows for the formation of microvilli in epithelial cells[19]. We were inspired by how proteins evolved to control when, where, and how much they bind to actin and we wondered if we could engineer such a protein as a tool to study the role of actin binding in cell.

Bcl-xL and BH3 are a domain and motif from proteins involved in the apoptosis pathway. They bind to each other tightly to prevent cell death and were originally targets for drug development to treat cancer[20–23]. In cells, it was shown that inhibiting Bcl-xL and BH3 interaction with small molecule competitive binders increased cell death in cancer cells, while healthy cells showed no increase is cell death[24]. Bcl-xL and BH3 were first demonstrated as a useful tool for protein engineering when they were used to make an inducible Ras GTPase enzyme[25], and later an inducible Cas9 for gene editing[26,27]. We took inspiration from this work to develop our own inducible actin binder.

Actin binding at tight junctions

As discussed in Chapter 2, tight junctions are responsible for regulating paracellular transport of ions, proteins, and immune cells through epithelial cell layers. ZO family proteins (ZO-1 and ZO-2), among other functions, link tight junction transmembrane proteins to actin filaments. We found that ZO-1 lacking the actin binding site (ABS) significantly reduces barrier function. Furthermore, we found that when we stably expressed ZO-1 with actin binding domains with varying affinities for actin, there was a maximum barrier function with a weak link to actin and a reduced barrier function. This led us to ask the question, does turning on actin binding in ZO-1 after epithelial cell-cell contacts are formed recover wildtype barrier function? If it does, what it the timing of recovering barrier function? In this study, we begin to understand time scales of tight junction reorganization by inducing actin binding in ZO-1 at the tight junction in live cells and measuring barrier function in concert.

Actin binding during macrophage phagocytosis

Actin is also involved in macrophage phagocytosis. Phagocytosis is the process where a macrophage engulfs and digests pathogens, bacteria, cells, cell debris, and foreign material[28–30]. Actin regulation and binding has been shown to be involved in many stages of phagocytosis[29]. During probing, actin-enriched protrusions from the macrophage wave around the cell to probe for something to eat[31,32]. During sensing, the macrophage determines whether or not to eat something. Receptors in the membrane of the macrophage bind to their target, and must cluster to activate signaling cascades[17,28,33–36]. In the picket fence model, transmembrane proteins that bind to the actin

cytoskeleton act as "pickets" affecting the diffusion and clustering of receptors in the membrane[16,37,38]. Last, the cell engulfs and internalizes its target, which, again, is dependent on actin to mediate. To study actin and how it interacts with the cell membrane influences the phases of phagocytosis, we engineered the switchable actin binder to be embedded in the membrane to control when and how much actin tethering at the membrane takes place during phagocytosis.

Here we show the development of a switchable actin binder that allows us to control where, when, and how much actin binds in the cell. For our design strategy, we explored domain order, linker length, and actin binding domain to develop a switchable actin binder that works in live cells. We then show that it is tunable, where varying the concentration of the small molecule to dissociate Bcl-xL and BH3 results in varying amounts of actin binding in live cells. We controlled where actin was binding in the cell by building fusion proteins and localized actin binding to the tight junction and the cell membrane. Lastly, we show that we can dynamically alter barrier function by inducing actin binding to ZO-1, and inhibit phagocytosis by tethering actin to the plasma membrane.

Results

Design Strategy

We took inspiration from previous work to engineer an activatable Cas9 enzyme[26,27], and designed our switchable actin binder such that the binding of Bcl-xL and BH3 sterically inhibits actin binding, but upon the application of on a small molecule inhibitor A-1155463 (A115) the actin binding domain is exposed (Figure 1A). The design space we explored included the order of domains, linker length between domains, and actin binding motif used (Figure 1B). For our studies we used short actin binding motifs actin binding site (ABS) of ZO-1 (22 amino acids) and Lifeact (17 amino acids) which we modeled to span the distance between Bcl-xL and BH3 and we predicted to be inhibited. One challenge in the design process is that the structure of these motifs is unknown. To accommodate for these uncertainties we explored a broad design space by varying linker length.

To test for changes in actin binding in live cells, we expressed each design for a switchable actin binder in HeLa cells fused to GFP for visualization. We quantified changes in actin enrichment by fixing cells after 30 min with 10 μM A115 and measuring colocalization with F-actin as stained with phalloidin. Actin enrichment was quantified as the average intensity of the switchable actin binder where actin is (indicated by the presence of fluorescently-tagged phalloidin) over the average intensity of the switchable actin binder in the cytoplasm (indicated by the absence of fluorescently-tagged phalloidin). Our initial screen of designs showed that actin binding domain, linker length and domain order influence how the construct colocalizes with actin with the administration of A115 (Figure 1C). The most promising designs were Bcl-xL-ABS-BH3 and BCL-XL-lifeact-BH3 as both showed significant changes in actin enrichment. However, the Lifeact switchable actin binder had significant actin binding even in its inhibited state (Figure 1C).

We therefore decided to move forward with the ABS from ZO-1 with no linkers: Bcl-xL-ABS-BH3. We believe that the longer linker lengths surrounding Lifeact had too much flexibility, preventing a steric inhibition of actin binding. All of our designs with BH3 at the N-terminus of the protein showed both low actin enrichment and no inducible activity (Figure 1C). This configuration may have inhibited actin binding, regardless of whether the small molecule induced a conformation change.

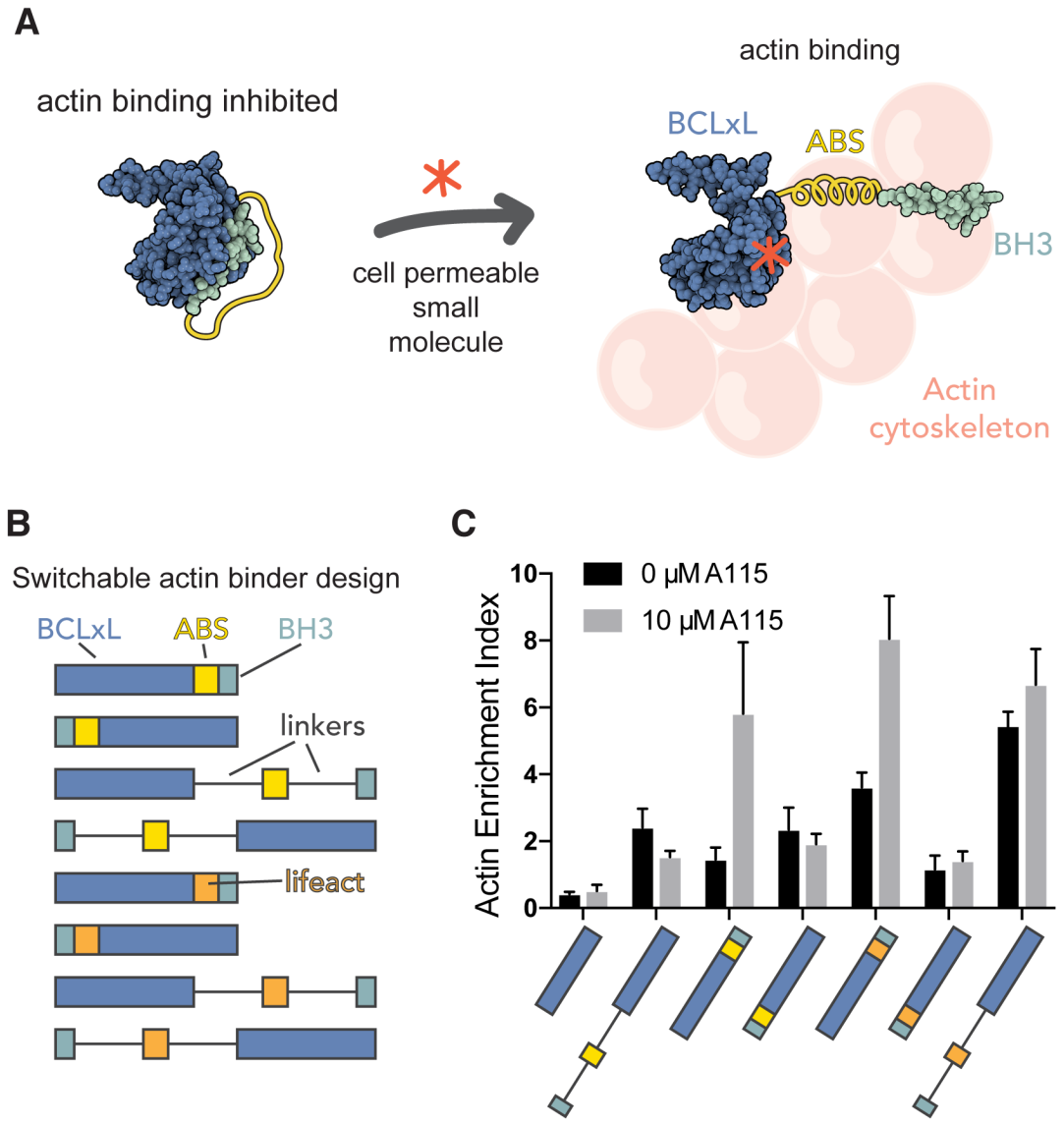

Figure 1 Design of a switchable actin binder

A) Schematic of a the switchable actin binder showing the inhibition of actin binding by the interaction Bcl-xL and BH3 and the disruption of this interaction with a small molecule to reveal the actin binding domain.
B) Designs assessed in the development of a switchable actin binder.
C) Quantification of actin enrichment, a measure of colocalization of GFP-tagged switchable actin binder designs with phalloidin (to stain F-actin) in HeLa cells with and without 30 minute incubation with 10 µM.

Characterization of the switch.

After picking our best candidate for a switchable actin binder we wanted to better understand the timing of how the switch worked. We verified our actin enrichment assay by visualizing changes in localization of the switchable actin binder over 30 minutes with live imaging. We found that over the course of 30 minutes we were able to see a change in localization of the switchable actin binder (Figure 2A). We predicted that as the switchable actin binder changes localization we would see regions with less actin to decrease in intensity and regions with more actin to increase in intensity. To quantify this, we measured intensity changes in various regions of interest in the cell and found that some regions decreased in intensity while others increased (Figure 2B). This indeed suggests that the switchable actin binder is changing location from an unbound state that is diffuse in the cytoplasm to binding to actin.

We hypothesized that the proportion of activated switches would increase as we increase the concentration of A115; that we could alter the amount of the switch that was bound to actin in a dose dependent manner. To test this, we incubated HeLa cells expressing Bcl-xL-ABS-BH3 with increasing amounts of A115 and measured actin enrichment as colocalization with phalloidin. We found that the switchable actin binder is tunable; the switchable actin binder increasingly colocalizes with phalloidin with an increase in A115 concentration after 30 minute incubation (Figure 2C).

We next assessed whether the switchable actin binder was reversible and on what time scale the switchable actin binder dissociated from actin after removal of the A115. Preliminary results show that actin binding was not reversible on the order of hours. While further work is necessary to fully understand the rate of dissociation, this data suggests that after an initial incubation for 30 minutes the A115 can be washed off to minimize off-target effects while maintaining robust actin binding for hours (Figure 2D).

Actin binding at tight junctions

We hypothesize that turning on actin binding in ZO-1 will recover barrier function. To test this hypothesis, we inserted the switchable actin binder surrounding the actin binding site of ZO-1 such that when expressed in cells the ABS of ZO-1 is auto-inhibited and after the application of A115 ZO-1 will be able to bind to actin. (Figure 3A). We expect that if actin binding was fully inhibited barrier function would be reduced from wildtype ZO-1 levels to those of ZO-1 lacking the ABS (ZO-1ΔABS). When ZO-1 actin switch was stably expressed in cells and was presumably in an autoinhibited state we found that barrier function was significantly reduced compared to cells expressing ZO-1, decreasing 75% (Figure 3B). Interestingly, the ZO-1 actin switch cells did not reduce barrier function as much as ZO-1ΔABS cells did, suggesting that the ABS was only partially blocked by our switch. Future studies are needed understand the degree of partial blocking.

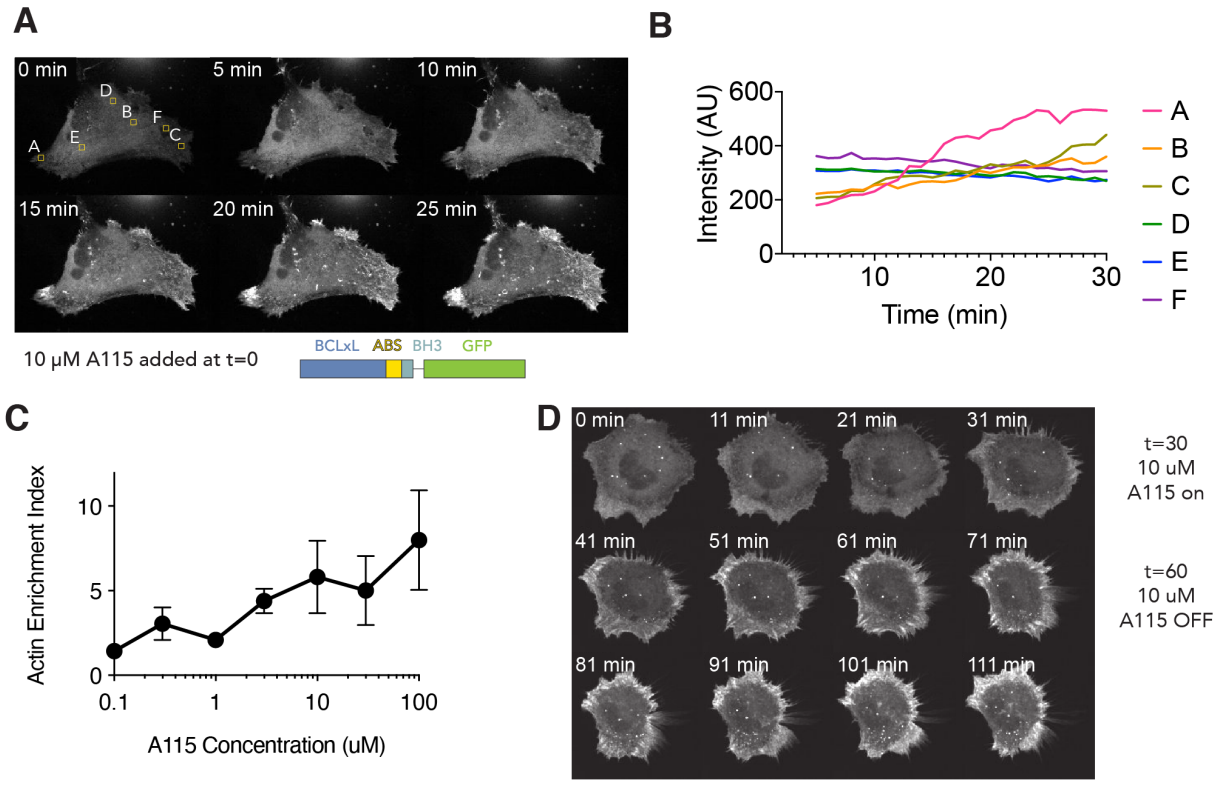

Figure 2 Characterization of the switchable actin binder

A) Micrographs in a time series showing localization of switchable actin binder after administration of 10 µM of A115 at time 0 min.
B) Intensity over time of regions labelled in Figure 1A.
C) Actin enrichment index measured for varying concentration of A115 in HeLa expressing a GFP-tagged switchable actin binder.
D) Micrographs in a time series showing localization of switchable actin binder after administration of 10 µM of A115 at time 30 min followed by removal of A115 at time 60 min.

We next tested whether barrier function was rescued with the application of A115 and found that barrier function increased with A115 dose, with higher concentration able to rescue barrier function to wildtype levels after three hours (Figure 3C). While these results are promising, we also found a dose response of barrier function to application of A115 to wildtype cells, with increasing dose decreasing barrier function (Figure 3D). This implies that A115 has off-target effects, and within 3 hours, drives significant changes in barrier function. To confirm that this wasn't an off-target effect of A115 we tested multiple small molecules known to interact specifically with Bcl-xL, and all decreased barrier function (data not shown). This suggests that inhibiting endogenous Bcl2 or Bcl-xL in cells significantly decreases barrier function. To isolate the influence of the ZO-1 actin switch, we normalized barrier function results in Figure 3C to wildtype ZO-1 levels.

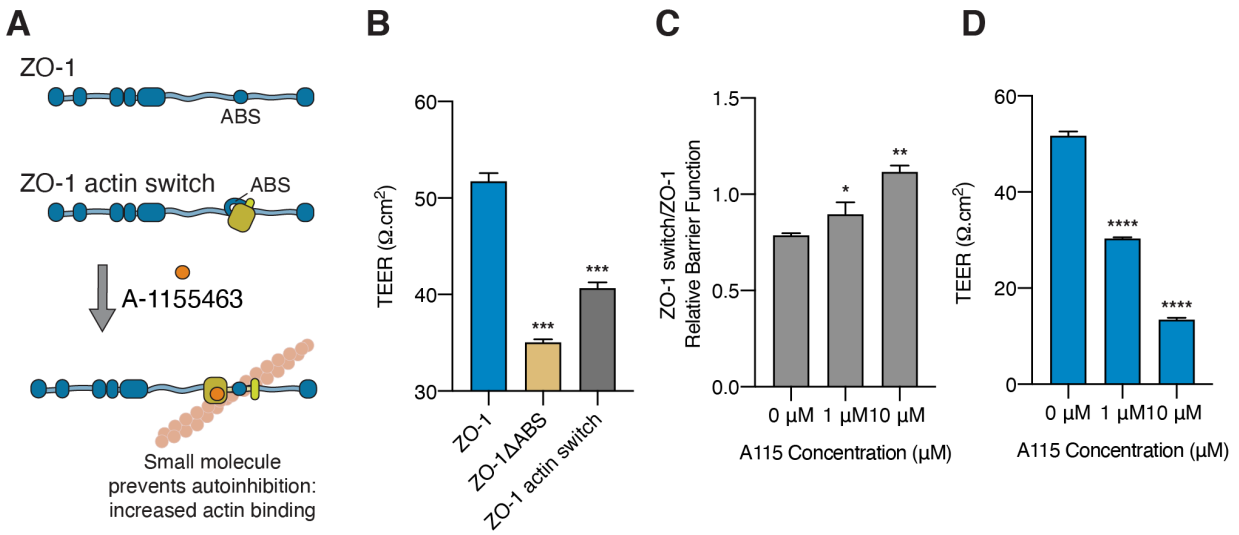

Figure 3 A switchable actin binder in ZO-1 recovers wildtype barrier function on the order of hours.

A) Schematic of design of ZO-1 with actin switch.
B) TEER measurements of MDCK II with ZO-1 and ZO-2 knocked out expressing ZO-1, ZO-1 lacking its actin binding site (ABS), and ZO-1 with the actin switch. *** $p < 0.001$
C) Relative barrier function as measured with TEER, ZO-1 actin switch/ZO-1 after administration of 0 μM, 1 μM, and 10 μM for 3 hours. * $p < 0.05$, ** $p < 0.01$
D) TEER measurements of MDCK II with ZO-1 and ZO-2 knocked out expressing ZO-1. **** $p < 0.0001$

Actin binding to the membrane during macrophage phagocytosis

In addition to examining actin binding in the specific context of tight junctions and ZO-1 we were also interested in localizing actin binding to other sub-cellular contexts. We designed the switchable actin binder to embed into the membrane with a CAAX motif[39,40]. The goal of this construct was to provide a method to control when and how much actin is tethered to the plasma membrane (Figure 4A). The biological process we were interested in examining is macrophage phagocytosis. Macrophages are a type of immune cell responsible for engulfing and digesting targets, whether it be pathogenic bacteria, dying cells, or even cancer. To examine how actin tethering to the membrane affects Fc receptor mediated phagocytosis we expressed the switchable actin binder with a CAAX motif (Bcl-xL-ABS-BH3-GFP-CAAX) in RAW 264.7 macrophages and measured phagocytosis with a bead eating assay.

In our bead eating assay, glass beads with a labeled lipid bilayer coated with antibody are incubated with macrophages and the amount of bead internalized is assessed. We found that raw macrophages expressing the membrane switchable actin binder ate significantly fewer beads when exposed to A115, while A115 does not alter the amount of beads internalized by wildtype raw macrophages (Figure 4B). These findings imply that actin bound to the membrane inhibits phagocytosis, so we designed experiments to explore which stage of phagocytosis (probing, early signaling and cup formation, pseudopod extension, or phagosome closure) is affected by membrane bound to the membrane.

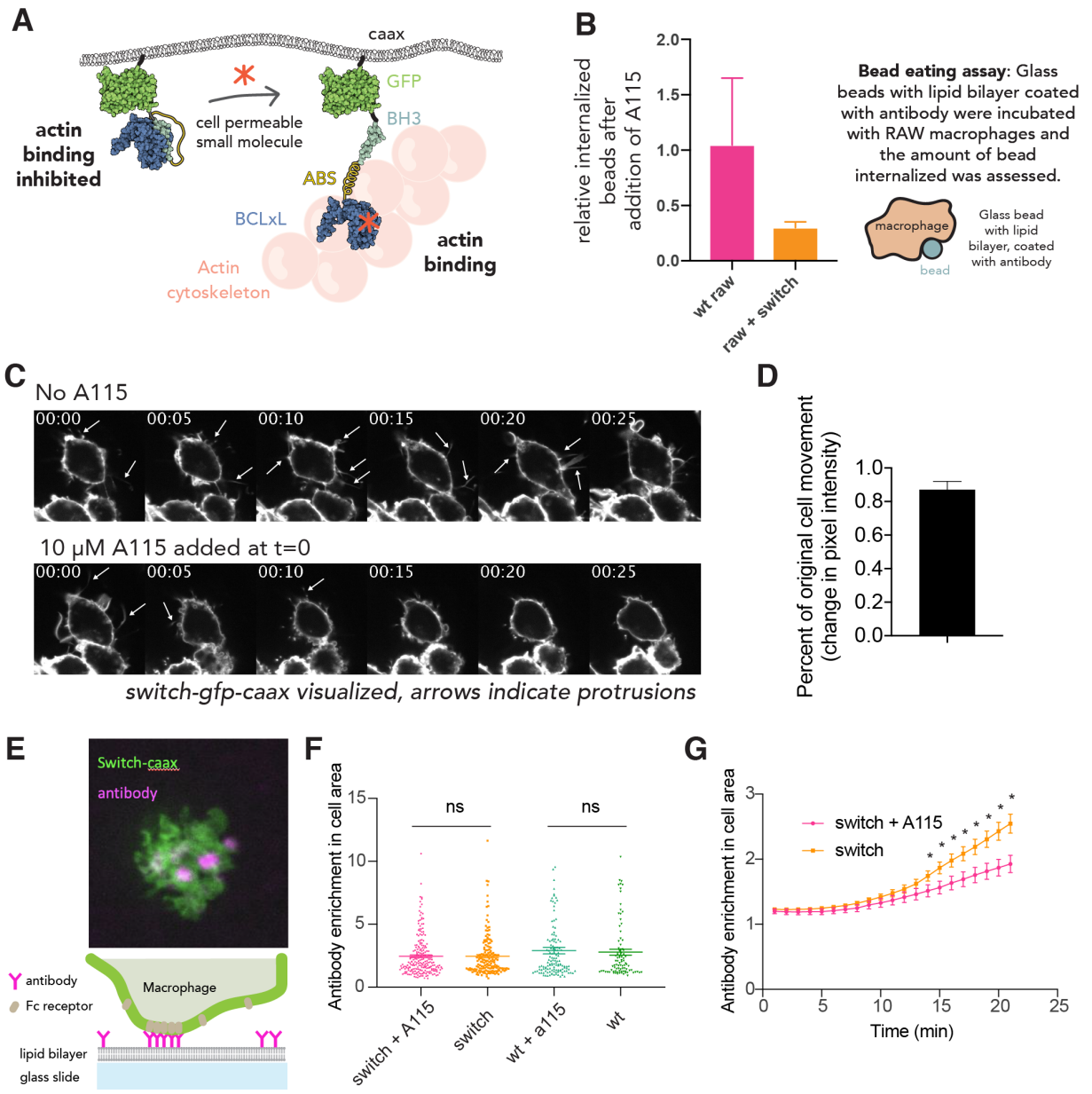

Figure 4 Actin tethering to the cell membrane decreases macrophage phagocytosis by decreasing probing and changing dynamics of antibody enrichment.

A) Schematic of our design of membrane switchable actin binder.
B) Relative number of glass beads with lipid bilayer coated with antibody internalized by macrophages after the addition of 10 μM A115.
C) Micrographs in a time series showing raw macrophages expressing the membrane switchable actin binder before and after the addition of 10 μM of A115 at time 0 min. Arrows indicate macrophage protrusions.
D) Quantification of macrophage movement as the difference in pixels between frames of a time series.
E) Micrograpah of macrophage dropped onto a supported lipid bilayer coated with antibody (magenta) expressing the membrane switchable actin binder (green, switch-caax) and schematic of experiment setup.
F) Quantification of antibody enrichment in the cell area of a raw macrophage dropped onto a supported lipid bilayer coated with antibody with or without administration of 10 μM of A115 after 60 minutes.
G) Quantification of antibody enrichment in the cell area over time of a raw macrophage dropped onto a supported lipid bilayer coated with antibody with or without administration of 10 μM of A115 after 60 minutes. * $p < 0.05$.

To explore whether probing, or the movement of long actin-rich membrane extensions around a macrophage, decreases with application of A115. We took time lapse videos of macrophages expressing the membrane switchable actin binder. We found that the number of protrusions and cell movement decreases after the addition of A115 (Figure 4C and 4D).

Lastly, we were interested in how the dynamics of clustering of receptors in the macrophage changes with actin tethered to the membrane. To explore this question, we made a supported lipid bilayer (SLB) with antibody that can diffuse and move freely in the SLB. We then dropped macrophages expressing the membrane switchable actin binder onto the opsonized SLB and measured how the antibody clustered under the cell (Figure 4E). We calculated antibody enrichment as intensity of the antibody in the cell area divided by intensity of antibody outside of the cell taken using total internal reflection fluorescence (TIRF) microscopy. We found that antibody is enriched after 60 minutes to a similar degree under cells expressing the switchable actin binder with or without the application of A115 in wildtype macrophages and macrophages expressing the membrane switchable actin binder (Figure 4F). This suggests that A115 does not have off-target affects in wildtype RAW macrophages that could alter antibody enrichment. We found that the dynamics to reach the same final enrichment are altered with the application of A115. Macrophages expressing the switchable actin binder enrich antibody at a faster initial rate compared to macrophages expressing the switchable actin binder when A115 is added (Figure 4G). This suggests that actin tethering to the membrane slows the clustering of receptors.

Discussion

Designing a switchable actin binder

Here we show the design, characterization and two potential applications for a switchable actin binder. While our design methodology was devised with the express purpose of developing this switchable actin binder, we believe that this methodology is widely applicable to other autoinhibited protein switches. We imagine a suite of proteins that could target protein binding in cells.

We believe that there is an opportunity for more optimization of a switchable actin binder. There are many native actin binding domains which preferentially bind to different actin structures[41,42], designing a switchable actin binder based on these domains could allow for scientists to target protein binding with more specificity. The switchable actin binder could be made with protein domains that dimerize with the addition of a small molecule (such as FRB/FKBP/rapamycin[43]) which could be engineered to study how a decrease in actin binding affects biology. In addition to Bcl-xL andBH3, there are photo-activatable domains[44,45] which could be engineered to allow for targeted actin binding.

As we did not have structural information for the ZO-1 ABS or Lifeact, we designed the switchable actin binder rather blind. As structures are known for many actin binding domains, we believe that

an alternative design route would be to use modeling software to specifically design switchable actin binders knowing which amino acids are responsible for actin binding to sterically block. Our workflow to measure actin binding with a quick cell assay can be adapted for the development of other switchable binders.

Characterization

We show that the switchable actin binder is tunable, with increasing concentration of A115 there is increased colocalization of the switchable actin binder with F-actin. While we showed the tunable nature of the switch in live cells, in further work it would be useful to better characterize the switchable actin binder outside of the cell. A more concrete understanding of how drug concentration influences the concentration of open and closed switchable actin binders is also needed, ideally with structural studies. Furthermore, to better understand the dynamics of the switch, it would be useful to examine purified switchable actin binders *in vitro*.

The fast-acting nature of inducing actin binding, on the scale of minutes, makes the switchable actin binder particularly useful for studying many actin-driven processes, such as phagocytosis, endocytosis, migration, and cell division, which occur on the order of hours.

Actin binding at tight junctions

The switchable actin binder seemed perfectly applicable to study actin binding at the tight junction as the actin binding site (ABS) of ZO-1 was used in the development of this tool. However, this system brought to light that there are off-target effects of the A115 family of drugs that dramatically and quickly alter barrier function. As an easy next step, we would like to incubate with A115 then wash out, especially given that robust actin binding is maintained for hours after the application of A115 in HeLa cells. The mechanism, of how A115 dramatically decreases barrier function in wildtype cells is also unknown. Though this may explain why this class of drugs failed to advance in clinical trials[46,47].

Even given the off-target effects, our results hint that actin binding can reorganize the tight junction on the order of hours. This suggests that targeting actin binding at the tight junction may be a method of modulating barrier function for therapeutic delivery.

Actin binding to the membrane in macrophage phagocytosis

To examine phagocytosis we developed a membrane bound switchable actin binder. We have shown that tethering actin to the membrane leads to decreased phagocytosis and that two key stages of phagocytosis, probing and receptor clustering are affected by membrane tethering. Our fluorescence recovery after photobleaching (FRAP) data shows that the t1/2 (half the time it takes to reach maximum fluorescence recovery) of the membrane switchable actin binder is greater when A115 is applied, suggesting diffusion is slowed (Supplemental Figure 1). This data supports a picket fence model where actin adjacent to the membrane bound to transmembrane proteins can

slow diffusion of receptors in the membrane. To build upon our work, FRAP experiments on macrophage receptors, rather than the membrane switchable actin binder itself, will help elucidate the degree to which the diffusion rate of receptors with no direct actin binding changes when there is more actin tethered to the membrane. Our data about the role of membrane/actin interactions during phagocytosis are tantalizing and this work opens the door to more questions.

Can we modulate receptor clustering by tuning actin binding at the membrane? As a next step, we propose exposing macrophages to varying concentrations of A115 and assessing changes in the dynamics of antibody enrichment under cells. Does actin binding at the membrane alter efficiency of engulfment after an activation signal? At cooler temperatures beads bind to cells but are not engulfed, we can examine engulfment in isolation by only administering A115 after beads are bound to cells, then use temperature to induce engulfment.

Our design of the switchable actin binder is broadly localized to the entire plasma membrane. In future work we could fuse the switchable actin binder to various binding domains to specifically locate the switch to induce actin binding only at the phagocytic cup. For example, the switch could be fused to specific lipids (e.g. PIP2 which is enriched in the phagocytic cup) or fused to various receptors (e.g. Fc receptor) to confine actin binding to the phagocytic cup. Actin driven processes at the membrane occur in many systems beyond macrophage phagocytosis. We believe that this tool is widely applicable to study a wide variety of cellular processes, such as endocytosis and cell migration.

Conclusion

Overall, we show the development of a tunable, inducible, and movable actin binder that allows us to control when, where, and how much actin binds in a cell. Here, we demonstrate how the switchable actin binder can be used to study barrier function and macrophage phagocytosis. We also suggest compelling future studies to develop more switchable actin binders and learn more about the role of actin tethering to the membrane in biological processes. We believe that this tool will be widely applicable and look forward to seeing how it is adapted from other scientists in the future.

Methods

Generation of constructs

The switchable actin binding designs were designed with a truncated Bcl-xL (Q07817-1, 4-198) and BH3 (APPNLWAAQRYGR ELRRMADEGEGSFK) in various orientations, ABS (PAMKPQSVLTRVKMFENKRSASLETKKD) or lifeact (MGVADLIKKFESISKEE) with linkers (GGGGS or GGGGSGGGGS) of different lengths, linked to eGFP in a pcDNA3.1 backbone. Initial designs were created by Pinecone (https://ccc.serotiny.bio/pinecone) and manufactured by Genscript. ZO-1 (human ZO-1 AA1-1748), ZO-1ΔABS (human ZO-1 AA1-1748, ΔAA1257-1284), ZO-1 actin switch with the switchable actin binder in place of the ABS

((human ZO-1 AA1-1748, ΔAA1257-1284) were cloned in a pHR backbone using Gibson assembly. To embed the switchable actin binder in the plasma membrane we added a CAAX motif (MSKDGKKKKKKSKTKCVIM) to the C-terminus of the switchable actin binder: Bcl-xL-ABS-BH3-eGFP-CAAX in pHR backbone using Gibson assembly.

Cell culture and cell lines

MDCK II cells were a gift from Keith Mostov (UCSF) and maintained at 37°C and 5% CO_2 in high glucose DMEM (4.5 g/l), supplemented with 10% fetal bovine serum (FBS) and penicillin-streptomycin (pen-strep). Similarly, HeLa cells were maintained at 37°C and 5% CO_2 in high glucose DMEM (4.5 g/l), supplemented with 10% FBS, and pen-strep. RAW 264.7 macrophage-like cell line was obtained from the UC Berkeley Cell Culture Facility. Cells were cultured in RPMI 1640 media (Corning) supplemented with 10% heat-inactivated fetal bovine serum (HI-FBS, Thermo Fisher Scientific) and 1% Pen-Strep (Thermo Fisher Scientific) in non-tissue culture-treated 10 cm dishes (VWR) at 37°C, 5% CO2.

Constructs were cloned using PCR and Gibson assembly into pHR or pc3.1 backbone plasmids. Cell lines were created through lentivirus infection. Briefly, HEK293 cells were transfected with TransIT-293 (Mirus) according to manufacturer's instructions with three plasmids, pMD.2g, p8.91 and pHR with viral protein constructs. Cells were grown for 2 days, after which media was collected and virus was concentrated with Lenti-X (Clontech) according to manufacturer's instructions. For MDCK II cells, lentivirus was added to freshly passaged MDCK II cells, and cells were grown for two days before passaging and removing media. For RAW 263.7 macrophages, 1 mL of lentiviral supernatant was added to 5x105 RAW 264.7 macrophages and cells were spinoculated at 300 x g for 30 minutes at room temperature. Cells were resuspended and plated into a 10 cm non-tissue-culture dish. MDCK II cell lines created with fluorescently tagged proteins were sorted and normalized for expression using the UC Berkeley Flow Cytometry Facility (BD Bioscience Influx Sorter). Cell lines were confirmed with confocal imaging.

Immunostaining and imaging

HeLa cells were imaged on glass bottomed 8 well chambers that had been coated with 10ug/ml fibronectin in PBS for 30 min in a glass-bottom cell culture dish. Fixation methods were optimized for each antibody used. Cells were either fixed in 4% PFA at room temperature for 20 minutes. Cells fixed in PFA were first permeabilized with 0.2% (v/v) Triton X-100 at room temperature for 10 minutes. To block, fixed cells were incubated in 5% (w/v) BSA in PBS at room temperature for 1 hour. Cells were then incubated with phalloidin for 30 min at room temperature. Cells were imaged on a Ti Eclipse microscope (NIKON) using a 60x 1.49 NA objective and an iXon Ultra EMCCD (Andor). For live cell imaging, cells were plated identically, but not fixed, and imaged on the same microscope. All live cells were maintained at 37°C, 5% CO2 with a stage top incubator (Okolab) during imaging.

Actin enrichment assay

To assess colocalization of the switchable actin binder designs with F-actin, HeLa cells were imaged on glass bottomed 8 well chambers that had been coated with 10ug/ml fibronectin in PBS for 30 min in a glass-bottom cell culture dish. We transfected HeLa cells plated on using lipofectamine 3000 (Thermo Fisher # L3000001) according to manufacturer's instructions. We allowed cells to grow for 24 hours before administering A-1155463 (Fisher Scientific NC1298858) in varying doses for 30 minutes. Cells were then fixed as above and stained with phalloidin. Cells were imaged using confocal microscopy (Nikon). Image analysis and processing was performed in MATLAB. The phalloidin channel was used as a mask, and an actin enrichment index was calculated such that $Actin\ enrichment\ index = \frac{Average\ construct\ intensity\ inside\ phalloidin\ mask}{Average\ construct\ intensity\ inside\ phalloidin\ mask}$.

Barrier function assay

Cells were plated on 24-well Transwell inserts (polyester (PE), 0.4 μm pore size (Corning)) coated with 30 μg/mL Collagen I (Cellmatrix) at a cell density of 3.33E4 cells/cm^2. Transepithelial electrical resistance measurements (TEER) was performed using the ENDOHM6 cup chamber (WPI) with EVOM2 (WPI) in cell culture media.

ZO-1, ZO-2, and double knockout (dKO) cell lines were developed in chapter 2[11], were created by first building a Cas9-expressing MDCK II cell line. Briefly, a lentiCas9-Blast (Addgene) plasmid was used to create stably expressing-Cas9 cell lines by selection under 5 ug/mL blasticidin for 7 days. Cas9 expression was confirmed with immunoblot. Three guide RNAs (gRNAs) for TJP1 were examined to create the ZO-1 KO. The three pLenti-gRNA-puro plasmids were transduced into Cas9-expressing cells before selection in 10 μg/mL puromycin for 6 days. Knockout was initially confirmed with immunofluorescence imaging of ZO-1. Clonal cell lines were created by dilution plating, where a single cell suspension (5 cells/mL) was plated in a 96-well tissue culture dish. On day 7, each well was checked for a single colony, and on day 14, cells were passaged. Knockout was verified with immunofluorescence, immunoblot, and genomic sequencing. dKO cells were created by following the protocol above with multiple TJP2 gRNAs and several TJP1 KO clones. After double knockout verification, a clone generated from gRNA 2 for TJP1 and gRNA 1 for TJP2 was used in subsequent experiments.

Bead Eating

Cell-like reconstituted target-particles were generated according to previously published protocol[34] summarized in the following sections.

Formation of cell-like target particles

40 μL of 4.07 μm silica beads (Bangs Laboratories) were cleaned using a 3:2 mixture of H2SO4:H2O2 (Piranha) for 30 minutes while sonicating. Cleaned beads were spun down at 1000 x g and washed 3 times with 1 mL pure water before being resuspended in 400 μL of water. Cleaned beads were stored at room temperature. To form SLBs, 40 μL of SUVs was added to 160

μL of MOPS buffer (25 mM MOPS (3-(N-morpholino)propanesulfonic acid), Thermo Fisher Scientific), 125 mM NaCl, pH 7.4), along with 20 μL of clean bead slurry. The mixture was incubated at room temperature for 15 minutes while rotating continuously. Coated beads (also referred to as target particles) were spun down at 50 x g for 1 minute, and 200 μL of the solution was removed and replaced with PBS (Corning).

Addition and quantification of protein on target particles

AlexaFluor647-labeled anti-biotin mouse IgG (clone BK-1/39, Thermo Fisher Scientific) were diluted in PBS to appropriate concentrations for target particle experiments. 50 μL of SLB-coated beads was added to 50μL of protein dilution, and beads were incubated at room temperature for 20 minutes with continuous rotation.

Target particle phagocytosis assay

35,000 macrophages were seeded in wells of a tissue-culture flat-bottom 96-well plate (Falcon) in 100 μL of RPMI 1640 medium. Post-seeding, cells were incubated at 37°C for 3-4 hours prior to target particle addition. 100 μL of target particles were prepared for each well with appropriate protein concentrations, and 95 μL of the 100 μL were added. Macrophages were incubated with target particles at 37°C for exactly 20 minutes. After incubation, wells were washed twice with PBS to remove excess particles. PBS containing 1 μM of CellTracker Green (CMFDA, Thermo Fisher Scientific) and 10 μM Hoechst 33342 (Thermo Fisher Scientific) was added to wells to stain the cytoplasm and nuclei, respectively. Wells were imaged after 10 minutes of staining using a spinning-disk confocal microscope (Nikon) at 20x. Images were acquired in an automated grid pattern at the same location within each well to reduce bias in image acquisition. For each well, at least 100 cells were imaged. Images were than analyzed using a custom CellProfiler (v2.1.1, Broad Institute (Carpenter, A.E. et al., 2006)) project program to identify single cells and quantify the internalized target particle fluorescence intensity (of LISS-Rhodamine lipid) within each cell. Average internalized fluorescence per cell was calculated per condition. Independent replicates were conducted on different days, and replicates were normalized to average eating for all conditions to control for day-to-day variation.

Probing assay

To assess changes in probing activity, we performed live-imaging using confocal microscopy (Nikon, described above) of macrophages expressing the membrane switchable actin binder with and without the presence of A-1155463. To quantify changes in movement, each frame of the time lapse image taken was subtracted from the previous, and an average value was calculated for each frame difference.

SLB TIRF imaging and quantification

Formation of planar SLBs

To image footprints of macrophages and GPMVs, planar SLBs were formed onto coverslips via fusion of SUVs to RCA-cleaned glass coverslips. PDMS (Polydimethylsiloxane, Sylgard) placed atop RCA-cleaned glass formed the imaging chamber, and 50 μL of MOPS buffer and 50 μL of non-fluorescent SUV solution were added. The SUVs were incubated for 20 minutes at room temperature. Excess SUVs were then removed by gently washing 5X with 60 μL of PBS. Appropriate antibody dilutions were prepared, 60 μL were added to the washed SLB and incubated for 20 minutes. Excess protein was removed by gently washing the SLB 2x with PBS. The fluidity of proteins on the SLB was confirmed by using a spinning-disk confocal (Nikon) to examine diffusion of labeled molecules after photobleaching a small region of interest.

TIRF imaging of cell interfaces

Macrophages were added directly to planar SLBs containing AlexaFluor647-labeled anti-biotin IgG. Cells or GPMVs were allowed to settle for 60 minutes prior to imaging. Engaged GPMVs or cells were located and identified using reflection interference contrast microscopy (RICM). Images were acquired using RICM and TIRF microscopy for all relevant fluorescent channels. For live cell imaging, the planar SLBs containing AlexaFluor647-labeled anti-biotin IgG were placed at 37°C, 5% CO2 with a stage top incubator (Okolab), and macrophages were added directly and imaged using RICM and TIRF microscopy.

Quantification of TIRF images

Images were quantified by identifying ROIs in RICM so as to not bias analysis by segmenting on a fluorescent channel. RICM images were flattened using a background (no cells) image, then outlines of SLB-bound cells or GPMVs were identified. Fluorescence inside and outside these ROI outlines was measured and averaged for each fluorescent channel. The outside background measurement was subtracted from the average signal inside of the footprint. This was implemented in MATLAB and data was processed and analyzed using MATLAB.

Acknowledgements

I would like to thank Emily Suter for her assistance with the materials and methods section.

Supplemental Figures

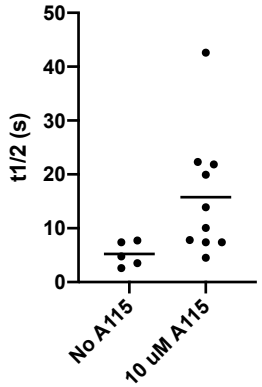

Supplemental Figure 1 Fluorescent recovery after photobleaching (FRAP) t1/2 of membrane switchable actin binder in HeLa cells after 30 minute incubation increased with application of 10 μM A115.

References

1. Schmidt, A. & Hall, M. N. Signaling to the actin cytoskeleton. *Cell Dev Biology* **14**, 305–338 (1998).

2. Stricker, J., Falzone, T. & Gardel, M. L. Mechanics of the F-actin cytoskeleton. *J Biomech* **43**, 9–14 (2010).

3. The Actin Cytoskeleton and Actin-Based Motility. https://cshperspectives.cshlp.org/content/10/1/a018267.full (n.d.).

4. Lanzetti, L. Actin in membrane trafficking. *Curr Opin Cell Biol* **19**, 453–458 (2007).

5. Smythe, E. & Ayscough, K. R. Actin regulation in endocytosis. *J Cell Sci* **119**, 4589–4598 (2006).

6. Šamaj, J. *et al.* Endocytosis, Actin Cytoskeleton, and Signaling. *Plant Physiol* **135**, 1150–1161 (2004).

7. Schaks, M., Giannone, G. & Rottner, K. Actin dynamics in cell migration. *Essays Biochem* **63**, 483–495 (2019).

8. Yonemura, S. Cadherin–actin interactions at adherens junctions. *Curr Opin Cell Biol* **23**, 515–522 (2011).

9. Ishiyama, N. *et al.* Force-dependent allostery of the α-catenin actin-binding domain controls adherens junction dynamics and functions. *Nat Commun* **9**, 5121 (2018).

10. Tsukita, S., Tsukita, S., Nagafuchi, A. & Yonemura, S. Molecular linkage between cadherins and actin filaments in cell—cell adherens junctions. *Curr Opin Cell Biol* **4**, 834–839 (1992).

11. Belardi, B. *et al.* A Weak Link with Actin Organizes Tight Junctions to Control Epithelial Permeability. *Dev Cell* (2020) doi:10.1016/j.devcel.2020.07.022.

12. Itallie, C. M. V., Tietgens, A. J., Krystofiak, E., Kachar, B. & Anderson, J. M. A complex of ZO-1 and the BAR-domain protein TOCA-1 regulates actin assembly at the tight junction. *Mol Biol Cell* **26**, 2769–2787 (2015).

13. Hartsock, A. & Nelson, W. J. Adherens and tight junctions: Structure, function and connections to the actin cytoskeleton. *Biochimica Et Biophysica Acta Bba - Biomembr* **1778**, 660–669 (2008).

14. Yu, D. *et al.* MLCK-dependent exchange and actin binding region-dependent anchoring of ZO-1 regulate tight junction barrier function. *Proc National Acad Sci* **107**, 8237–8241 (2010).

15. Castellano, F., Chavrier, P. & Caron, E. Actin dynamics during phagocytosis. *Semin Immunol* **13**, 347–355 (2001).

16. Diakonova, M., Bokoch, G. & Swanson, J. A. Dynamics of Cytoskeletal Proteins during Fcγ Receptor-mediated Phagocytosis in Macrophages. *Mol Biol Cell* **13**, 402–411 (2002).

17. Rougerie, P., Miskolci, V. & Cox, D. Generation of membrane structures during phagocytosis and chemotaxis of macrophages: role and regulation of the actin cytoskeleton. *Immunol Rev* **256**, 222–239 (2013).

18. Atherton, P., Stutchbury, B., Jethwa, D. & Ballestrem, C. Mechanosensitive components of integrin adhesions: Role of vinculin. *Exp Cell Res* **343**, 21–27 (2016).

19. Pelaseyed, T. *et al.* Ezrin activation by LOK phosphorylation involves a PIP2-dependent wedge mechanism. *Elife* **6**, e22759 (2017).

20. Oberstein, A., Jeffrey, P. D. & Shi, Y. Crystal Structure of the Bcl-XL-Beclin 1 Peptide Complex BECLIN 1 IS A NOVEL BH3-ONLY PROTEIN. *J Biol Chem* **282**, 13123–13132 (2007).

21. Maiuri, M. C. *et al.* Functional and physical interaction between Bcl-XL and a BH3-like domain in Beclin-1. *Embo J* **26**, 2527–2539 (2007).

22. Campbell, S. T., Carlson, K. J., Buchholz, C. J., Helmers, M. R. & Ghosh, I. Mapping the BH3 Binding Interface of Bcl-x L , Bcl-2, and Mcl-1 Using Split-Luciferase Reassembly. *Biochemistry-us* **54**, 2632–2643 (2015).

23. Willis, S. N. *et al.* Proapoptotic Bak is sequestered by Mcl-1 and Bcl-xL, but not Bcl-2, until displaced by BH3-only proteins. *Gene Dev* **19**, 1294–1305 (2005).

24. Shoemaker, A. R. *et al.* A Small-Molecule Inhibitor of Bcl-XL Potentiates the Activity of Cytotoxic Drugs In vitro and In vivo. *Cancer Res* **66**, 8731–8739 (2006).

25. Rose, J. C. *et al.* A computationally engineered RAS rheostat reveals RAS–ERK signaling dynamics. *Nat Chem Biol* **13**, 119–126 (2017).

26. Rose, J. C. *et al.* Rapidly inducible Cas9 and DSB-ddPCR to probe editing kinetics. *Nat Methods* **14**, 891–896 (2017).

27. Rose, J. C., Stephany, J. J., Wei, C. T., Fowler, D. M. & Maly, D. J. Rheostatic Control of Cas9-Mediated DNA Double Strand Break (DSB) Generation and Genome Editing. *Acs Chem Biol* **13**, 438–442 (2017).

28. Aderem, A. & Underhill, D. M. MECHANISMS OF PHAGOCYTOSIS IN MACROPHAGES. *Annu Rev Immunol* **17**, 593–623 (1999).

29. Botelho, R. J. & Grinstein, S. Phagocytosis. *Curr Biol* **21**, R533–R538 (2011).

30. Aderem, A. Phagocytosis and the Inflammatory Response. *J Infect Dis* **187**, S340-5 (2003).

31. Fritz-Laylin, L. K. *et al.* Actin-based protrusions of migrating neutrophils are intrinsically lamellar and facilitate direction changes. *Elife* **6**, e26990 (2017).

32. Flannagan, R. S., Harrison, R. E., Yip, C. M., Jaqaman, K. & Grinstein, S. Dynamic macrophage "probing" is required for the efficient capture of phagocytic targets. *J Cell Biology* **191**, 1205–1218 (2010).

33. Erwig, L.-P. *et al.* Differential regulation of phagosome maturation in macrophages and dendritic cells mediated by Rho GTPases and ezrin–radixin–moesin (ERM) proteins. *Proc National Acad Sci* **103**, 12825–12830 (2006).

34. Joffe, A. M., Bakalar, M. H. & Fletcher, D. A. Macrophage phagocytosis assay with reconstituted target particles. *Nat Protoc* **15**, 2230–2246 (2020).

35. Stuart, L. M. & Ezekowitz, R. A. B. Phagocytosis Elegant Complexity. *Immunity* **22**, 539–550 (2005).

36. Flannagan, R. S., Jaumouillé, V. & Grinstein, S. The Cell Biology of Phagocytosis. *Annu Rev Pathology Mech Dis* **7**, 61–98 (2012).

37. Mylvaganam, S. M., Grinstein, S. & Freeman, S. A. Picket-fences in the plasma membrane: functions in immune cells and phagocytosis. *Semin Immunopathol* **40**, 605–615 (2018).

38. Ostrowski, P. P., Grinstein, S. & Freeman, S. A. Diffusion Barriers, Mechanical Forces, and the Biophysics of Phagocytosis. *Dev Cell* **38**, 135–146 (2016).

39. Hancock, J. F., Cadwallader, K., Paterson, H. & Marshall, C. J. A CAAX or a CAAL motif and a second signal are sufficient for plasma membrane targeting of ras proteins. *Embo J* **10**, 4033–9 (1991).

40. Choy, E. *et al.* Endomembrane Trafficking of Ras The CAAX Motif Targets Proteins to the ER and Golgi. *Cell* **98**, 69–80 (1999).

41. Harris, A. R. *et al.* Biased localization of actin binding proteins by actin filament conformation. *Nat Commun* **11**, 5973 (2020).

42. Steric regulation of tandem calponin homology domain actin-binding affinity | Molecular Biology of the Cell. https://www.molbiolcell.org/doi/full/10.1091/mbc.E19-06-0317 (n.d.).

43. Choi, J., Chen, J., Schreiber, S. L. & Clardy, J. Structure of the FKBP12-Rapamycin Complex Interacting with Binding Domain of Human FRAP. *Science* **273**, 239–242 (1996).

44. Gil, A. A. *et al.* Optogenetic control of protein binding using light-switchable nanobodies. *Nat Commun* **11**, 4044 (2020).

45. Niopek, D. *et al.* Engineering light-inducible nuclear localization signals for precise spatiotemporal control of protein dynamics in living cells. *Nat Commun* **5**, 4404 (2014).

46. Harazono, Y., Nakajima, K. & Raz, A. Why anti-Bcl-2 clinical trials fail: a solution. *Cancer Metast Rev* **33**, 285–294 (2014).

47. Roberts, A. W. Therapeutic development and current uses of BCL-2 inhibition. *Hematology* **2020**, 1–9 (2020).

Chapter 5 – Concluding remarks

Throughout this dissertation, I presented my research into cell-cell barriers, how viruses break down cell-cell barriers, and how to control actin binding in cells. Each project has opened the door to future directions and new explorations.

Tight junctions and actin binding

The vast majority of our studies into tight junctions and actin binding were performed in a commonly used cell line, MDCK II. However, this cell line, canine kidney epithelial cells, is not representative of many organs with tight junctions. A next step to verify the relevance of our work in human cells and human disease is to explore tight junctions and actin binding in human cell types from other organs. These models will allow us to better understand our ability to manipulate actin binding, and the potential for exploring this avenue to develop therapeutics.

Viruses and cell barriers

Our work into how viruses hijack host proteins to disrupt barrier function is still in the preliminary stages. We have identified that NS1 PBMs from various strains disrupt barrier functions, but the mechanism for this disruption remains to be discovered. Future work includes teasing out which PDZ-domain binding partners are responsible for the barrier breakdown, and whether there is a common pathway that could be targeted with therapeutics to treat the flu. Similarly, we found that the E protein of SARS-CoV-2 reduces barrier function in A549 (lung epithelial cells), but our hypothesis that it was the PBM that mediates this interaction was wrong. Exploratory work into which binding partners of the E protein are responsible for the disruption to the barrier is needed.

Switchable actin binder

This project remains the most open-ended. As actin is involved in many critical cell processes across all cell types, this tool can be used to examine actin binding in many topics. Furthermore, more work can be done to develop more switchable actin binders.

Promising projects

As I began my graduate work, I never could have foreseen where the science would lead me. My research into the proteins involved in organizing the tight junction to control barrier function lead through many dead-end paths. Below are two projects that were dead-ends at the time, but with new tools and new knowledge that were not available at the time, they may be worth exploring further.

Measuring forces at the tight junction using a FRET tension sensor.

I hypothesized that forces exerted on ZO-1 played a role in tight junction assembly and maintenance, and I embarked on a project to measure forces acting through ZO-1. One method for measuring forces at cell-cell interfaces is by fusing a FRET tension sensor to a protein of interest

to measure forces across the protein. The FRET tension sensor module (TSmod) is composed of a FRET pair of protein fluorophores connected with an entropic protein spring. When relaxed, there is FRET between the two fluorophores, and when under tension, the protein string stretches moving the FRET pair apart and reducing FRET efficiency (Figure 1). The FRET tension sensor is the only current method that can measure forces at the tight junction specifically by measuring tension across ZO-1, rather than integrating forces across all cell-cell junctions.

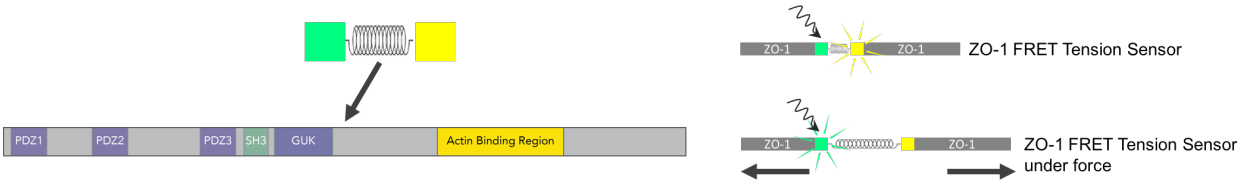

Figure 1 Left, schematic of the FRET tension sensor module (TSmod) inserted into ZO-1 between the actin binding region and binding domains to transmembrane proteins, Right, schematic of high FRET when not under tension and reduced FRET when ZO-1 is under tension.

The FRET tension sensor in ZO-1 was expressed double knockout cells (Figure 2A). I used a 2-p confocal microscope with a spectral detector to measure the intensity of emission of the donor and acceptor. I calculated a FRET index, which is the intensity of the acceptor emission normalized for expression and taking into account bleed-through of donor emission into the acceptor emission wavelengths. A control construct will be created with the tension sensor at the N-terminus of ZO-1, which will never be under tension, as well as ZO-1 with just the donor or acceptor fluorophore for calculating bleed-through. Preliminary results show that the FRET index is significantly lower in dKO cells expressing ZO-1 TSmod compared with ZO-1 TSmod N-term in live cells (Figure 2B, C), suggesting that ZO-1 is indeed under tension in polarized epithelial cells.

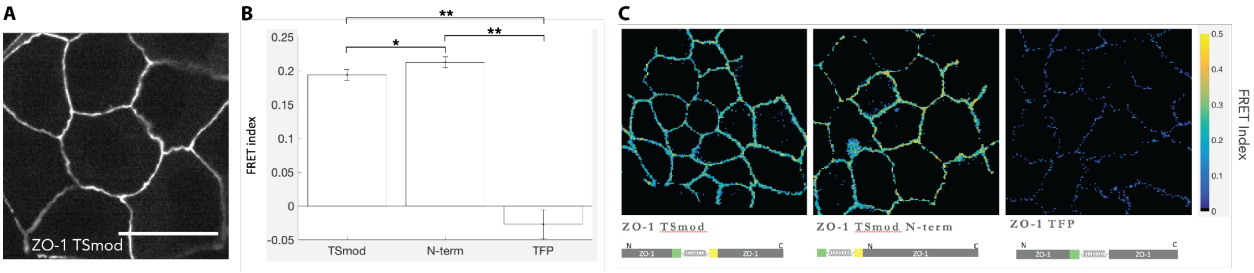

Figure 2 ZO-1 is under tension at the tight junction

A) Confocal image showing ZO-1 TSmod localizes to cell junctions in dKO MDCK II cells, reintroducing membrane undulations. Scale bar 10 μm.

B) Average FRET index in ZO-1 TSmod, ZO-2 N-term and TFP constructs. * $p < 0.05$, ** $p < 0.01$, N=5, technical replicates.

C) FRET index calculated pixel by pixel for ZO-1 TSmod, ZO-1 TSmod N-term and ZO-1 TFP constructs expressed in live cells.

Discovery of actin binding proteins that preferentially bind to different actin structures

For this project, we sought to identify novel proteins that preferentially bind to different structures. We used a method for spatially resolved proteomic mapping, where a peroxidase, APEX, fusion

to a protein probe will covalently tag nearby endogenous proteins with biotin allowing for subsequent identification with mass spectrometry[1]. We used an actin binding protein as a probe which we find to specifically locate to actin under tension or torque in live cells. By creating APEX fusion proteins that localize to different actin structures we can compare the relative abundance of labeled proteins and, for the first time, use an unbiased approach for identifying proteins found in proximity to actin under tension or torque. Identification of novel proteins, or new functions of known proteins, will extend our understanding of how mechanical forces influence cell behavior.

APEX2, an engineered ascorbate peroxidase, was fused with an actin-binding protein which localizes to specific actin structures. In the presence of H2O2 and biotin-phenol, APEX2 oxidizes biotin-phenol to a biotin-phenoxyl radical, which is highly reactive and short lived. Therefore, biotin will be conjugated to proteins that are proximal to the active site of APEX, with a previously reported biotinylation radius of about 20 nm. It should be noted, however, that biotinylation occurs at further distances at a decreased rate, and may be detected by MS. A general non-actin-binding cytoplasmic control is crucial for differentiating between common cytoplasmic proteins and actin-binding proteins. We developed a label-free relative quantification method to compare relative abundance of proteins from two separate APEX-protein constructs. To validate our methodology we expressed fusion APEX-utrophin-ABD and APEX-utrophin-ABD-mutant in HeLa cells, which localize to different actin structures in the cell. Additionally, we created an APEX-GFP construct which localizes to the cytoplasm, to distinguish between cytoplasmic proteins and our actin-binding proteins of interest (Figure 3).

APEX-utrophin-ABD, APEX-utrophin-ABD-mutant and APEX-GFP fusion proteins were expressed in HeLa cells, incubated with biotin-phenol and H2O2. Biotinylation localization was verified through fluorescent staining of biotin in cells after peroxide incubation (Figure 3 A-F). Streptavidin magnetic beads were used to enrich for biotinylated proteins for MS, and we confirmed that many different proteins were labelled with biotin with a western blot (Figure 3, g). Tandem MS (MS/MS) identified 431 distinct proteins. Gene ontology analysis of the complete list of proteins labeled by APEX-utrophin or APEX-utrophin-mutant showed that while both showed high representation of cytoskeleton proteins, there are some actin structures that were uniquely identified. Notably, APEX-utrophin labeled proteins that were categorized as the cell cortex and ruffle, while APEX-utrophin-mutant labeled proteins that were categorized as stress fiber and actomyosin (Table 1). These data, compiled by an unbiased gene ontology analysis of identified proteins, confirm our reported localization data. Utrophin-ABD localizes to all actin structures, including the cell cortex, while the utrophin-ABD-mutant preferentially localizes to stress fibers. By comparing the relative abundance of labeled proteins from the APEX-utrophin and APEX-utrophin-mutant we identified 20 actin-binding proteins of interest that were significantly enriched above the APEX-GFP cytoplasmic background. From this list alpha-catenin 1 and filamin-A were used as cross-linkers in an actin gel. Interestingly, we saw differences in the actin gel structure (Figure 3, H-I). We demonstrated that this method can be used to identify new proteins, which

can then be independently validated, showing the potential for using APEX to tag proteins that localize to actin under tension or torque.

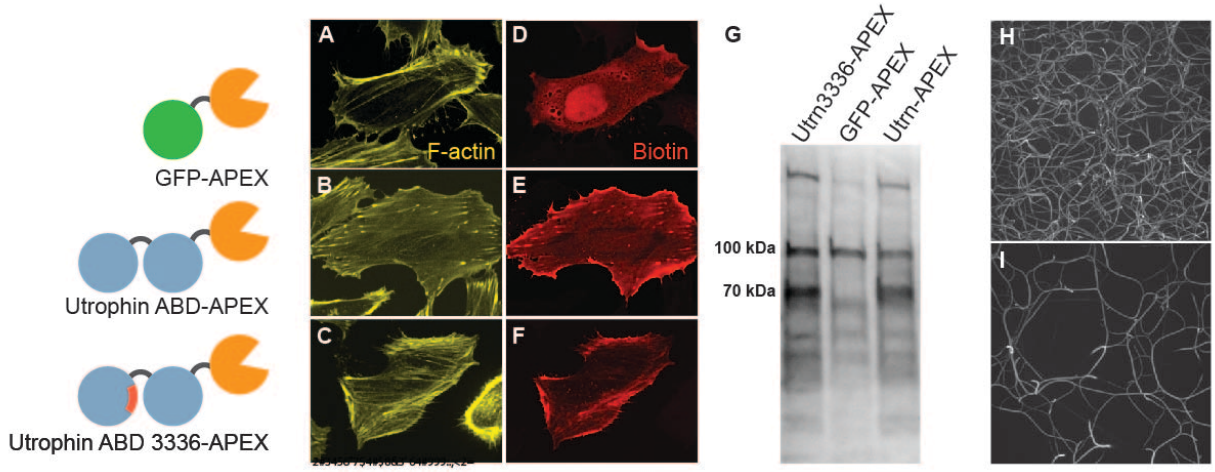

Figure 3 Method to identify proteins bound to distinct populations of actin

A-F: Localization of F-actin and biotin after peroxidase activation of APEX-utrophin-ABD, APEX-utrophin-ABD-mutant and APEX-GFP.

G: Western blot labeled for biotin showing a wide distribution in the size of proteins labeled with biotin.

H: 1875 nM alpha-actinin used as cross-linkers in an actin gel (visualized as white with phalloidin).

I: 1250 nM Filamin-A used as cross-linkers in an actin gel (visualized as white with phalloidin).

	Enriched in Utrophin-APEX		Enriched in Utrophin3336-APEX	
	Gene Ontology (GO)	p-value	Gene Ontology (GO)	p-value
Unique GO	ruffle (GO:0001726)	1.74E-04	contractile actin filament bundle (GO:0097517)	6.97E-04
	cell cortex (GO:0005938)	6.10E-03	stress fiber (GO:0001725)	6.97E-04
	cortical cytoskeleton (GO:0030863)	2.98E-02	actin filament bundle (GO:0032432)	1.29E-03
	cell leading edge (GO:0031252)	3.83E-02	actomyosin (GO:0042641)	2.25E-03
			myofibril (GO:0030016)	3.35E-03
			contractile fiber part (GO:0044449)	2.40E-02
Shared GO	cytoskeleton (GO:0005856)	4.24E-16	cytoskeleton (GO:0005856)	5.45E-09
	adherens junction (GO:0005912)	4.57E-12	adherens junction (GO:0005912)	3.13E-22
	actin cytoskeleton (GO:0015629)	5.60E-04	actin cytoskeleton (GO:0015629)	5.42E-06

Table 1 Gene ontology of proteins identified after proximity labelling using Utrophin-APEX and Utrophin3336-APEX constructs

References

1. Hung, V. *et al*. Spatially resolved proteomic mapping in living cells with the engineered peroxidase APEX2. *Nat Protoc* **11**, 456–475 (2016).